Progress Report No. 4

MECHANISM OF THE PHOTOVOLTAIC EFFECT IN II-VI COMPOUNDS

National Aeronautics and Space Administration
Lewis Research Center
Cleveland, Ohio

October 1, 1968 - March 31, 1969

School of Engineering
Department of Materials Science
Stanford University
Stanford, California

Grant NGR-05-020-214

Principal Investigator

Richard H. Bube, Professor

(This Report is the PhD Thesis of William D. Gill)

SU-DMS-69-R-49

Department of MATERIALS SCIENCE
STANFORD UNIVERSITY

ABSTRACT

The photovoltaic properties of efficient Cu_2S-CdS heterojunctions have been investigated with the following aims: (1) to develop a model for the band profile consistent with all the experimental observations, (2) to understand the nature of the complicated spectral response and V-I characteristics of these heterojunctions, (3) to understand the effects of heat treatment on the photovoltaic properties of the cells, and (4) to measure directly the ambipolar diffusion lengths that determine the active region of the heterojunction.

Fast and slow components of the spectral response of short-circuit photocurrent and the effects of secondary illumination on the primary response have been investigated. V-I characteristics and capacitance-voltage behavior have been examined for the cells in the dark and under illumination.

Diffusion length measurements were made using a light microprobe to inject minority carriers and the junction as a current collector. Light-induced reverse breakdown observed in these heterojunctions was also examined with the light microprobe.

Heat treatment of the cells resulted in decreased long wavelength response. Secondary illumination with photon energy greater than 1.5 eV partially restored the original response. Quenching of the enhanced short-circuit photocurrent was observed in two infrared bands at 0.8 eV and 1.1 eV. Slow components in the photoresponse show enhancement and quenching regions in agreement with secondary illumination results.

Diffusion lengths between 3×10^{-4} and 6×10^{-4} cm were measured in the CdS, and between $\leq 1 \times 10^{-5}$ and 3×10^{-5} cm in the Cu_2S.

Short wavelength light-induced reverse breakdown with a threshold of 0.2 volts was observed in both V-I characteristics and light microprobe measurements. Photocurrents up to 2000 times the incident photon flux were observed at low reverse bias. These breakdown effects were correlated with imperfections observed on the junction.

A model is proposed in which hole trapping at levels introduced in the CdS by heat treatment varies the transparency of a conduction band spike to photoexcited electrons tunnelling from the Cu_2S which are responsible for the long wavelength response. Enhancement and quenching effects are related to changes in hole occupancy of these levels. The reverse breakdown observed under short wavelength illumination is explained by light-induced Zener breakdown at high field points on the junctions.

ACKNOWLEDGMENTS

The author wishes to express his appreciation to Professor R. H. Bube, principal advisor, for suggesting the topic and for his suggestions and counsel in many discussions during this work.

The author is grateful to Professors J. L. Moll, G. L. Pearson, and W. E. Spicer, members of the reading committee, for their helpful suggestions during this investigation and in the preparation of this dissertation.

The author is indebted to Professor T. Takahashi, Visiting Scholar from Tohoku University, for his keen interest and for discussions on many aspects of this topic.

The contributions, in many stimulating discussions on this topic, of Mr. P. F. Lindquist, Dr. H. Matthews, and Mr. J. Harper are gratefully acknowledged.

The author wishes to thank Dr. H. W. Brandhorst, Jr. of Lewis Research Center, and Mr. L. R. Shiozawa of Clevite Corp. for several helpful discussions and for providing the thin film CdS solar cells.

A leave of absence from IBM Corporation for the duration of this work is gratefully acknowledged.

Finally, the author wishes to thank his wife, Sandra, for her encouragement and for her assistance in the preparation of this dissertation.

The work presented in this dissertation was supported partially by the National Aeronautics and Space Administration (Lewis Research

Center) and partially by the Advanced Research Projects Agency through the Center for Materials Research at Stanford University.

TABLE OF CONTENTS

LIST OF FIGURES

LIST OF TABLES

I. INTRODUCTION

1.1 Nature of the Problem

The photovoltaic properties of semiconductor p-n junctions and metal-semiconductor barrier cells have been studied extensively and are well understood in the framework of present semiconductor theory. These junctions have found extensive application as light detectors and as solar energy conversion devices. Heterojunctions, i.e., junctions formed at the interface between two semiconductors, are considerably more complex and are therefore only qualitatively understood at present. The complexity of heterojunctions is due to the complications inherent in forming a junction between semiconductors having different bandgaps, free carrier densities, electron affinities, and often different crystal structures. Despite these complications, there has been considerable interest in heterojunctions because the use of two semiconducting materials provides a great variety of possible band profiles and allows flexibility in designing device characteristics such as spectral response.

The heterojunction formed by Cu_2S and CdS is the subject of this thesis. It has been found that by very simple methods Cu_2S layers can be grown on CdS crystals resulting in heterojunctions having spectral response characteristics which are a good match to the solar spectrum.

The work described in this thesis has been directed toward understanding the photovoltaic properties of the Cu_2S-CdS heterojunction with the hope that through better understanding more efficient energy conversion devices will result.

Considerable research and development work has been done on Cu_2S-CdS heterojunctions and on Cu-CdS barrier cells. At the present time, heterojunctions formed on evaporated thin films of CdS can be reliably produced with solar conversion efficiency in the range of 5 to 6 percent. Many of the features of these efficient cells are now reasonably well understood, but a completely satisfactory model for the junctions has not yet emerged.

There are several reasons why the Cu_2S-CdS photovoltaic cells have been difficult to understand. The heterojunction is a complex one since the crystal structures and lattice parameters of the Cu_2S and CdS are very different. In addition, the Cu-S phase diagram is complex with several metastable phases existing in the composition and temperature range of interest. A second major difficulty in understanding the electrical properties of the junctions is the lack of knowledge of the physical parameters of Cu_2S itself. The problem is further complicated by several unusual features observed in the spectral response and V-I characteristics of the cells.

Most of the previous research on the photovoltaic properties of these junctions has been concentrated on spectral response measurements and the light-generated V-I characteristics of the cells. In the present research the electrical properties of efficient Cu_2S-CdS heterojunctions have been studied using a wide variety of experiments in an attempt to

obtain a new perspective on the problem. Experiments have been carried out mainly with junctions formed on single crystal CdS to avoid the additional complications inherent in polycrystalline films. However, where possible, parallel experiments have been made on thin film cells so that the results of work on single crystal cells could be related with some confidence to the more practical thin films.

The specific aims of the research presented in this thesis have been to (1) develop a model for the band profile consistent with all the experiments, (2) understand the nature of the complicated spectral response and V-I characteristics of the cells, (3) understand the effects of heat treatment which is a usual step in efficient cell production, and (4) measure directly the minority carrier diffusion lengths that determine the active region of the heterojunction.

1.2 Survey of Previous Research

In 1954, Reynolds et al.[1,2] found strong photovoltaic effects when copper contacts were made to CdS crystals. Open-circuit voltages of 0.45 volts and short-circuit currents of about 15 mamp/cm^2 were reported. The spectral response was found to extend to longer wavelengths than the bandgap of CdS. This observation was explained by a two-step excitation process through impurity levels in the CdS. This was the first reported observation of efficient photovoltaic effects involving CdS. Possible solar cell applications resulted in extensive investigation of CdS barrier cells at several laboratories. Williams and Bube[3] investigated the properties of photovoltaic cells made by plating various metals onto CdS crystals. These authors found that photoemission

from the metal into the CdS was responsible for the long wavelength response. The most efficient cells were found to be Cu-CdS barrier cells. Fabricius[4] and Grimmeiss and Memming[5] interpreted similar results in Cu-CdS cells being due to a p-n photoeffect in CdS, a result in agreement with earlier work by Woods and Champion.[6]

In 1962, Cusano[7,8] reported results on the heterojunction systems Cu_2Te-CdTe and Cu_2S-CdS. Cusano interpreted his results as due to a photovoltaic junction between p-type copper telluride and n-type cadmium telluride and a similar junction in the Cu_2S-CdS system. The absorption of useful radiation was interpreted as occurring almost entirely in the CdTe and CdS respectively. In addition, Cusano suggested that the Cu-CdS barrier cells investigated by other authors contain very thin Cu_2S layers forming heterojunctions at the CdS interface. The photovoltaic response of Cu_2S-CdS heterojunctions formed by vacuum evaporation of Cu_2S on CdS single crystals was reported by Selle et al.[9] These authors attributed the observed long wavelength response to an indirect absorption process in the Cu_2S. Research on evaporated and diffused Cu-CdS cells by Bockemuehl et al.[10] were explained by a double junction model. Keating[11,12] working with this kind of cell showed that a heterojunction model was more likely than a homojunction model. The possibility of a photoconducting CdS layer between the Cu_2S and the bulk CdS was pointed out. Duc Cuong and Blair[13] attributed the extrinsic response to impurities in the CdS layer.

Considerable reserach has also been carried out on broad-area photovoltaic cells involving the use of thin films of polycrystalline CdS. The first such thin film cell was reported by Nadjakov et al.[14] in

1954, using aluminum and gold to form barrier cells. At this time, several research laboratories investigated photovoltaic cells using vacuum deposited films of CdS with rectifying contacts of copper, cuprous oxide, and cuprous sulfide. In 1958, Cabannes[15] reported photovoltaic effects using copper on CdS films. In 1960, Moss[16] reported the fabrication of Cu-CdS thin film solar cells with energy conversion efficiencies approaching 1 percent. Subsequently, many laboratories investigated these cells in an effort to develop efficient, light-weight, large-area solar cells. Chamberlin and Skarman[17] investigating Cu_2S-CdS thin film cells formed by a chemical spraying technique reported efficiencies up to 4 percent. The most reliable and efficient cells are produced by a chemical dipping process due to Shirland and Hietanen,[18] in which the CdS surface is reacted with cuprous ions in an aqueous solution. The current state of the art is reliable production of 5 to 6 percent efficient cells of about 50 cm^2 area. These cells involve the heterojunction between evaporated CdS films and chemically formed Cu_2S layers.

Several complications arise in attempting to understand the detailed mechanism of the photovoltaic effect in CdS barrier cells and heterojunctions. The first question involves the nature of the junction itself, i.e., whether one is dealing with p-n junctions, heterojunctions or metal-semiconductor barrier-cells. It has been universally observed that the only efficient cells are those using copper or a copper compound as the rectifying contact to the CdS. Furthermore, the properties of cells made by electroplating copper onto CdS and those made by chemically forming a Cu_2S layer on the CdS are remarkably similar. Cuprous sulfide is a degenerate p-type semiconductor and therefore most

of the space-charge region of the Cu_2S-CdS heterojunction is on the CdS side of the interface. Similarity of the characteristics of Cu-CdS barrier cells and Cu_2S-CdS heterojunctions may be due to either (1) a thin layer of Cu_2S being formed at the CdS interface of the barrier cells, or (2) copper diffusion into the CdS depletion layer in both the barrier cells and the heterojunctions. In the first case, both types of cells are actually heterojunctions and their characteristics should be similar. In the second case, similar characteristics could be expected as long as the CdS side of the junction dominated the response, and provided the effective barrier heights for the copper and Cu_2S rectifying contacts were similar.

In dealing with Cu_2S-CdS heterojunctions, such as those formed by chemically reacting the CdS surface with cuprous ions, a major problem is understanding the band profile at the interface. Very little information is available on the properties of Cu_2S. Near room temperature the phase diagram is complicated, with a number of nearly stable modifications being possible. X-ray analysis of the layers formed on CdS nearly always indicates that a number of these phases are present. The dominant phase is orthorhombic Cu_2S which has a, b and c lattice constants of 11.88 A, 27.32 A, and 13.49 A respectively.[19] Optical studies have shown Cu_2S to have an indirect bandgap of 1.2 eV[20] and a higher energy gap at 1.8 eV. Because of the strength of the absorption the latter is probably a direct gap. The optical absorption coefficients determined in several studies[20-24] are shown in figure 1.1. The electron affinity is not known. Electrically, Cu_2S is a degenerate p-type defect semiconductor with resistivity in the range of 10^{-2} to 10^{-3} ohm-cm. Hall

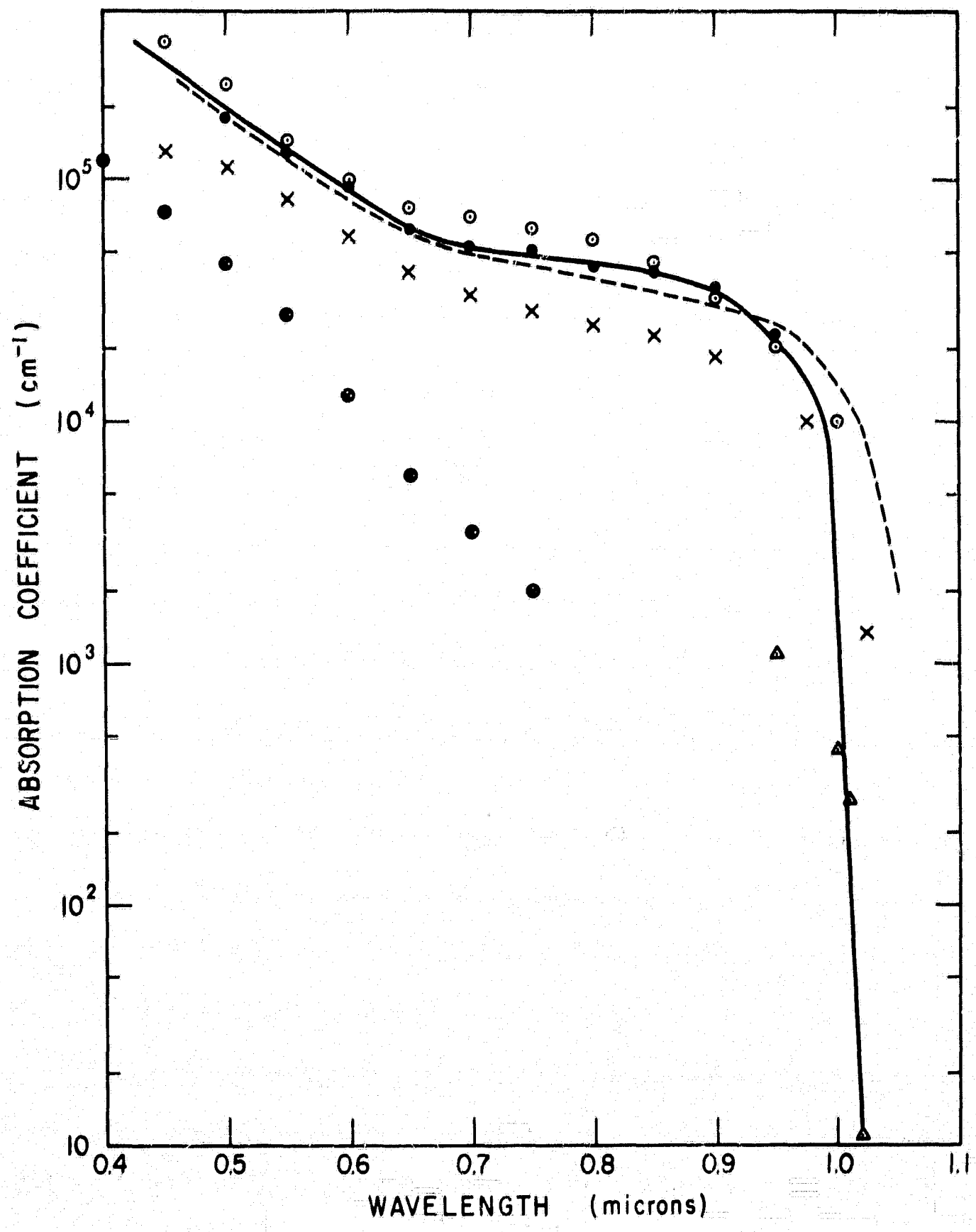

FIGURE 1.1: ABSORPTION COEFFICIENT OF Cu_2S. DATA FROM: ⊙ EISENMANN[21], ● SHIOZAWA et al.[23], DIP-FORMED Cu S, × SHIOZAWA et al.[23], VACUUM DEPOSITED Cu_2S, △ MARSHALL AND MITRA[20], ● SOROKIN et al.[22], DASHED LINE FROM SELLE AND MAEGE.[24] THE SOLID LINE IS THE CURVE JUDGED MOST RELIABLE FOR DIP-FORMED Cu_2S FILMS.

measurements show the mobility at room temperature to be about 10 to 25 $cm^2/V\text{-}sec$, and carrier concentrations greater than 10^{19} cm^{-3}.[25,26] Heterojunctions formed chemically in solution at around 90°C show a preferred orientation between the Cu_2S and the CdS crystals, with the a and c axes being aligned.[27]

Research on Cu_2S-CdS heterojunctions and Cu-CdS barrier cells has resulted in many models for the photovoltaic process.[3,5,10,23,28,29] Much of the confusion has resulted from the use of low efficiency cells in many of these investigations. In such cells the long wavelength response can reasonably be attributed to light absorption at impurity states and surface states.[13,30,31] In the high efficiency cells of more practical interest, quantum efficiencies greater than 0.1 are realized over much of the spectral response interval. Optical absorption considerations lead to the conclusion that the major long wavelength response of these cells originates in the Cu_2S layer.[23] The concern of the present work has been the photovoltaic properties of these efficient cells.

One of the major experimental observations on the Cu_2S-CdS cells has been the non-additive nature of the spectral response. In a conventional p-n junction solar cell, the response to white light may be fairly accurately obtained by integrating over the normalized spectral response curve. In the Cu_2S-CdS cells similar integration does not yield the output under white illumination, the usual result of integration predicting too small a value for the white output. This effect is due to the enhancement of long wavelength response by short wavelength light. The spectral response of the enhancing radiation has led to a

model in which the series resistance of the cells is modified by the photoconductivity of an insulating CdS layer at the interface.[23,32,33] Similar enhancement effects were studied on Cu-CdS cells,[13] where the enhancement effect was attributed to increased red absorption through impurity levels emptied by the short wavelength enhancing radiation.

The V-I characteristics of efficient Cu_2S-CdS heterojunctions show a crossover in the forward direction of the dark characteristic and the characteristic under illumination.[34] Current models explain this effect by the series resistance of the insulating CdS layer[34] or by changes in the barrier height under illumination.[23] The adequacy of series resistance model has been questioned in a recent publication.[35]

The well established features of the efficient Cu_2S-CdS heterojunction operation may be summarized as follows. The major light absorption is in the Cu_2S film with electron diffusion to the junction providing the photocurrent. Efficient cells require short heat treatments to improve shunt resistance. The heat treatment diffuses acceptors, probably copper, into the CdS widening the depletion layer.[23,35] As a result of the heat treatment the long wavelength response of the cells is degraded, but may be partially recovered by simultaneous, weak short wavelength illumination.[23,32,33,35] Spectral response of the enhancement effect indicates that light absorption in the partially compensated CdS layer at the junction is responsible for the enhancement.

II. THEORY

2.1 Heterojunctions

An extensive review of the theory of heterojunctions has been presented in the doctoral thesis of van Ruyven.[37] Only a very brief summary of the more important models is given here. Some considerations of the general theories relevant to the Cu_2S-CdS heterojunction are discussed in greater detail. Tunnelling in heterojunctions is also discussed since it plays an important role in the analysis of the experiments.

General Models for Heterojunctions

An abrupt junction model has been developed by Anderson[38] for Ge-GaAs heterojunctions. This treatment assumes transition from one crystal to the other with a discontinuity in a single plane of atoms. This approach is applicable in certain cases where the mismatch in lattice constants for the two semiconductors is very small. In Anderson's treatment the effects of dipoles and interface states are neglected. The transition region in this model is made up of two barriers which are the diffusion potentials in each material. The width of the transition region and the total capacitance of the junction are obtained by considering the individual depletion regions in series.

The effect of junction-grading is included in a model by Oldham and Milnes.[39] In this model the material parameters such as lattice constant, energy gap, and electron affinity are assumed to vary continuously across a finite region.

A third model for junction profiles in which interface states play a dominant role was introduced by van Ruyven.[37] The interface states can arise due to the mismatch in lattice constant and the difference in band structure. In this model the Fermi level is stabilized at the interface by surface states and the work function differences of the bulk materials are not important. An electric dipole at the interface compensates the difference in work functions between the semiconductor surfaces, and the total junction can be treated as back-to-back Schottky diodes separated by a very thin metal layer.

Considerations Applicable to the Cu_2S-CdS Heterojunction

In this section the effects of crystal structure, band gap, and conductivity of the two semiconductors forming the heterojunction are discussed for the situation applicable to the Cu_2S-CdS heterojunction. These semiconductors have different crystal structures, lattice constants, and band gaps. In addition, Cu_2S is a degenerate p-type semiconductor, while CdS is non-degenerate n-type.

Differences in crystal structure and lattice constants between the two component semiconductors cause serious structural problems at the interface. Efficient heterojunction properties depend on intimate contact across the junction. This means that a reasonable two dimensional match of the two crystal structures must be possible. In the

Cu_2S-CdS junction, the a-axis and the c-axis of the orthorhombic (Cu_2S) and hexagonal (CdS) structures are aligned. The a-axis lattice constant of Cu_2S is within 4 percent of being 3 times the CdS a-axis length. Along the c-direction the Cu_2S lattice constant is twice the CdS lattice constant within 0.4 percent.[27] The deviation from an exact match of multiples of the lattice constants results in large strains at the junction. The effects of such strain on the electrical properties of a heterojunction are difficult to estimate. There may be changes in the bandgaps near the junction and interface states are probably affected by such strains. The piezoelectric effect in CdS may also affect the electrical properties of the junction in the strained region.

The difference in the bandgaps of the two semiconductors forming a heterojunction is its most interesting feature. In the usual photocell involving a wide and a narrow bandgap semiconductor, the light is incident from the wide bandgap side ("back-wall" illumination). The long wavelength threshold of the spectral response is determined by the narrow bandgap semiconductor. The short wavelength cutoff is due to the wide bandgap material. Thus in principle the spectral response can be tailored over a wide range by suitable choice of a heterojunction couple. In practice the structural problems outlined above severely restrict the possible semiconductor combinations. In the Cu_2S-CdS case the long wavelength response is determined by the 1.2 eV bandgap of Cu_2S. However, because the Cu_2S is formed as a very thin layer ($\simeq 3 \times 10^{-5}$ cm) on the CdS, the light is usually incident through the Cu_2S ("front-wall" illumination). The short wavelength response is therefore no longer limited by the 2.4 eV bandgap of CdS.

The general nature of the band profile is determined by the conductivities of the bulk semiconductors. However, the details of the profile in the transition region are very sensitive to affinity differences, charged surface states, dipole layers, and cross-diffusion of impurities. A few possible band profiles for the Cu_2S-CdS system are sketched in figure 2.1. Since the Cu_2S is a degenerate semiconductor, the space charge penetration into the p-side of the heterojunction is very small and the junction may be treated in some respects as a metal-semiconductor Schottky barrier. The depletion width and junction capacitance may be calculated from the usual relationships for Schottky barriers[40] considering only the CdS side of the heterojunction. The profiles (a), (b) and (c) of figure 2.1 show the effects of electron affinity differences between the two semiconductors. Similar discontinuities in the band profile may result from charged interface states or dipole layers as in the case of junctions between different metals. Profile (d) shown in the figure is included since after heat treatment of the cells there is evidence for compensation of the Cu_2S by diffused-in copper.

Current Transport and Tunnelling

The current-voltage characteristics of p-n homojunctions was derived by Shockley[41] for a pure diffusion current. The form of the characteristic for the diode is

$$I = I_S\left[\exp\left(\frac{qV}{akT}\right)-1\right] , \qquad (2.1)$$

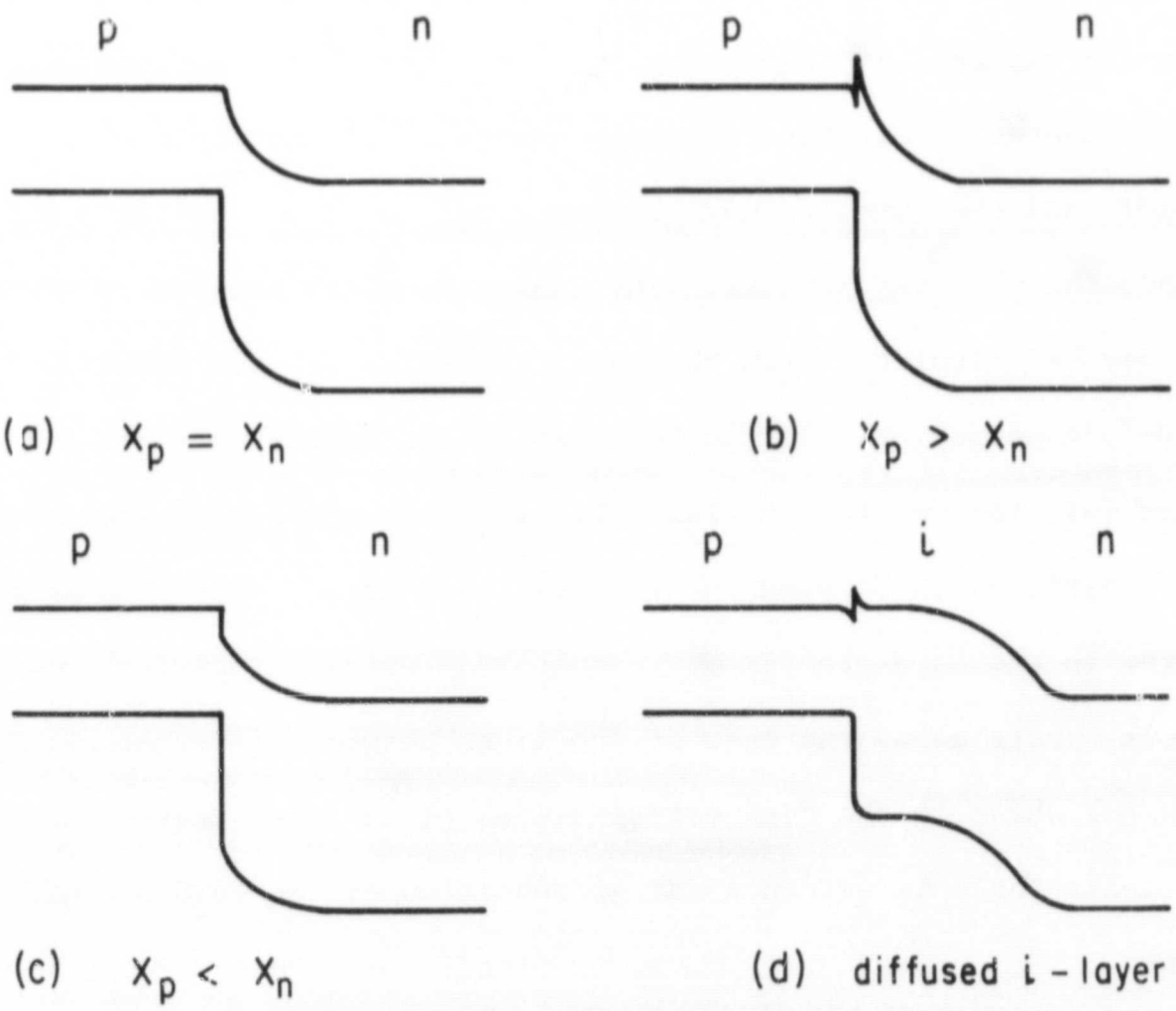

FIGURE 2.1: SOME POSSIBLE BAND PROFILES FOR THE Cu_2S-CdS HETEROJUNCTION. DISCONTINUITIES AT THE INTERFACE MAY BE DUE TO AFFINITY (X) DIFFERENCES AS SHOWN OR MAY RESULT FROM INTERFACE STATES OR DIPOLE LAYERS. THE Cu_2S IS SHOWN AS A DEGENERATE p-TYPE SEMICONDUCTOR.

where I is the total current, I_S is the reverse saturation current, V is the applied voltage, and a is a temperature independent constant equal to unity for the so-called "ideal" diode.

The situation may be somewhat altered in the case of heterojunctions. Because of the different bandgaps, the barrier in the conduction and valence bands is usually very different. In addition, the presence of discontinuities, especially potential "spikes," at the interface result in departures from the homojunction case due to the possibility of tunnelling as a mechanism for current transport. In many cases the temperature dependence of V-I characteristics of heterojunctions have resulted in temperature independent exponents in equation 2.1.[37,42,43] The characteristics fit an equation of the form

$$I = I_o(e^{\alpha V} - 1) , \qquad (2.2)$$

where α is a temperature independent coefficient. Characteristics of this sort are interpreted as indicating that tunnelling processes dominate the current transport.

Since the results of several measurements on the Cu_2S-CdS heterojunction are explained in terms of tunnelling processes, the remainder of this section will be devoted to developing the appropriate theory. Zener[44] originally treated the problem of quantum mechanical tunnelling in the electrical breakdown of thin insulating films. Franz[45] developed an expression for the transparency, T, for tunnelling through a barrier which is a convenient starting point for treatment of Zener breakdown in p-n junctions,[46,47] field emission in Schottky barriers[48] and tunnelling through barriers in heterojunctions.[37,42,43,49] Franz's expression which is derived using the WKB approximation is

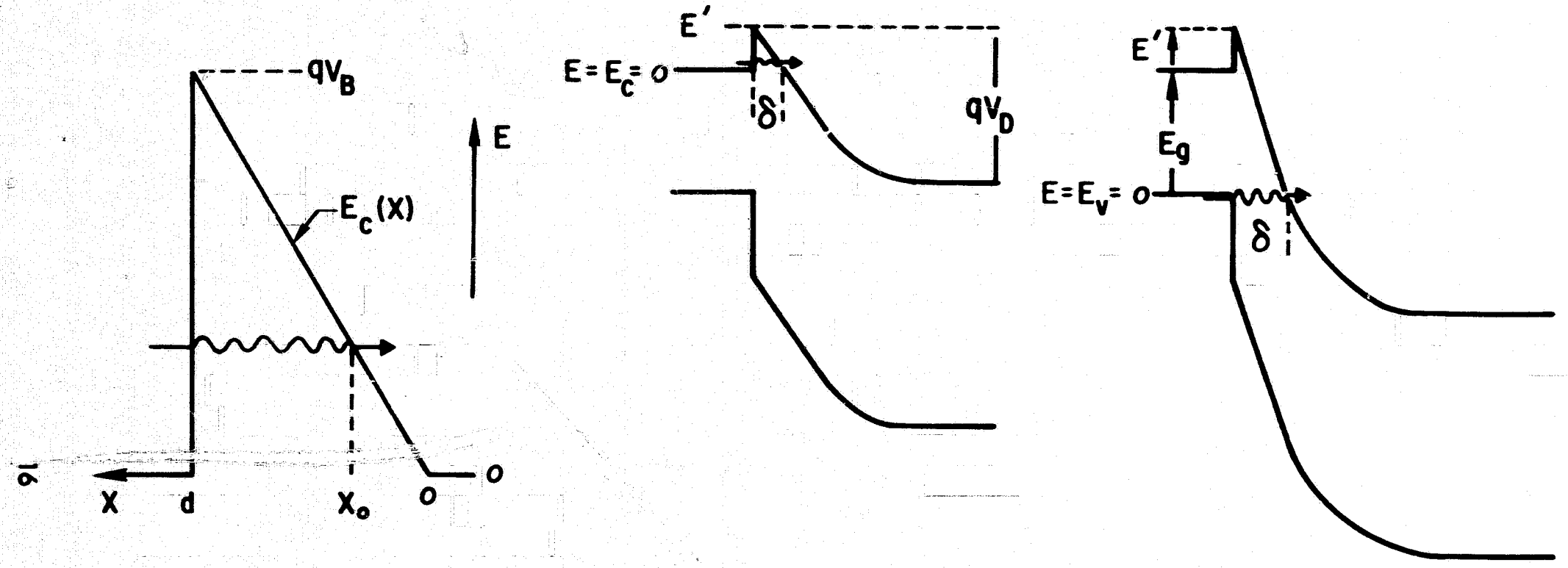

(a) TUNNELLING GEOMETRY (b) CONDUCTION BAND SPIKE (c) ZENER BREAKDOWN

FIGURE 2.2: GEOMETRY OF TUNNELLING PROCESSES.

$$T = \exp\left[- 2i \int_{x_1}^{x_2} k(x)\,dx \right] , \qquad (2.3)$$

where $k(x)$ is the electron wavevector, x_1 and x_2 are the classical turning points.

Consider first the tunnelling probability through a conduction band spike at the interface of a heterojunction. The spike may be represented as a triangular barrier as shown in figure 2.2(a). Then, for an electron tunnelling through the spike at some energy E above the base of the spike, the wavevector $k(x)$ may be written as

$$\hbar^2 k^2(x) = 2m^*[E - E_c(x)] = -2m^*|E_c(x) - E| , \qquad (2.4)$$

where m^* is the effective mass and $E_c(x)$ is the conduction band edge. Using equations (2.3) and (2.4) the transparency of the barrier at energy E is

$$T(E) = \exp\left[- \frac{2}{\hbar} \int_{x_o}^{d} [2m^*(E_c(x) - E)]^{1/2}\, dx \right] . \qquad (2.5)$$

For the triangular barrier approximation

$$E_c(x) = \left(\frac{qV_B}{d} \right) x . \qquad (2.6)$$

Integrating equation (2.5) gives

$$T(E) = \exp\left[- \frac{4}{3\hbar} (2m^*)^{1/2} \frac{d}{qV_B} (qV_B - E)^{3/2} \right] . \qquad (2.7)$$

Equation (2.7) can now be adapted for the two tunnelling situations considered in the Cu_2S-CdS heterojunctions. The applicable geometries are illustrated in figure 2.2(b) and (c) and correspond to tunnelling through a conduction band spike and band-to-band tunnelling or Zener breakdown. In both cases a triangular barrier is assumed with tunnelling taking place through the bottom of the barrier (E = 0 in equation 2.7). The junction is assumed to be an abrupt transition from Cu_2S to CdS with the tunnelling being entirely in the CdS forbidden gap.

For tunnelling through the conduction band spike the barrier height is the height of the spike E' above the Cu_2S conduction band edge. The width of the barrier δ is determined from the depletion width as

$$\delta = \left[\frac{\varepsilon}{2q(N_D-N_A)}\right]^{1/2} \left[V_D^{1/2} - (V_D - \frac{E'}{q})^{1/2}\right] , \qquad (2.8)$$

where V_D is the diffusion potential for the junction and (N_D-N_A) is the net ionized donor density in the CdS. Equation (2.8) assumes a step junction, an approximation which is probably reasonably valid for the cells before heat treatment. Putting d = δ and letting E = 0 in equation (2.7), the transparency of the conduction band spike is

$$T(E_c) = \exp\left\{-\frac{4}{3\hbar}\left[\frac{m^*\varepsilon V_B}{(N_D-N_A)}\right]^{1/2}\left[V_D^{1/2} - (V_D-V_B)^{1/2}\right]\right\} . \qquad (2.9)$$

For the case of band-to-band tunnelling, an exactly analogous treatment is followed. The barrier height is the Cu_2S band gap E_g plus the height of the conduction band spike E'. The barrier width is the width of the forbidden region at the Cu_2S valence band edge.

Since Zener breakdown is found to be important only at high field regions on the junction and the cell is reverse biased, the appropriate expression for δ is different from equation (2.8). The barrier transparency for Zener breakdown is

$$T(E_V) = \exp\left\{-\frac{4}{3\hbar}\left[2m^*(E_g + E')\right]^{1/2}\delta\right\} , \qquad (2.10)$$

where the barrier width δ is some function of the applied voltage and the net charge density in the depletion region.

If it is assumed that the tunnelling current is predominantly through the base of the barrier, the current density J is

$$J = B \exp\left[-\frac{4}{3\hbar}(2m^*qV_B)^{1/2}\delta\right] , \qquad (2.11)$$

where the coefficient B is a function of the density of states and the wavefunctions on either side of the barrier. Since these are not known, B will be assumed constant.

2.2 Diffusion Lengths

A light microprobe has been used to make direct measurements of the minority carrier diffusion lengths on both sides of the Cu_2S-CdS heterojunction. Since several geometries were used in the experiments, a brief analysis will be given for each of the conditions.

Excess carriers are injected into the semiconductor by generation of electron-hole pairs with a small light spot. The electron and hole densities are governed by the continuity equations and the equations

for electron and hole currents. Exact solution of these equations shows that the ambipolar diffusion constants are measured by any measurement of the excess carrier distribution away from the point of injection. The ambipolar diffusion equation for a homogeneous semiconductor is[50]

$$-\frac{p-p_o}{\tau_p} + D\left[\frac{n(d^2p/dx^2) + p(d^2n/dx^2)}{n+p}\right] = 0 , \qquad (2.12)$$

where the electric field is assumed to be zero. In this equation, D is the ambipolar diffusion constant given by

$$D = \frac{n+p}{(n/D_p) + (p/D_n)} , \qquad (2.13)$$

where D_p and D_n are the hole and electron diffusion constants. If the semiconductor is n-type and $n \gg p$, $D \simeq D_p$ the minority carrier diffusion constant, and equation (2.12) reduces to

$$D_p \frac{d^2p}{dx^2} - \frac{p-p_o}{\tau_p} = 0 . \qquad (2.14)$$

This result shows that as long as the injected minority carrier density $\Delta p = p-p_o$ is small compared with the majority carrier density, the approximate solutions obtained by solving the equation of continuity for minority carriers only is justified.

The simplest geometry involves one-dimensional flow from the light spot to a collector. The continuity equation for minority carriers is

$$\frac{dp}{dt} = G - \frac{\Delta p}{\tau_p} - \frac{1}{q}\underline{\nabla} \cdot \underline{J}_p , \qquad (2.15)$$

where G is the hole generation rate and τ_p is the minority carrier lifetime. The hole current density is

$$\underline{J}_p = q\mu_p p\underline{E} - qD_p\underline{\nabla}p \ . \qquad (2.16)$$

Substituting equation (2.16) into equation (2.15) and considering steady-state conditions in one dimension leads to

$$G - \frac{p}{\tau_p} - \mu_p E \frac{dp}{dx} - \mu_p p \frac{dE}{dx} + D_p \frac{d^2p}{dx^2} = 0 \ , \qquad (2.17)$$

where $p = p-p_o$ is assumed. For a small light spot, G is assumed zero everywhere except at x = 0. Also, since we are dealing with minority carriers, space charge neutrality is assumed so that equation (2.17) reduces to

$$-\frac{p}{\tau_p} + D_p \frac{d^2p}{dx^2} = 0 \ . \qquad (2.18)$$

Equation (2.18) has the solution

$$p = p_{x=0} \exp[-x/L_p] \ , \qquad (2.19)$$

where $L_p = \sqrt{D_p \tau_p}$ is the hole diffusion length. In the diffusion length experiments the heterojunction was used as a collector. The current collected by the junction is proportional to the hole density at the edge of the depletion region. Thus, a plot of the logarithm of photocurrent versus junction distance from the light spot should yield a straight line with slope = $-1/L_p$. This solution is a reasonable approximation for a planar collector some distance from the light source.

Another case of interest is the solution for a line source and a line collector both at the surface of the semiconductor.[51,53] The diffusion equation in cylindrical coordinates is

$$\frac{\partial^2 p}{\partial r^2} + \frac{1}{r}\frac{\partial p}{\partial r} - \frac{p}{D_p \tau_p} = \frac{1}{D_p}\frac{\partial p}{\partial t} , \qquad (2.20)$$

where r is the radial distance. Putting $(\partial p/\partial t) = 0$ and letting $x = (r/L_p)$, this equation becomes

$$\frac{d^2 p}{dx^2} + \frac{1}{x}\frac{dp}{dx} - p = 0 . \qquad (2.21)$$

The solution to equation (2.21) is

$$p = p_o \frac{iH_o^{(1)}(ix)}{iH_o^{(1)}(ix_o)} , \qquad (2.22)$$

where p_o is the hole density at the small radius r_o equal to the width of the light line, and $iH_o^{(1)}(ix)$ are Hankel functions. The diffusion current density is

$$J_p = \frac{qD_p p_o}{L_p} \cdot \frac{-H_1^{(1)}(ix)}{iH_o^{(1)}(ix_o)} . \qquad (2.23)$$

The Hankel functions $iH_o^{(1)}(ix)$ and $-H_1^{(1)}(ix)$ have been tabulated.[54] The diffusion length is determined from the slope, at some point r, of the logarithm of photocurrent versus r from

$$L_p = \frac{iH_o^{(1)}\ (i\ r/L_p)}{H_1^{(1)}\ (i\ r/L_p)} \frac{1}{(\text{slope})_r} \quad . \tag{2.24}$$

The exact dependence on source distance of current collected at a planar junction perpendicular to the surface from a parallel line source on the surface is given by van Roosbroeck[52] including the effect of surface recombination. The solutions are presented graphically in a dimensionless form in van Roosbroeck's paper and will not be reproduced here. For surface recombination velocity s = 0, the solution is exactly given by equation (2.19) above. When the reduced surface recombination velocity S = sL/D is finite the solution peaks as the source approaches the collecting junction. For S = 1, the exponential solution of equation (2.19) is a good approximation for source distances from the junction greater than three times the diffusion length.

One other geometry that must be considered is that applicable to angle-lapped junctions.[55,56] Calculation of collection efficiency in this case uses the results of Loferski and Wysocki[57] who analyzed the short-circuit photocurrent for monochromatic radiation including the effects of absorption coefficient, surface recombination, and diffusion lengths. When this theory is applied to the case of highly absorbed light incident on the surface of a thin layer of semiconductor parallel to a collector junction a distance y below the surface, the collection efficiency, Q reduces to

$$Q = \left[\frac{sL}{D} \sinh\left(\frac{y}{L}\right) + \cosh\left(\frac{y}{L}\right)\right]^{-1} \quad . \tag{2.25}$$

The asymptotic form of this solution for y > L is

$$Q = \frac{2}{1+(sL/D)} \exp(-y/L) \quad . \tag{2.26}$$

For the bevel angle geometry the thickness of the layer y varies with distance from the intersection of the junction plane and the surface. The collection efficiency becomes

$$Q = \frac{2}{1+(sL/D)} \exp\left[-\frac{x\sin\theta}{L}\right] , \tag{2.27}$$

where x is the distance of the source from the intersection of the junction plane and the surface, and θ is the angle the junction plane makes with the surface. The conditions necessary for equation (2.27) to be valid are: (1) $\alpha >> 1/L$, (2) $\alpha >> s/D$, and (3) $y > L$. Here α is the absorption coefficient and y is the thickness of the layer.

III. EXPERIMENTAL

3.1 Cell Fabrication

The major part of this investigation was carried out on heterojunctions formed on single crystals of CdS, which had high conductivity (0.3 to 50 Ω-cm) due to excess cadmium. The crystals were purchased from Clevite Corporation and in most cases were used as-grown. Some of the purchased crystals were high resistivity material. These were annealed in cadmium vapor for several days at 900°C to increase their conductivity. Several cells were also made from an as-grown high conductivity CdS crystal grown in this laboratory.[58] Apart from series resistance variations, no differences were noted in cell characteristics due to the various sources of CdS crystals. The crystal orientations were determined from Laue patterns[59] and then samples with dimensions of about 1.5 mm by 5 mm by 0.5 mm were cut from the larger crystals. The samples were cut so that the c-axis was perpendicular to the surface on which the heterojunction was to be formed. Exceptions to this orientation were the cleaved crystals. Good cleavage planes for CdS are the prismatic planes making the c-axis lie in the plane of the junction.

The two large area surfaces of the samples were polished using 0.3 micron alumina to obtain a reasonably good optical finish. The samples were then masked and the regions where contacts to the CdS

were to be made were etched in dilute (15 - 20%) HCl solution. Indium contacts were vapor deposited on the etched regions and fine copper wires were indium soldered to the contacts. During the soldering process sufficient indium diffusion takes place to ensure formation of ohmic contacts. At this stage contacts were checked for ohmic behavior by verifying that the V-I characteristics were linear over a wide voltage range.

The treatment of the surface on which the heterojunction was to be formed varied depending on the nature of the experiments to be carried out. Whenever possible the surface was lightly etched to remove polishing damage. For this purpose an optical quality etchant[60] was used consisting of an approximately 0.3 molar solution of $KMnO_4$ in concentrated H_2SO_4. Etching was carried out for 2 minutes at room temperature. Because etching developed surface roughness which resulted in non-planar junction interfaces, most of the angle-lapped junctions were not etched. Since surface damage was expected to penetrate only one or two microns, and the surface layer converted to Cu_2S was generally about 5 microns thick for these samples, it was felt that the original surface damage would be unimportant.

The Cu_2S-CdS heterojunctions were formed by a dipping process in an aqueous solution containing copper ions in the cuprous state. A saturated solution of CuCl in distilled water was used. Hydroxyl amine hydrochloride was added to the solution, and sufficient HCl was added to adjust the pH to about 3.0, in order to reduce all the copper to the Cu^{2+} state. Various temperatures between 70°C and 100°C were used for dipping. Duration of the dipping process varied

depending on desired Cu_2S layer thickness, CdS orientation, temperature of the bath and surface treatment. In most cases, dipping times between 1 minute and 2 hours were used.

After dipping, ohmic contacts were made to the Cu_2S with evaporated gold or with silver paint. Copper wires were then attached using silver paint. Samples which were to be angle-lapped for light microprobe measurements were mounted on a bevelled polishing block and lapped to the desired bevel angle using 0.3 micron alumina.

After dipping to form the heterojunction, heating of the cells was avoided until preheat treatment characteristics of the cells had been measured. Lapping procedures required potting the samples, for which purpose a low melting point (65°C) glass (glycol phthalate) was used. Since the temperature during potting was lower than the temperature of the solution in the dipping process, this was not considered a significant heat treatment. Many of the cells were heat-treated to compare their characteristics before and after short annealing times. The heat treatments were short times (10 seconds to 5 minutes) at 250°C in air.

Where possible, results obtained on single crystal cells were compared with the characteristics of an evaporated polycrystalline cell. The thin film cell was a standard 50 cm^2 cell supplied by L. Shiozawa of Clevite Corporation. These cells have been heat treated during fabrication for about 1 minute at 250°C in air. Since measurements on such a large area cell were not convenient, small cells were obtained by cutting up the larger cell.

3.2 Sample Properties

In order to facilitate discussion of experimental results the properties of cells specifically referred to appear in Table 3.1.

Table 3.1

Properties of Cu_2S-CdS Cells Referred to in the Experiments.

Cell	Surface	ρ_{CdS} (Ω-cm)	Dipping Process	Geometry
#1	polished ⊥c etched	1.1	5 min 80°C	no bevel
#2	cleaved //c	1	1 min 100°C	no bevel
#3	polished ⊥c	1.9	1 hour 95°C	-5°
#4	polished ⊥c etched	54	1 hour 75°C	+5°
#5	polished ⊥c	1	2 hours 90°C	-5°
#6	polished ⊥c	0.3	1 hour 90°C	-2°
#7	cleaved //c	1	1 min 95°C	cleaved @ 90°, ⊥ to junction plane
#8	polished ⊥c	0.6	2 hours 95°C	-5°
#9	polished ⊥c	0.8	15 min 90°C	+5°
#10	polished ⊥c	54	2 hours 75°C	-5°

In Table 3.1, the convention of Davies and Gentry[61] is used in defining positive and negative bevel angles. For a positive bevel angle, the acute angle is between the junction plane and the CdS surface. For a negative angle, the acute angle is between the junction plane and the Cu_2S surface.

3.3 General Measurements

To avoid confusion between two kinds of V-I characteristics obtained with light incident on the sample, the following nomenclature will be adhered to throughout this thesis: "V-I characteristics under illumination" will refer to experiments in which an external voltage is impressed on the sample; "light V-I characteristics" will refer to the characteristics obtained by varying the load resistance across the cell with no external voltage supply in the circuit.

Voltage-Current (V-I) Characteristics

The rectifying properties of the heterojunctions were determined from dark V-I characteristics using a Tektronix 575 curve tracer with a polaroid camera attachment to photograph the characteristics. V-I characteristics were also obtained under strong illumination with a focussed microscope illuminator and various Corning glass filters as the light source. The filter combinations most commonly used were a 2-64 filter which passes wavelengths longer than 6500 A, a 1-69 filter which passes only wavelengths shorter than about 10,000 A, and a 1-69 + 4-96 combination which passes a band between 3600 A and 6000 A. The characteristics of major interest in these measurements

were the cell series resistance in the light and dark, the reverse breakdown in the dark and under various illuminations, and the magnitudes of the photocurrent and photovoltage. The cell series resistance was determined from the slope of the V-I characteristic at high forward currents.

On many of the cells V-I characteristics in the dark and under illumination were also obtained from point-by-point measurements. In these measurements, voltages were impressed across a cell and a small resistor in series. A Keithley 610 A electrometer was used to measure the applied voltage, and a Keithley 149 microvoltmeter across the small resistor was used to measure the current.

Capacitance-Voltage (C-V) Characteristics

The measurement of junction capacitance as a function of applied bias voltage is a standard technique for determination of depletion widths, junction doping profiles and diffusion potentials. The heterojunctions being investigated usually have much higher conductances than do good semiconductor p-n junctions and Schottky barriers. However, useful and reliable data were obtainable on most samples by careful attention to the geometry so as to keep the series resistance very small and the conductance within the limits of the capacitance bridge. A Boonton 75D capacitance bridge operating at 1 MHz was used. The signal level was maintained at less than 20 mvolts. An external dc voltage bias supply was used.

Spectral Response

Spectral response measurements were made using a Bausch and Lomb 500 cm grating monochromator with a tungsten-ribbon light source. The monochromator slits were set at 2 mm to give a band pass of 130 A. The output of the monochromator was focussed on the samples to give maximum intensity. Calibration of the light intensity at the sample holder was made with a Perkin-Elmer thermopile. Data were normalized to the intensity measured at 9000 A which was 300μwatt/cm^2 ± 20 percent. The accuracy of this absolute intensity measurement was verified using a calibrated Si photocell.[62]

The short-circuit photocurrent responses were measured using a Keithley 149 microvoltmeter across a small resistor (10 to $10^4\Omega$) in series with the sample. Measured voltages were always kept under 1 millivolt so that short-circuit conditions were well approximated. Measurements of open-circuit photovoltage were made with a Keithley 410 A electrometer having an input impedence of 10^{14} ohms.

Light V-I Characteristics

The measurement of the photocurrent and photovoltage developed across a variable load resistance generates the light V-I characteristic. For these measurements a series circuit consisting of the sample, a small resistor (10Ω) and a variable load resistor was used. Photocurrent was measured across the small resistor using the Keithley 149 and photovoltage was measured across the sample with the Keithley 410 A. The light source for these experiments was tungsten radiation through the monochromator with the grating acting as a mirror. For

one sample direct sunlight was used to check the approximate solar conversion efficiency of these cells.

Temperature Dependence

The temperature dependence of the V-I characteristics was measured from 113°K to 373°K. An Air Products Inc. cryotip system was used to make low temperature measurements. In this system, cooling is by the Joule expansion of nitrogen gas through a porous plug. The low-temperature measurements were made with the sample in vacuum. High temperature measurements were made with the sample in a dry nitrogen ambient. Dark V-I characteristics were obtained point-by-point using the technique described above. The Tektronix 575 curve tracer was also used to obtain photographs of the V-I characteristics in the dark and under strong illumination at several temperatures.

3.4 Secondary Light Experiments

Investigations of the sample response to a primary light source while under illumination by a secondary (bias) light source were carried out using three different methods.

(1) The spectral response of the short-circuit photocurrent due to the primary radiation was measured with and without secondary illumination on the sample. The primary light source was light from the monochromator and the secondary source was a microscope illuminator operated from a regulated dc power supply. Interference filters or Corning glass filters were used to obtain the desired wavelengths of secondary light. The experimental procedure was to turn on the

secondary source, eliminate the photocurrent caused by the secondary light using the zero offset of the Keithley 149, then measure the response due to the primary light in the usual manner.

(2) The effect of varying the secondary wavelength on the short-circuit-current response to a fixed primary light signal was measured. The apparatus used is shown schematically in figure 3.1. The primary source was a microscope illuminator and a suitable narrow bandpass interference filter. This light was chopped at 114 Hz by a rotating slotted disc. The secondary light source was the output of the B & L monochromator. A parallel path for short-circuit photocurrent was provided so that the chopped signal had a low impedence path (170Ω) through the input of the Type B preamplifier of a Princeton Applied Research HR-8 Lock-in Amplifier. The dc signal due to the secondary light was provided with a higher impedance path still sufficiently small that short-circuit conditions were maintained.

(3) The sample was illuminated with the secondary light for a short interval followed by a variable delay time in the dark. The transient response to primary radiation was then measured. For these experiments the B & L monochromator was used as both primary and secondary light sources. The sample was illuminated with the desired secondary wavelength for a short time, then a shutter was closed and during the dark interval the monochromator was reset to the primary wavelength. The short-circuit photocurrent due to the primary radiation was measured with the Keithley 149 across a small resistor. The output of the Keithley was recorded on a Moseley X-Y recorder as a function of time. The response time of the system was about 0.25 seconds.

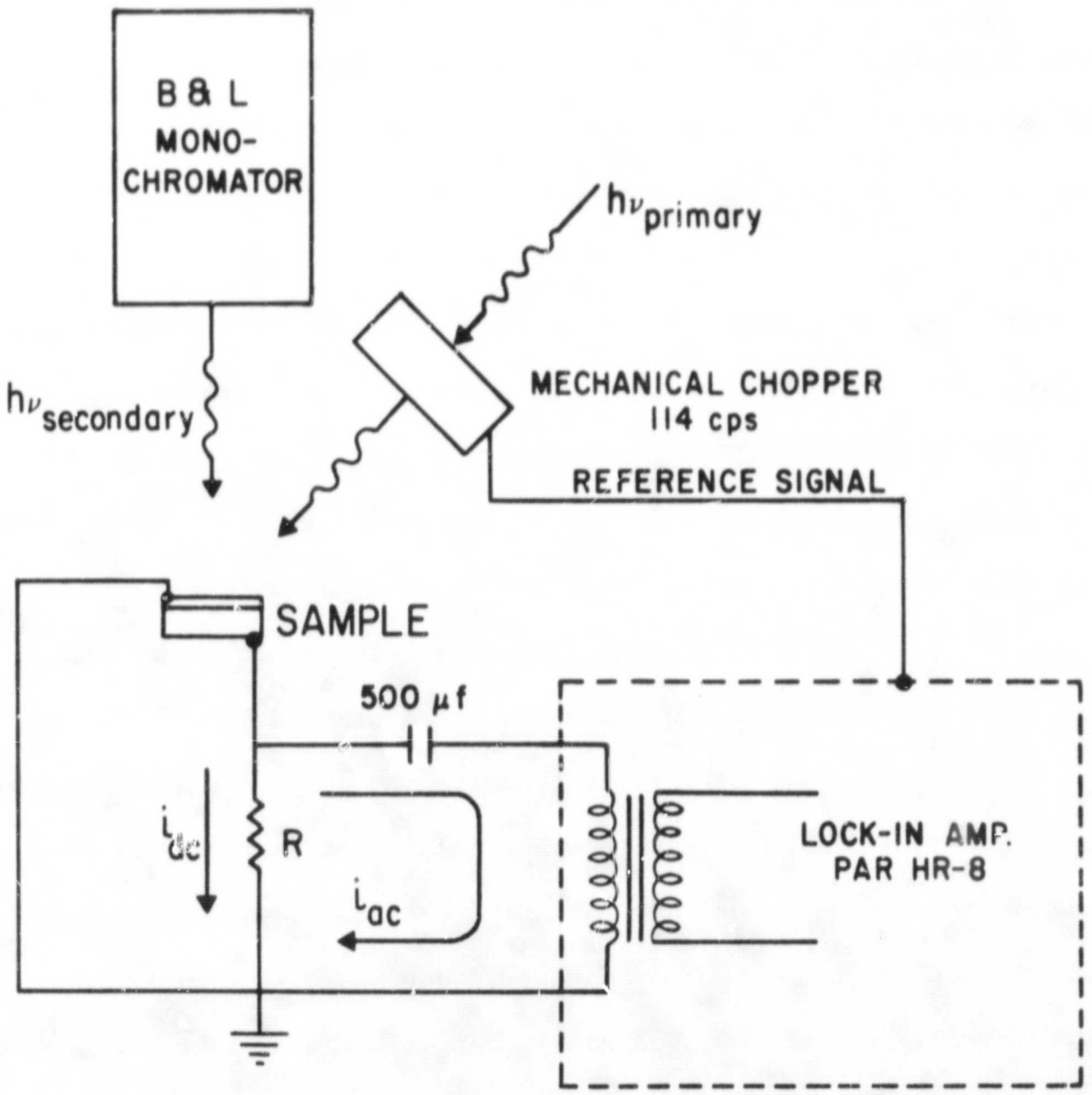

FIGURE 3.1: SCHEMATIC OF THE APPARATUS FOR BIAS LIGHT EXPERIMENTS WITH CHOPPED PRIMARY LIGHT.

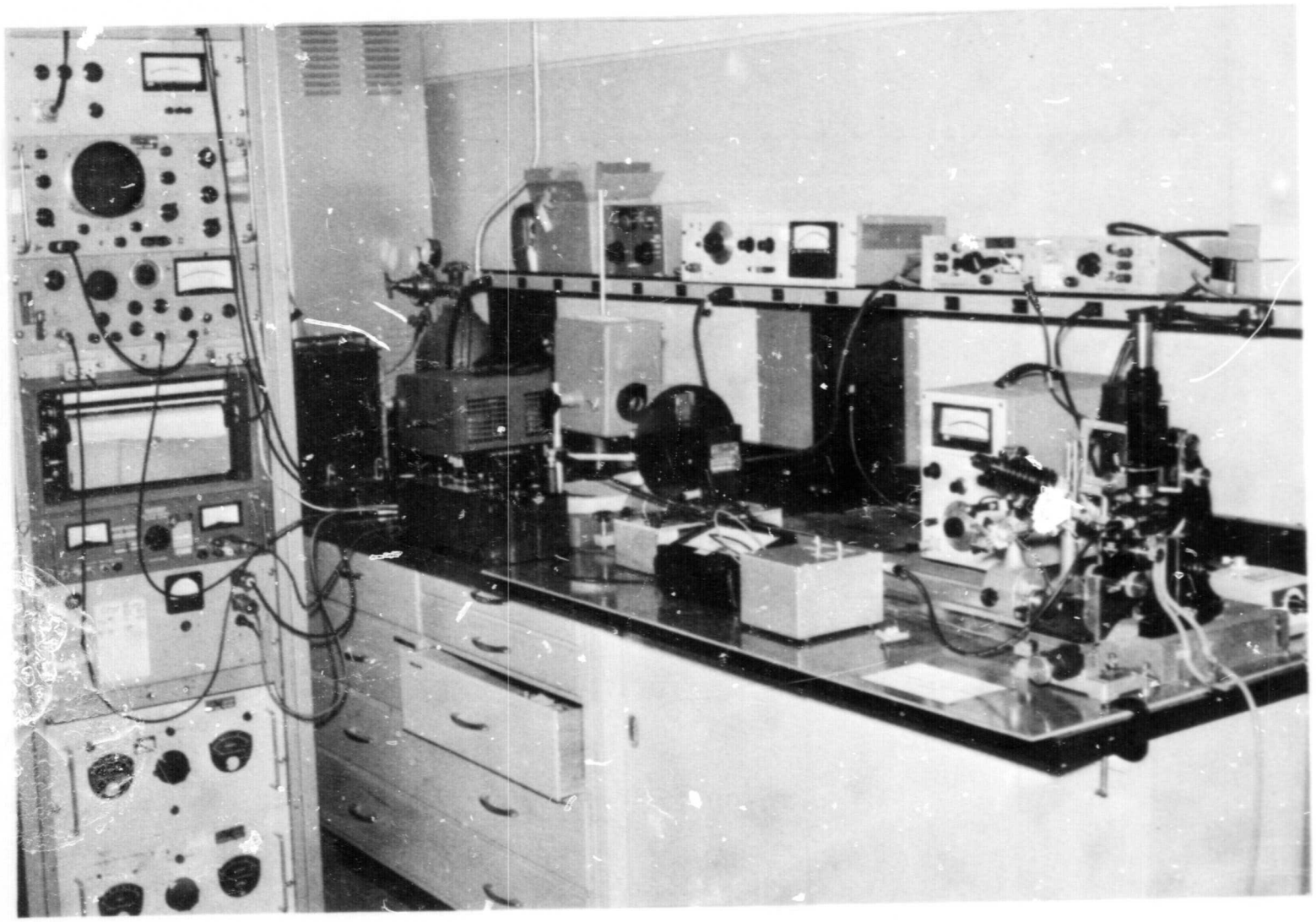

FIGURE 3.2: PHOTOGRAPH OF THE LIGHT MICROPROBE APPARATUS.

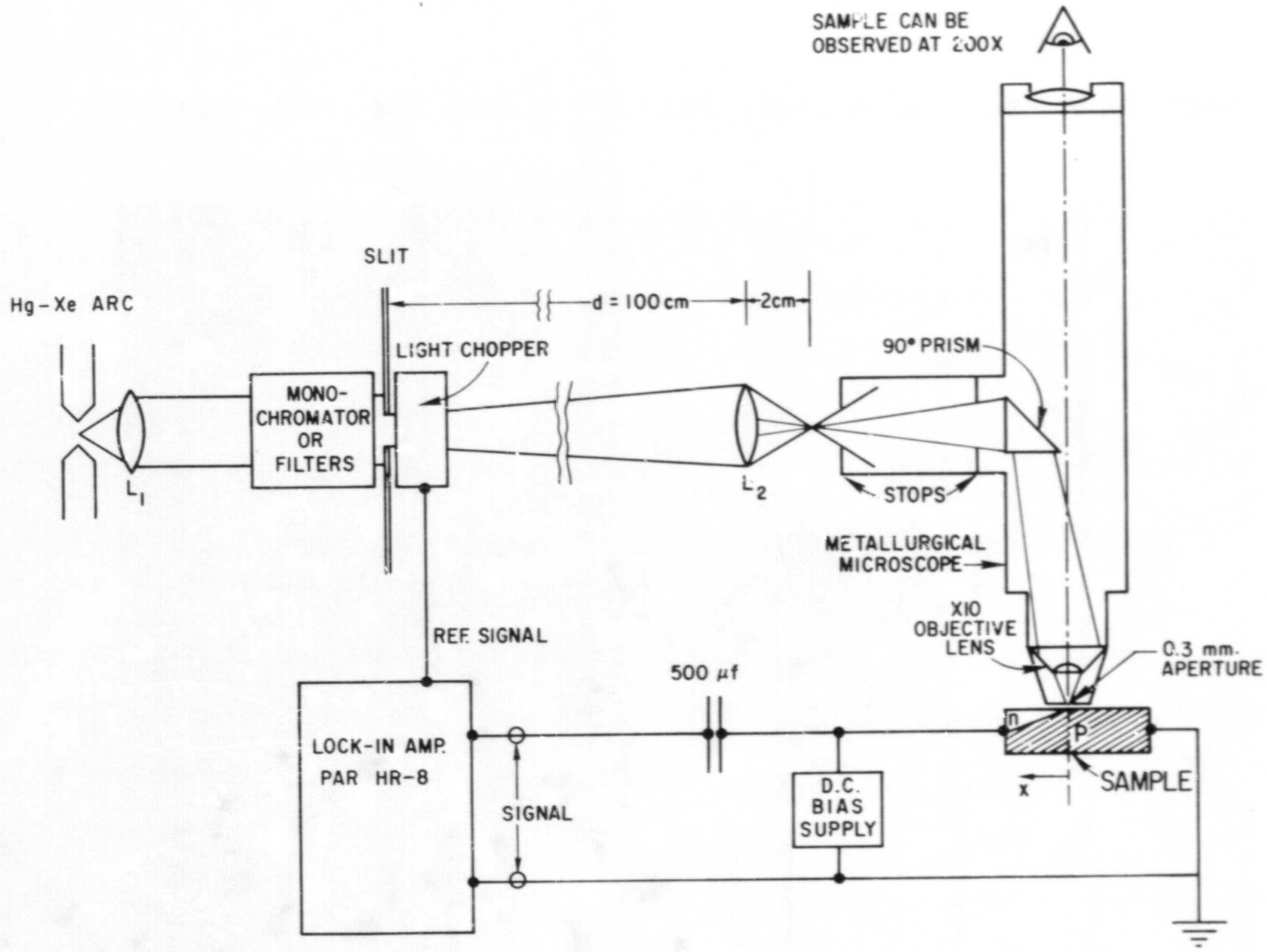

FIGURE 3.3: SCHEMATIC DIAGRAM OF THE LIGHT MICROPROBE.

3.5 Light Microprobe Description

A light microprobe was designed and built to allow investigation of photoresponse across the junction on a microscopic level.[56,63] The system was used to measure minority carrier diffusion lengths, spectral response across the junction, uniformity of response along the junction, and V-I characteristics under illumination as a function of position of the injected carriers. A photograph of the light microprobe apparatus is shown in figure 3.2, and a schematic diagram of the light microprobe is shown in figure 3.3. The collimated beam of a 200 watt Hg-Xe arc is passed through a monochromator or suitable Corning glass filters and illuminates a slit 0.4 mm wide by 10 mm long. The light passing through the slit is mechanically chopped at 114 Hz, passes through lens L_2, and into the side port of a metallurgical microscope. The light is totally reflected by a 90° prism and imaged on the sample by the microscope objective lens. The size of the image is determined by the focal length of the microscope objective and for a given lens L_2 by the distance d from the slit to L_2. As the prism only obscures half the microscope field the sample can be viewed through the microscope in the usual way. To keep the beam divergence angle as small as possible a long focal length objective (10.25 mm) is used. The slit is reduced a factor of 50 by lens L_2 and another factor of 10 by the objective for an overall demagnification of 500X. Thus a line image is formed on the sample 20 microns long by 0.8 microns wide. The width of the image is very near the theoretical resolution limit which for 5000 A light is 0.6 microns. To further decrease the light spot would require a larger aperture objective lens resulting

in a divergence angle ≈90° making focussing extremely critical. The sample is held on a mount which can be rotated to make the projection of the junction plane parallel to the line image. The entire shielded sample holder is mounted on a calibrated precision motion which allows accurate positioning perpendicular to the line image to better than ±0.5 micron. Motion in the two other orthogonal directions is made with a standard micromanipulator.

The photocurrent generated in the sample is detected by a Princeton Applied Research HR-8 Lock-in Amplifier using a low input impedance (100Ω) Type B preamplifier. A reference signal from the light chopper is also fed into the lock-in amplifier. Signal currents as small as 10^{-11} amp can be measured with reasonable signal-to-noise ratios, which is found to be adequate sensitivity for the photocells being measured.

External bias voltage can be applied to the sample from a battery power supply. A large capacitor (500 μf) in the circuit is used to block dc currents from passing through the lock-in amplifier.

Attenuation of scattered light, i.e. light incident on the sample outside the line image, is necessary for diffusion length measurements where it is desirable to detect a decrease by at least two orders of magnitude in the collected photocurrent. Scattering of light is due to imperfect optical elements, multiple reflections in the light path, reflections from the sample surface reflected back to the sample from the objective lens, and scattering by surface roughness. Aperture stops must be used with care since the resolution limit decreases with decreasing aperture. The most serious scattering problem was reflected

light from the semiconductor surface being reflected back from the objective lens. This scattering was reduced severalfold by a 0.3 mm diameter aperture just above the surface of the sample (see figure 3.3).

3.6 Light Microprobe Measurements

Diffusion Lengths

Because the diffusion lengths in the system Cu_2S-CdS were expected to be small, the angle-lapped junction method for measuring diffusion lengths was used. Fig. 3.4(a) shows the geometry of the samples for this experiment. The bevel angle θ was chosen to give maximum spatial resolution to the experiment keeping in mind that at very small angles interface roughness becomes a serious problem. In the angle-lapped method highly absorbed light must be used. Minority carriers created very near the surface diffuse in the y-direction to the edge of the space-charge region where they are collected by the field across the junction. Moving the light spot in the x-direction results in a corresponding increase in the distance y measured normal to the junction by the amount

$$y = x \sin \theta \ . \qquad (3.1)$$

Since the number of carriers reaching the space-charge region is proportional to exp[-y/L] (see equation (2.26)), where L is the ambipolar diffusion length and the decrease in light intensity is

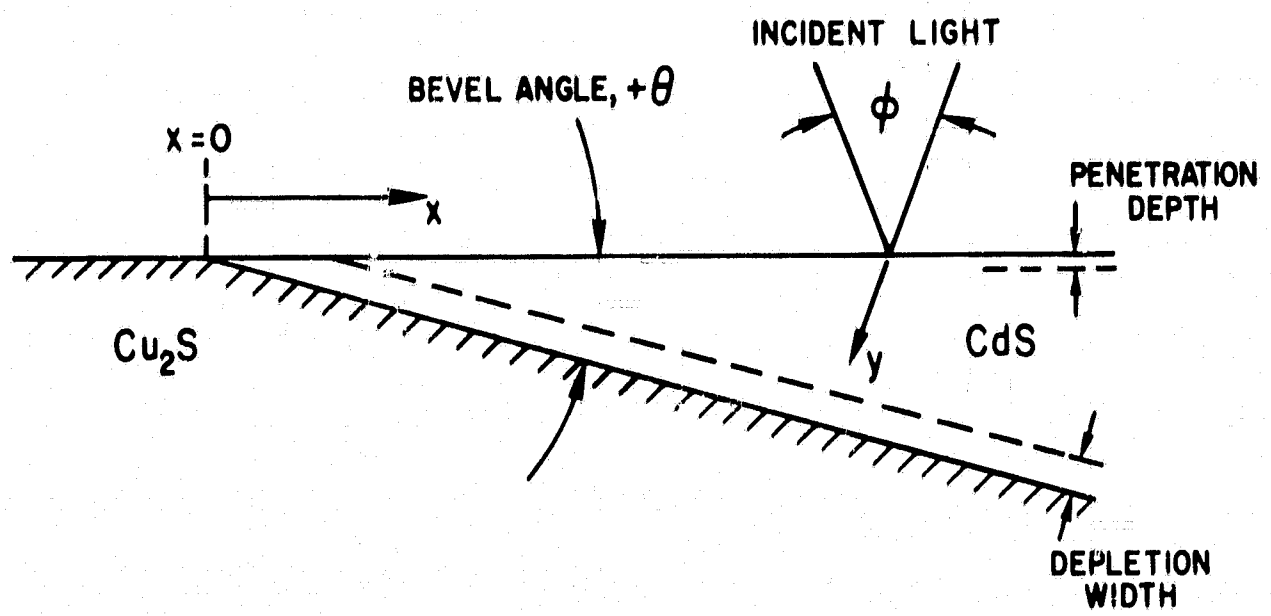

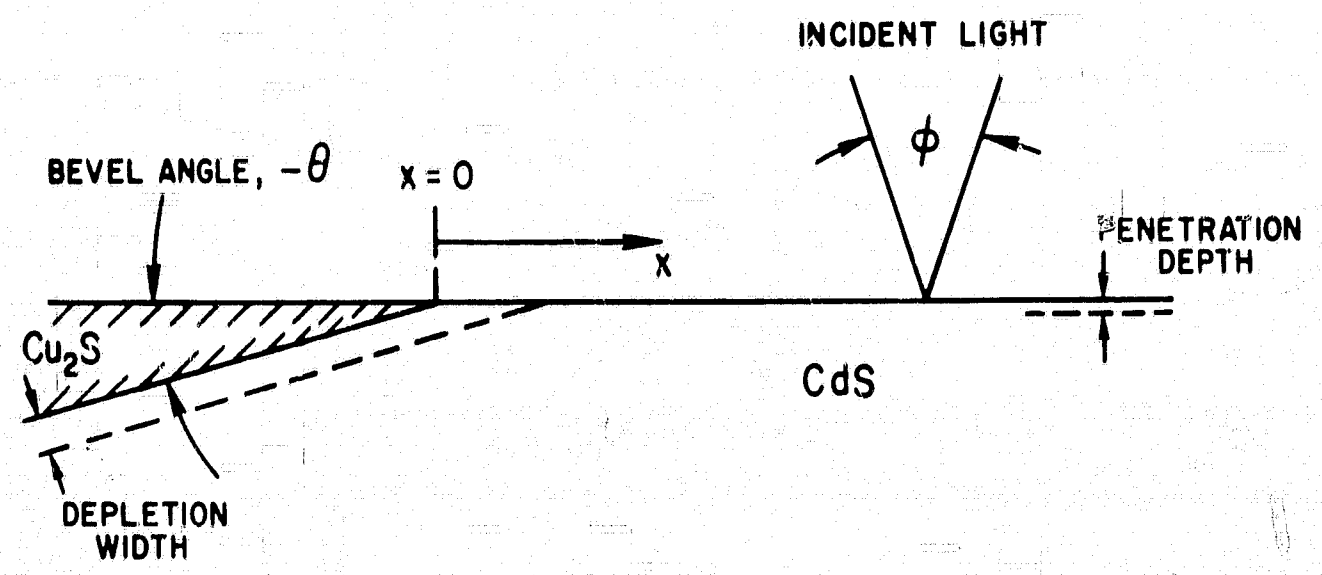

FIGURE 3.4: GEOMETRY OF THE ANGLE-LAPPED JUNCTIONS FOR POSITIVE AND NEGATIVE BEVEL ANGLES.

approximately given by

$$I = I_o \exp[-\alpha y] \ , \qquad (3.2)$$

the ultimate limit on diffusion lengths which are measurable depends on the absorption coefficient. For CdS the maximum absorption coefficient ($\lambda \leq 4800$ A) is 8.5×10^4 cm^{-1}.[64] Since to measure the diffusion length by this method requires $\alpha \geq 1/L_p$ we see that the minimum measurable diffusion length in CdS is

$$(L_p)_{min} \simeq 3\left(\frac{1}{\alpha_{max}}\right) = 3.6 \times 10^{-5} \text{ cm} \ .$$

For a 5° bevel angle, a motion of 4 microns in the x-direction would correspond to $(L_p)_{min}$ in the y-direction. As the sample could be positioned to within 0.5 microns, a 5° angle was used. A few samples were also bevelled at 2° when examining the Cu_2S side of the junction. Because of the higher absorption coefficient at short wavelengths of Cu_2S the minimum measurable diffusion length L_n is about 1.5×10^{-5} cm.

Corrections for scattered light were made on the experimental curves when the collected photocurrent had decreased by 1.5 to 2 orders of magnitude. The contribution of scattered light was determined in two ways: (1) the response curve measured at large distances from the junction was extrapolated into the junction region and this current was subtracted from the steeper response curve near the junction; (2) the light spot was scanned parallel to the edge of the crystal but just of the surface. The measured photocurrent was then equal to one-half the scattering contribution for the spot incident on the sample away from any edges. The two measurements of the photocurrent due to

scattered light were in good agreement on several samples, so the first method was adopted for all the measurements. The good agreement between the two methods indicates that reflections from the sample surface were not an important source of scattered light. In general, the corrections made to the data were only significant at distances from the junction equal to 3 to 4 times the diffusion length and therefore were not a serious source of error.

Spectral Response Across the Junction

The light microprobe was used to measure the spectral response at various positions across the interface. Since the major interest was to determine the contribution of the CdS side to the long wavelength response, a cell with a -5° bevel angle was used. A monochromator was placed in the light beam of the light microprobe and spectral response curves were obtained for various positions of the light spot relative to the Cu_2S-CdS interface.

Photocurrents Under Applied Bias Voltage

The effects of applied bias voltage on the photocurrent were investigated. The measurements were similar to those used for diffusion length measurements except that a dc bias voltage was now applied across the sample. Measurements were made keeping the bias voltage fixed and varying the position of the light probe relative to the interface, and keeping the light probe position fixed and varying the bias voltage. In addition, variations in the photocurrent along the interface were measured by scanning a 2μ x 2μ light spot parallel to

the junction. The latter measurements were made with and without reverse bias applied.

IV. RESULTS: MACROSCOPIC STUDIES OF THE HETEROJUNCTION PROPERTIES

In this chapter, experimental results pertaining to the entire junction area of samples are presented. Experimental results obtained with the light microprobe and various surface effects are discussed in the following chapter.

4.1 V-I Characteristics

General Features

The V-I characteristics of cell #1 before any heat treatment are shown in figure 4.1 for T = 295°K and T = 132°K. The forward characteristics show a slight crossover of the light and dark curves occurring at small forward currents. Under strong illumination an open circuit photovoltage of 0.42 volts is developed. The reverse characteristics, however, are quite unusual. In the dark, a "soft" reverse breakdown is observed, but reverse current is less than 1μamp out to -3 volts. Strong long wavelength illumination (λ>6800 A) generates an appreciable photocurrent which has the normal effect of displacing downward the V-I characteristic by an amount equal to the photocurrent. Illumination with light containing wavelengths equal to or shorter than the CdS bandgap initiates reverse breakdown at about -0.4 volts. This effect makes reversed-biased junctions extremely sensitive to short

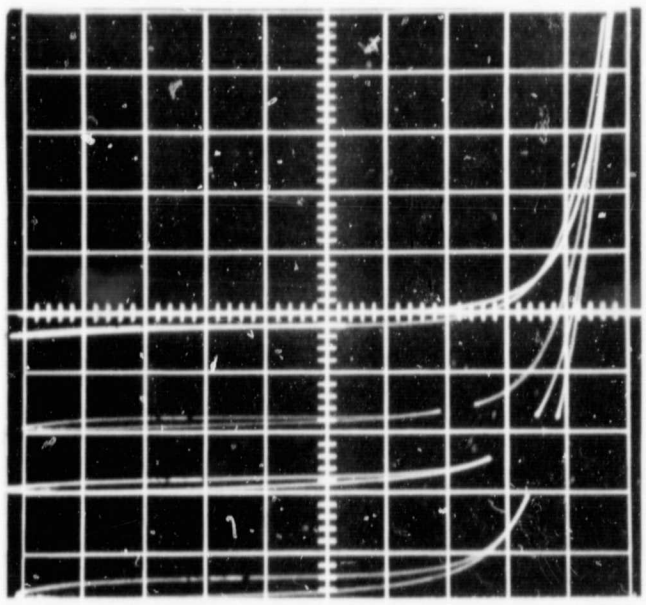

(a) T = 295 °K
VERT. = 0.1 ma/div
HORIZ. = 0.1 v/div

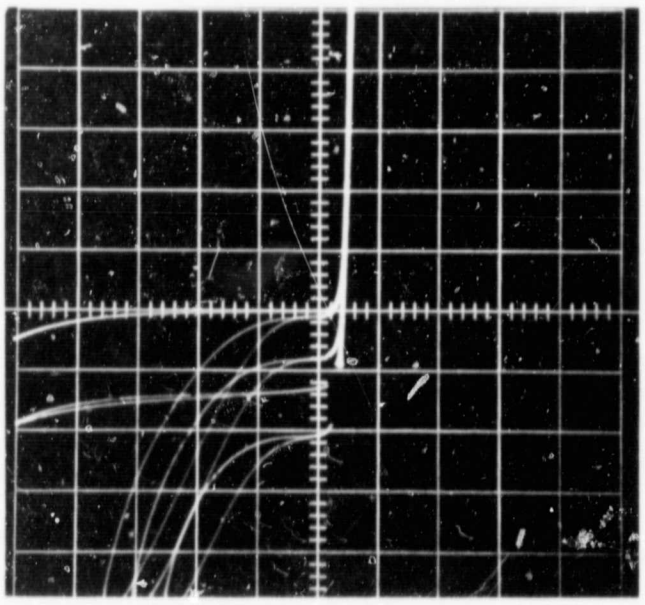

(b) T = 295 °K
VERT. = 0.2 ma/div
HORIZ = 1.0 v/div

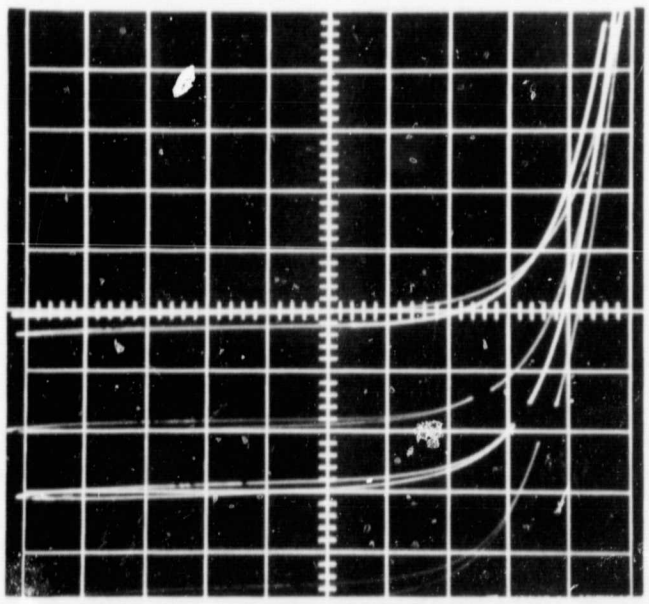

(c) T = 132° K
VERT. = 0.1 ma/div
HORIZ. = 0.1 v/div

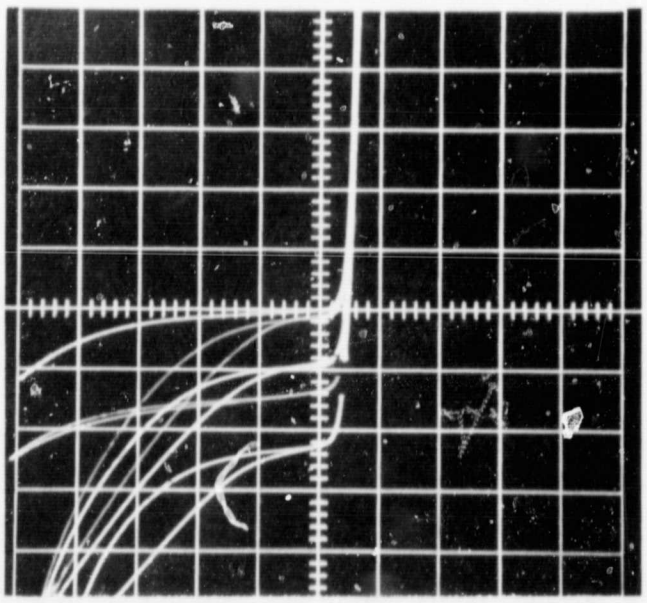

(d) T = 132 °K
VERT = 0.2 ma/div
HORIZ. = 1.0 v/div

FIGURE 4.1: V - I CHARACTERISTICS OF CELL # 1 BEFORE HEAT TREATMENT. ILLUMINATION CONDITIONS IN ORDER OF INCREASING SHORT-CIRCUIT CURRENT WERE (1) DARK, (2) 3000A < λ < 6000A, (3) 3000A < λ < 10000A, (4) λ > 6500A, (5) UNFILTERED TUNGSTEN RADIATION.

wavelength radiation since the light-induced breakdown is in effect a photocurrent gain process. The observed breakdown is nondestructive. Comparison of the characteristics at the two temperatures shows relatively minor differences. The series resistance of the cell, measured from the forward V-I characteristics, increased with cooling from 8Ω to 30Ω. The dark reverse current increased and the light-induced breakdown current decreased slightly. Little effect of cooling is seen on the photovoltage or photocurrent.

The V-I characteristics of the same cell after heat-treatment for 1 minute at 250°C in air are shown in figure 4.2. In the forward direction the dark current has decreased drastically. Illumination (with the same light as before heat treatment) causes very large increases in the forward current resulting in anomalous forward characteristics in which $I_{light} > I_{dark}$. Long wavelength light is much less effective in this regard. In the reverse direction, the dark current remains less than 1 μamp out to -6 volts and the short wavelength light-induced breakdown is almost negligible. The short-circuit photocurrents are generally reduced, reflecting a drastic decrease in long wavelength response. Open-circuit photovoltages increase slightly to about 0.48 volts. Even though the photocurrent generated by the long wavelength radiation is negligible, the V_{oc} generated by this same light is 0.44 volts. At lower temperatures V_{oc} increases to about 0.6 volts.[65] Some of the V-I characteristics before and after heat treatment have been replotted in figure 4.3 for easier comparison.

It was noticed that after heat treatment the forward characteristic in the dark showed transient behavior after short wavelength

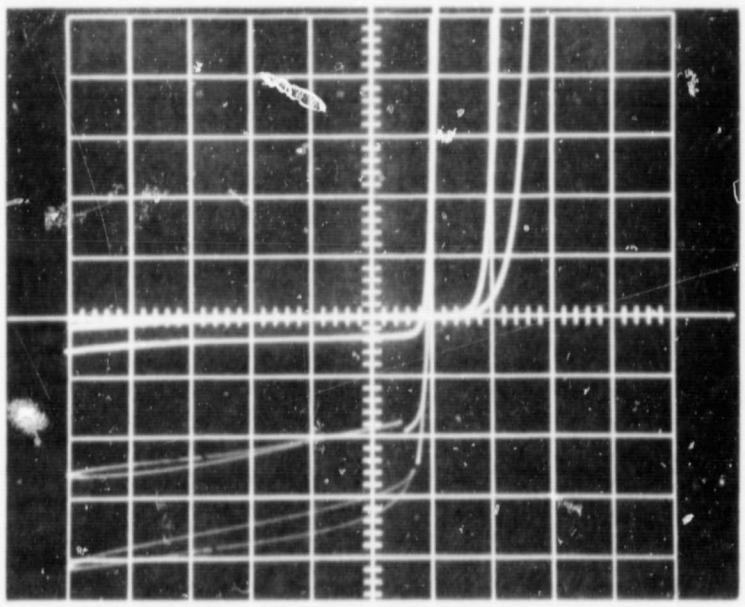

(a) T = 288 °K

VERT. = 0.05 ma/div

HORIZ. = 0.5 v/div

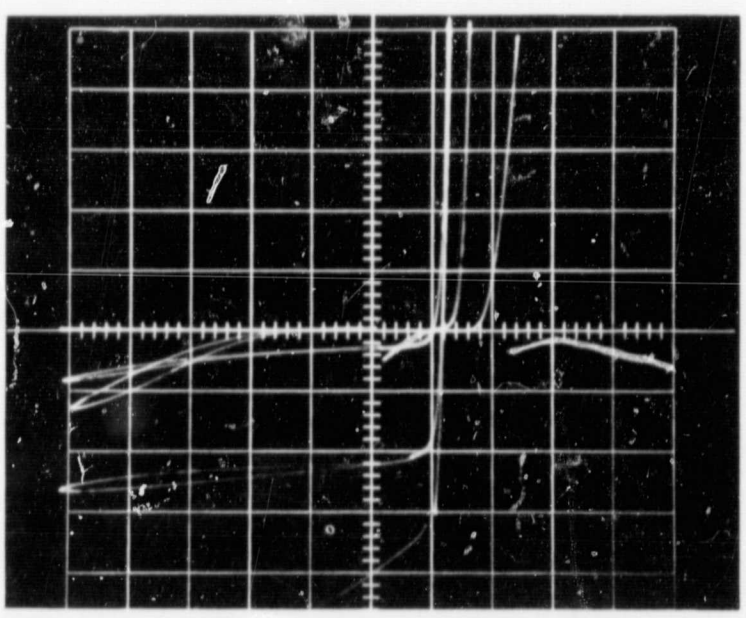

(b) T = 113 °K

VERT. = 0.05 ma/div

HORIZ. = 0.5 v/div

FIGURE 4.2: V-I CHARACTERISTICS OF CELL # 1 AFTER 1 min. AT 250°C IN AIR. ILLUMINATION CONDITIONS IN ORDER OF INCREASING SHORT-CIRCUIT CURRENT WERE (1) DARK, (2) $\lambda > 6500$ A, (3) 3000 A $< \lambda <$ 6500 A, (4) 3000 A $< \lambda <$ 10000 A (5) UNFILTERED TUNGSTEN RADIATION.

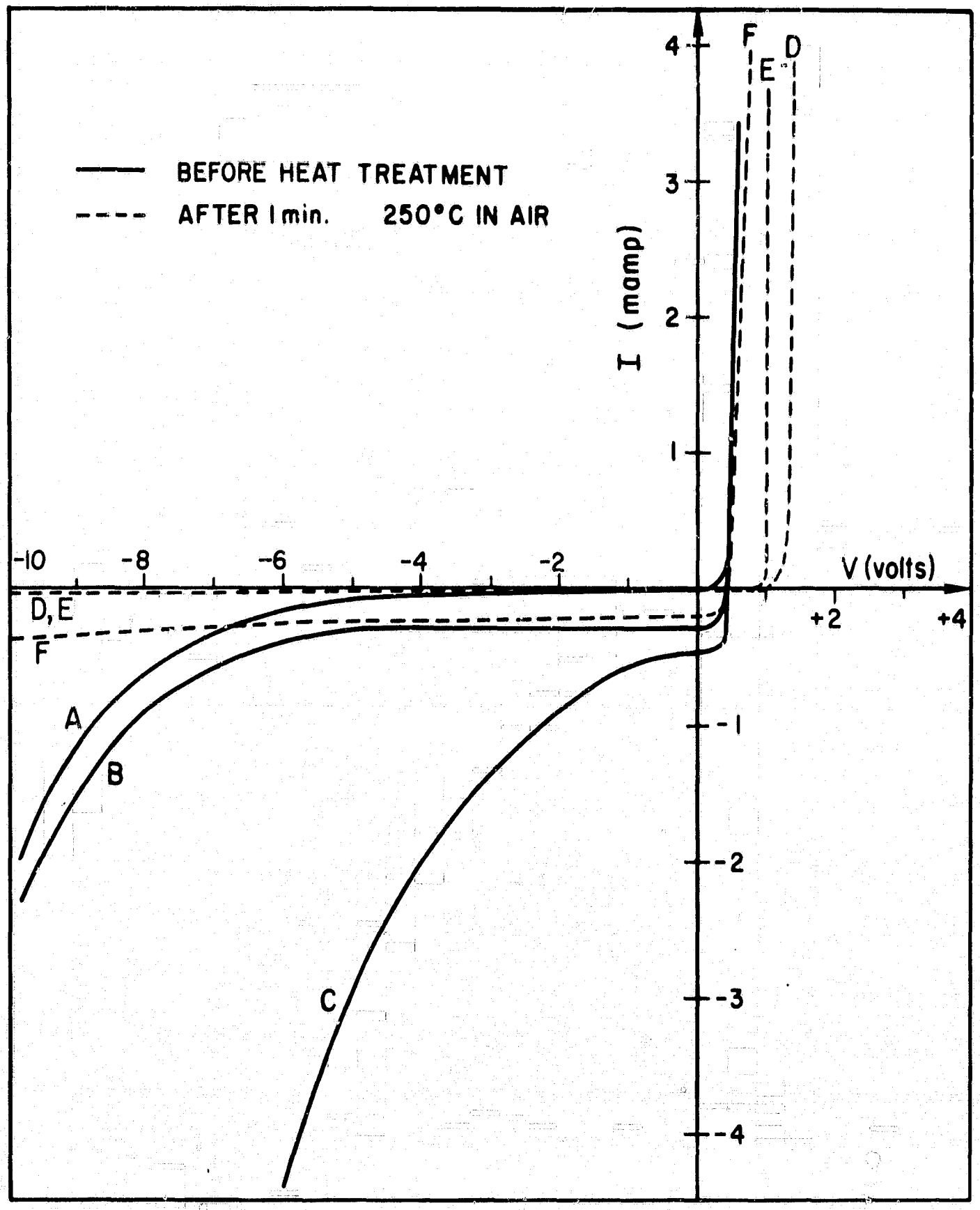

FIGURE 4.3: V - I CHARACTERISTICS OF CELL # 1 BEFORE AND AFTER HEAT TREATMENT. CURVES A and D ARE THE DARK CHARACTERISTICS, B and E ARE FOR RED ILLUMINATION (A >6800A), AND F and C ARE FOR WHITE ILLUMINATION.

illumination. As the forward bias was slowly increased the dark current was observed to decrease until a stable dark V-I characteristic was formed. The time required to reach this stable characteristic varied directly as the magnitude of forward current.

The main features of the V-I characteristics described above are fairly typical of those measured on all the more efficient cells.

Temperature Dependence of the Forward Characteristics

The temperature dependence of the forward V-I characteristics were examined for cell #1 before and after heat treatment and for the sample of the Clevite thin film cells. The characteristics obtained from cell #1 before heat treatment are shown in figure 4.4. From 132°K to 295°K there was essentially no temperature dependence. The forward current fits an equation of the form

$$I = I_o(e^{\alpha V}-1) \ , \qquad (4.1)$$

where I_o is the intercept with the current axis of the extrapolated linear portion of the ln I vs V curve, and α is a temperature independent parameter. Above 0.4 volts a break to a higher slope was evident at all temperatures.

After heat treatment for 1 minute at 250°C the forward current of this cell decreased by about 5 orders of magnitude. The measured forward characteristics are plotted in figure 4.5. For bias voltages less than 0.9 volts, the current has an exponential dependence on the applied bias as in equation (4.1). The parameter α is again fairly

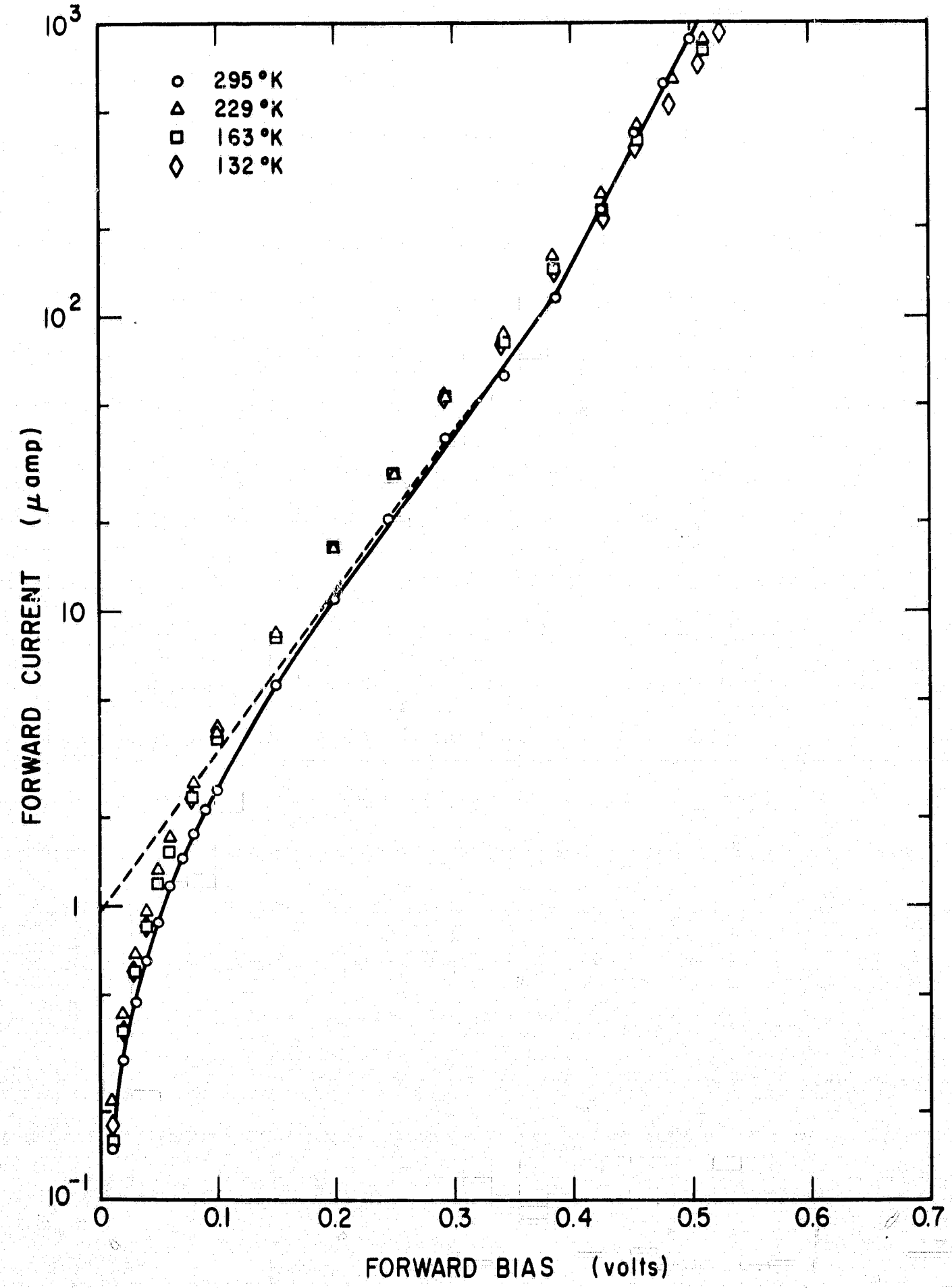

FIGURE 4.4: FORWARD V-I CHARACTERISTICS OF CELL # 1 BEFORE HEAT TREATMENT. THE CURVES ARE DRAWN FOR THE T = +22 °C DATA. THE DASHED LINE CORRESPONDS TO THE EQUATION $I = I_o(e^{\alpha V} - 1)$ WITH $\alpha = 12.5$.

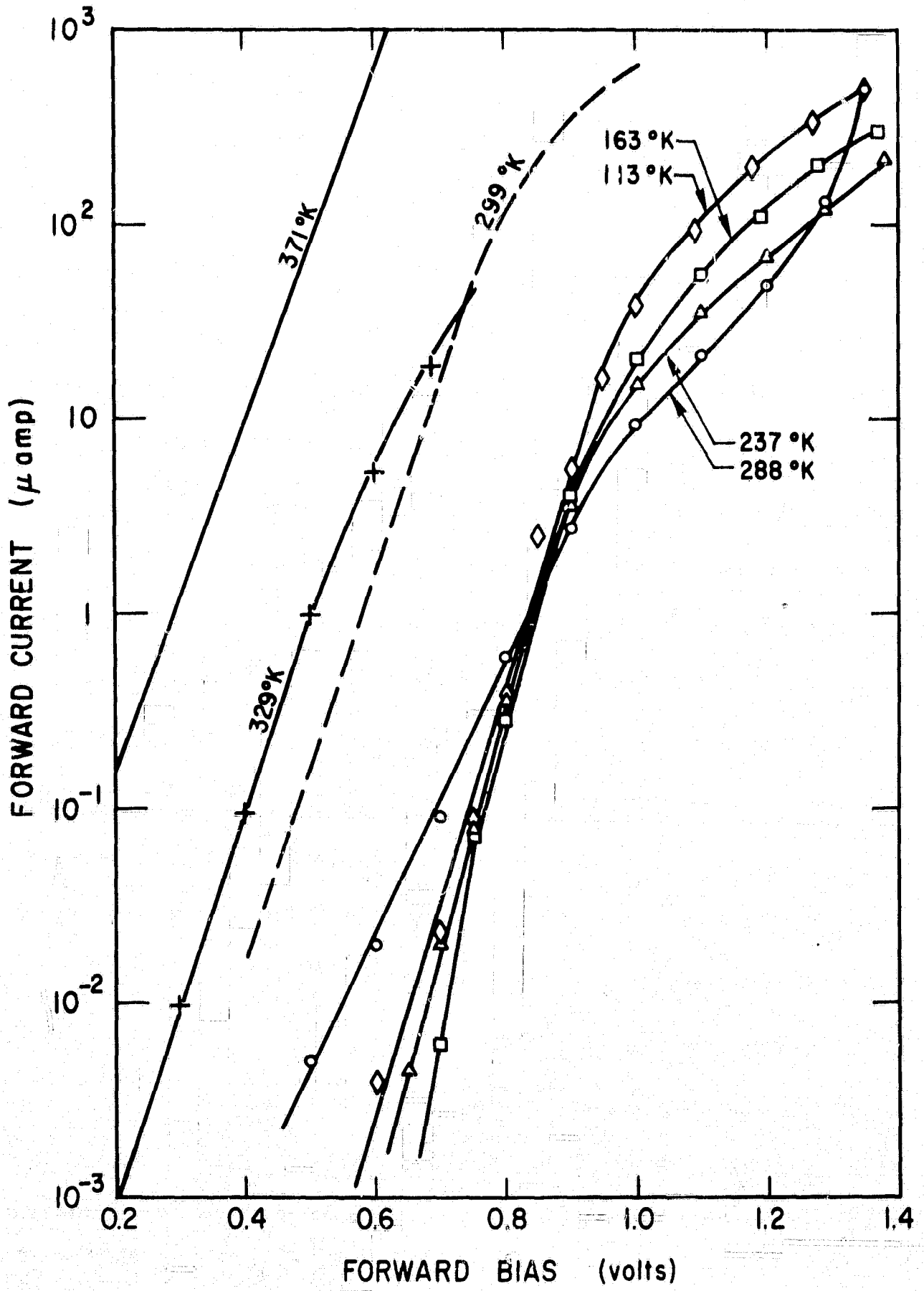

FIGURE 4.5: V-I CHARACTERISTICS OF CELL # I AFTER HEAT TREATMENT FOR I MINUTE AT 250°C IN AIR. THE BROKEN LINE CURVE WAS THE STABLE CHARACTERISTIC OBTAINED AFTER COOLING THE CELL FROM 375 °K WITH 0.5 VOLTS APPLIED.

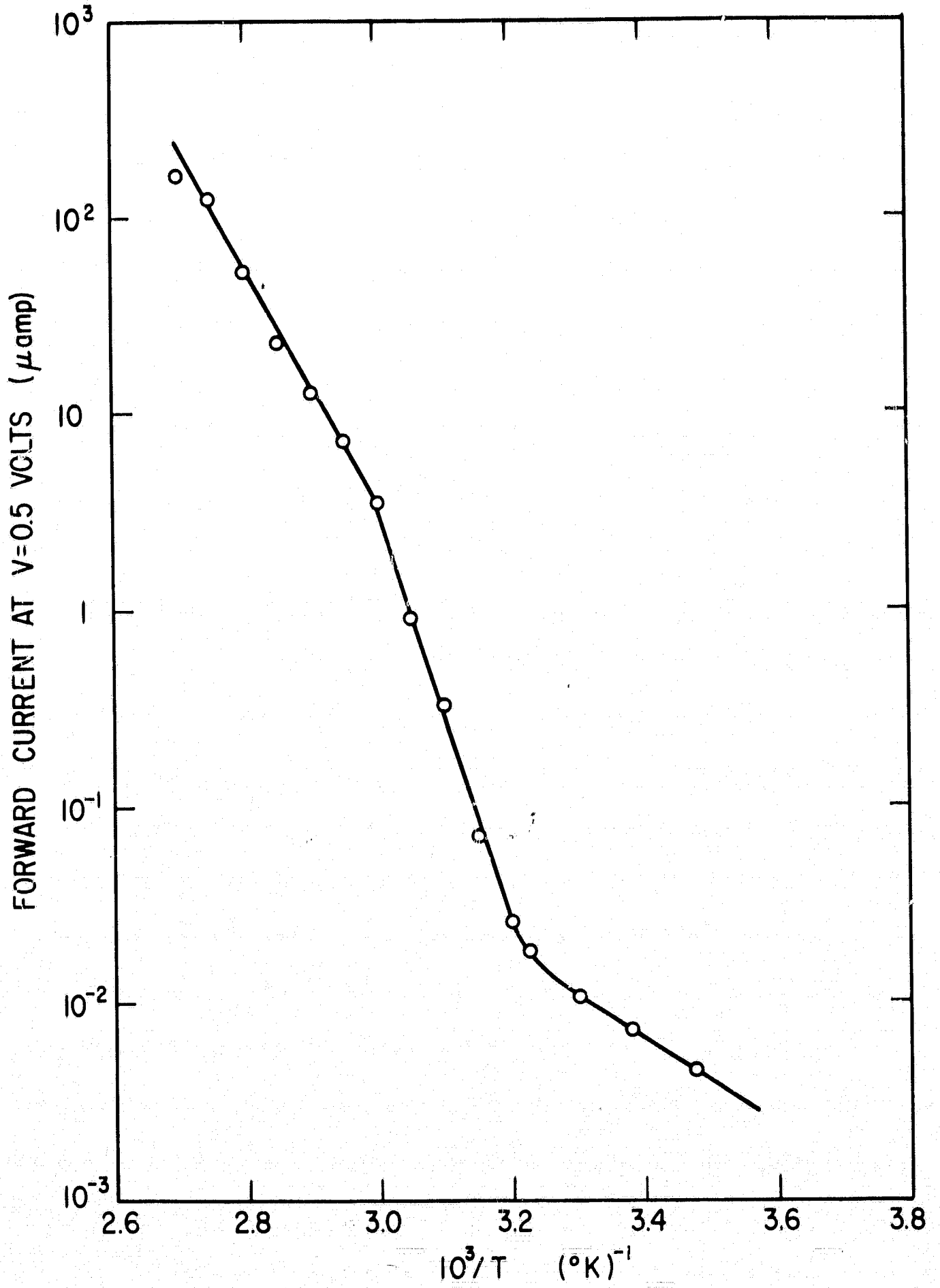

FIGURE 4.6: FORWARD CURRENT AT V = 0.5 VOLTS VERSUS RECIPROCAL TEMPERATURE FOR CELL # 1 AFTER HEAT TREATMENT.

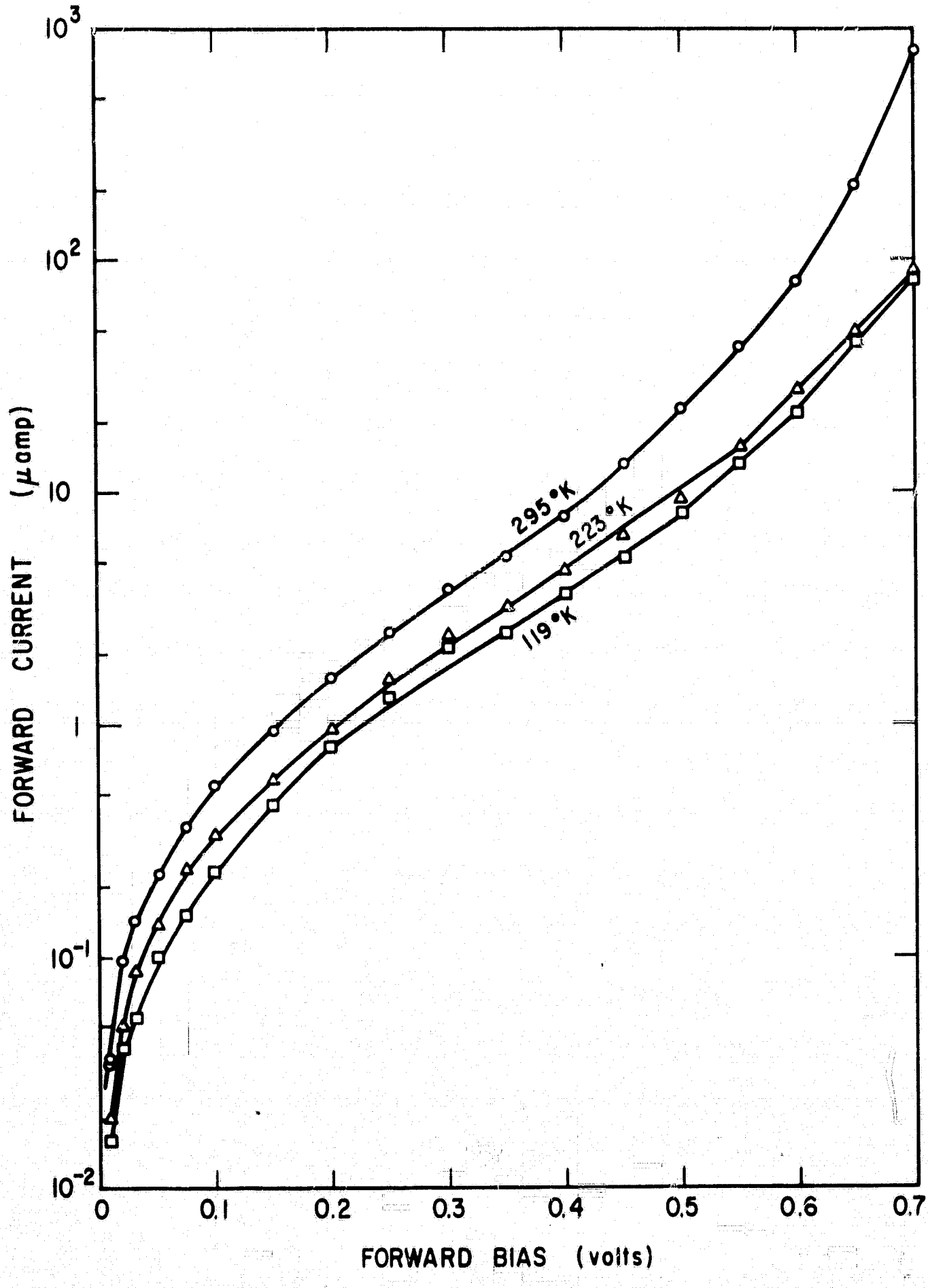

FIGURE 4.7: FORWARD V-I CHARACTERISTICS OF THE CLEVITE EVAPORATED CdS CELL. THE SAMPLE AREA WAS 0.225 cm^2.

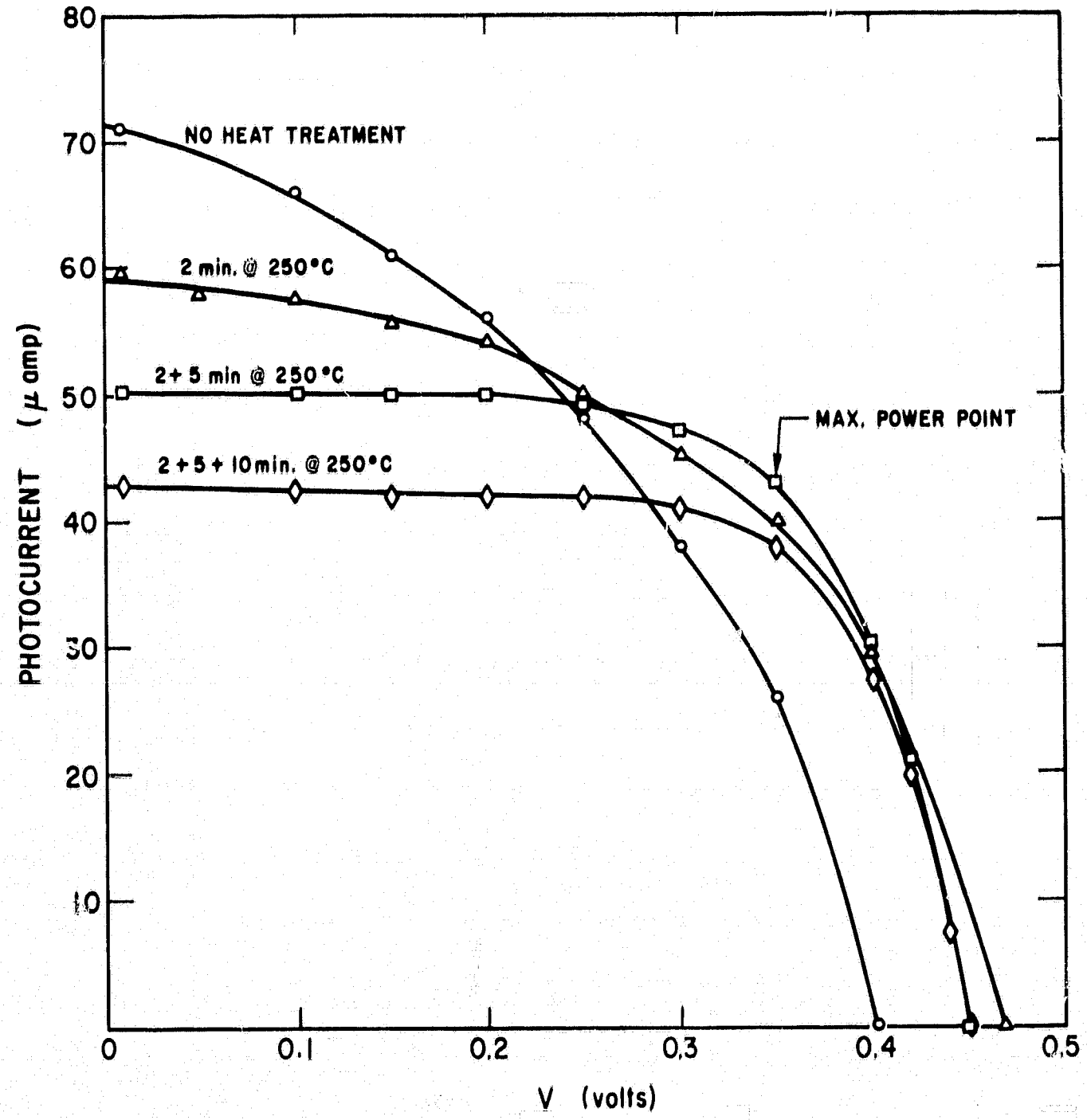

FIGURE 4.8: EFFECT OF HEAT TREATMENT IN AIR ON THE LIGHT V-I CHARACTERISTICS OF CELL # 2. ILLUMINATION WAS FRONTWALL WITH WHITE LIGHT FROM A TUNGSTEN SOURCE.

temperature insensitive except for the value at T = 288°K where α has a considerably lower value. The pre-exponential term I_o is no longer approximately constant but varies in a complicated manner. At the higher temperatures a rapid increase in I_o was observed. In the higher temperature region (288°K $\leq$ T < 373°K) the variation of forward current with temperature was measured at a fixed forward bias of 0.5 volts. The result is shown in figure 4.6 as a function of reciprocal temperature. The steep slope region between 310°K and 333°K is probably due to the value of the parameter α increasing as well as I_o increasing. An activation energy of 1.2 eV was obtained from the region above 333°K where α was approximately constant.

After the measurements at 371°K the 0.5 volt bias was removed and the cell was cooled to room temperature. The curve of figure 4.6 was then repeated and found to be in good agreement with the first run. This time the 0.5 volt forward bias was left on while the cell was cooled to check if the breaks in the curve of figure 4.6 were present on cooling. Cooling the sample to 280°K resulted in no decrease in the forward current from the 373°K value. Attempts to return to the original current condition at 288°K by strong illumination with and without bias applied and by heating to 371°K with no bias applied were not successful. The current at 371°K with 0.5 volts applied remained unchanged, but in the vicinity of room temperature a new stable forward V-I characteristic was measured. The new characteristic is shown as the dashed curve in figure 4.5.

Temperature dependence of the forward V-I characteristics of a piece of Clevite thin film cell is shown in figure 4.7. These films

undergo short heat treatment during fabrication. The results fit equation (4.1) over a limited range with parameters I_o and α being essentially temperature independent.

Effect of Heat Treatment on Light V-I Characteristics

Previous work has shown that the efficiency of CdS solar cells improves with short heat treatment. The effect of a series of heat treatments on the light V-I characteristics of cell #2 are shown in figure 4.8. The short circuit current decreases monotonically with increased heat treatment. Open-circuit photovoltage increases with short heat treatment, then with increased heat treatment V_{oc} decreases slightly and remains approximately constant. The slope of the light V-I characteristic at the intersection with the current axis is often related to the internal shunt resistance of a cell. As a result of heat treatment the shunt or leakage resistance of cell #2 increased, resulting in more nearly square-shaped characteristics and hence higher efficiencies. The decreasing short-circuit current was due to reduced long wavelength response after heat treatment.

4.2 Capacitance - Voltage Results

In all cases where good ohmic contacts were made to both sides of the junction and reverse currents were sufficiently low, reliable C-V characteristics resulted. Information on the net donor density could be obtained from the slope of plots of $1/C^2$ versus V.[66] Such a plot is illustrated in figure 4.9 for cell #3. The net donor density calculated from the constant slope of this plot compares well with the

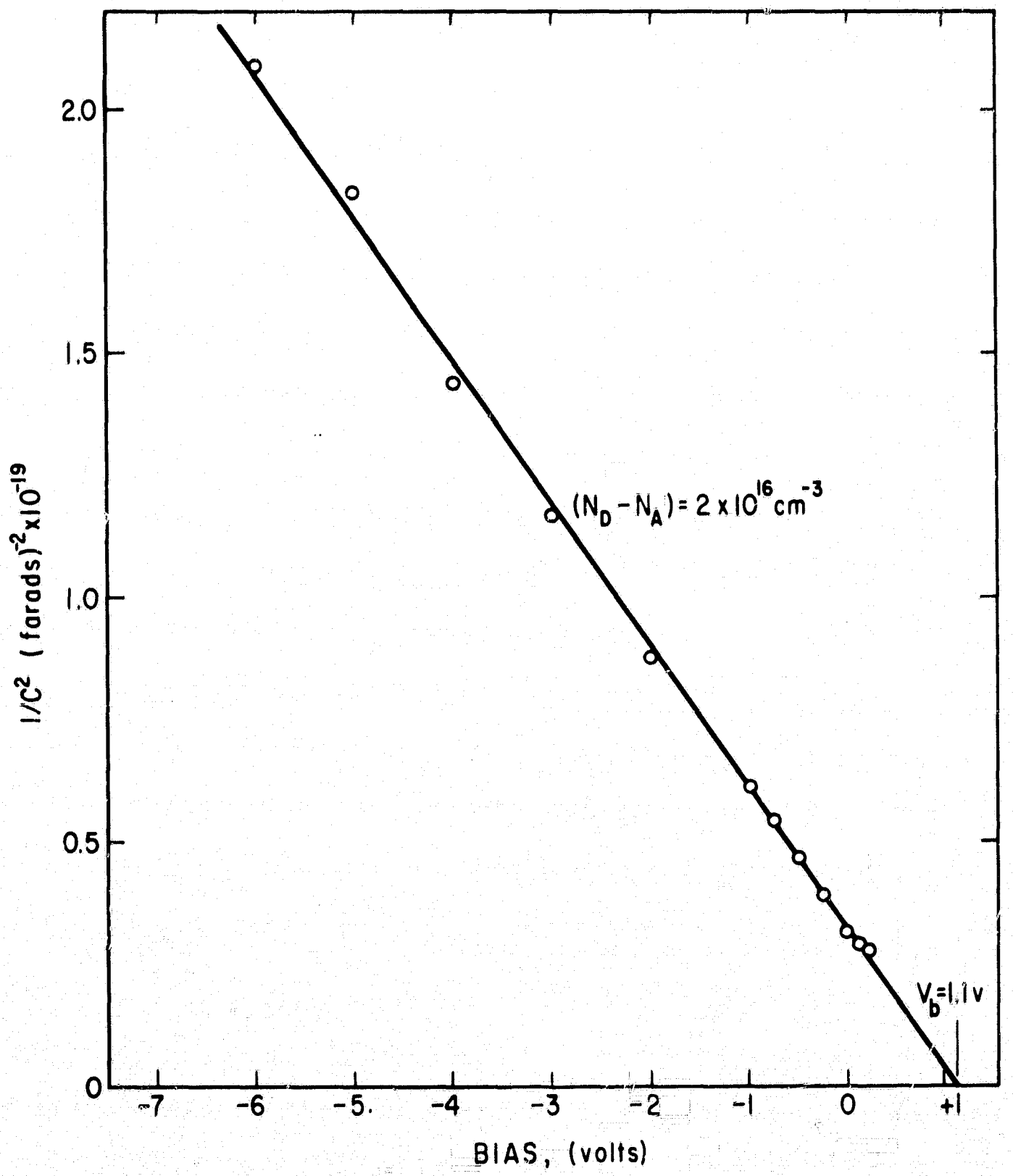

FIGURE 4.9: $1/C^2$ VERSUS APPLIED BIAS VOLTAGE FOR A NON-HEAT TREATED CELL (CELL # 3).

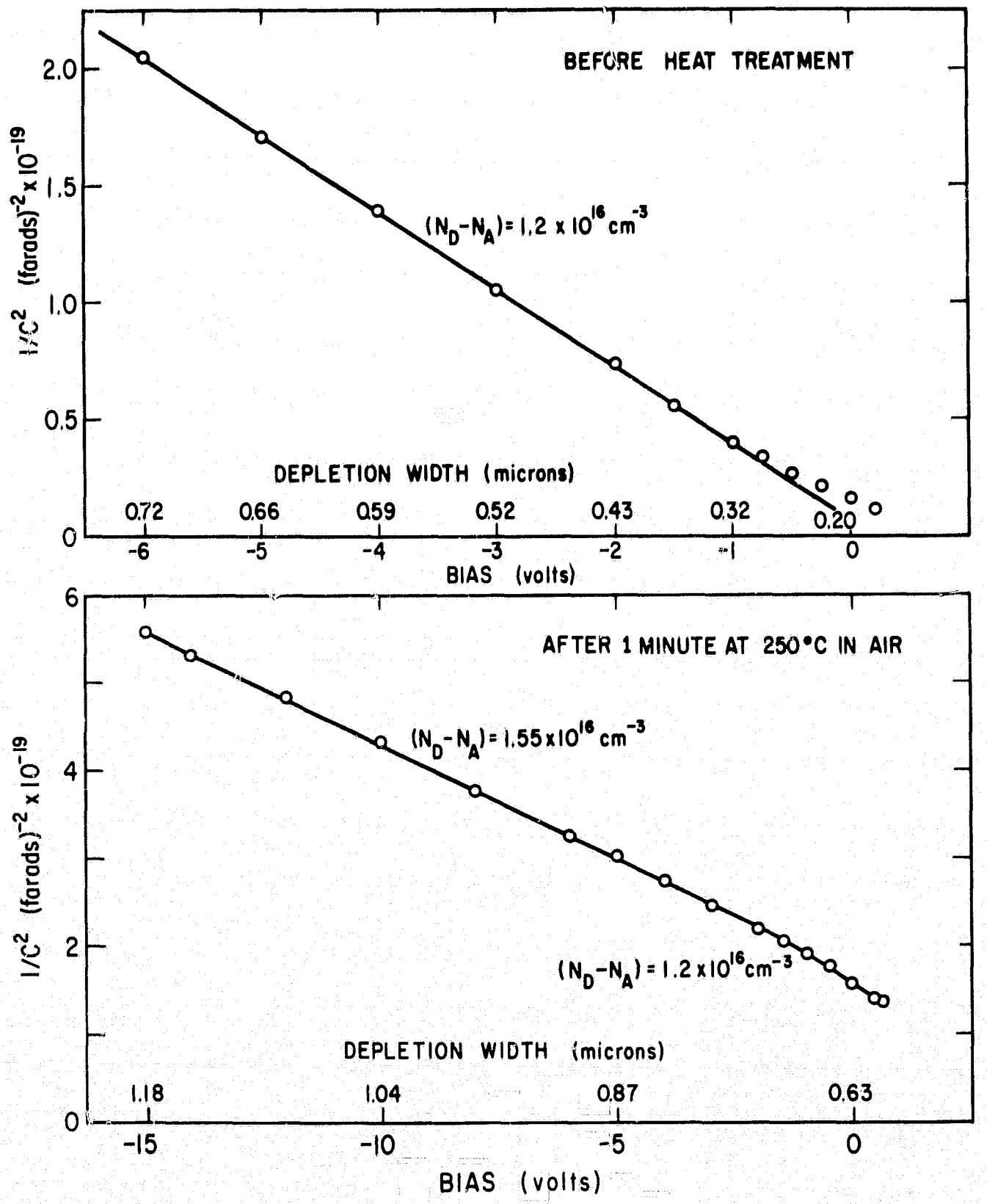

FIGURE 4.10: $1/C^2$ VERSUS BIAS VOLTAGE FOR CELL # 1 BEFORE AND AFTER HEAT TREATMENT.

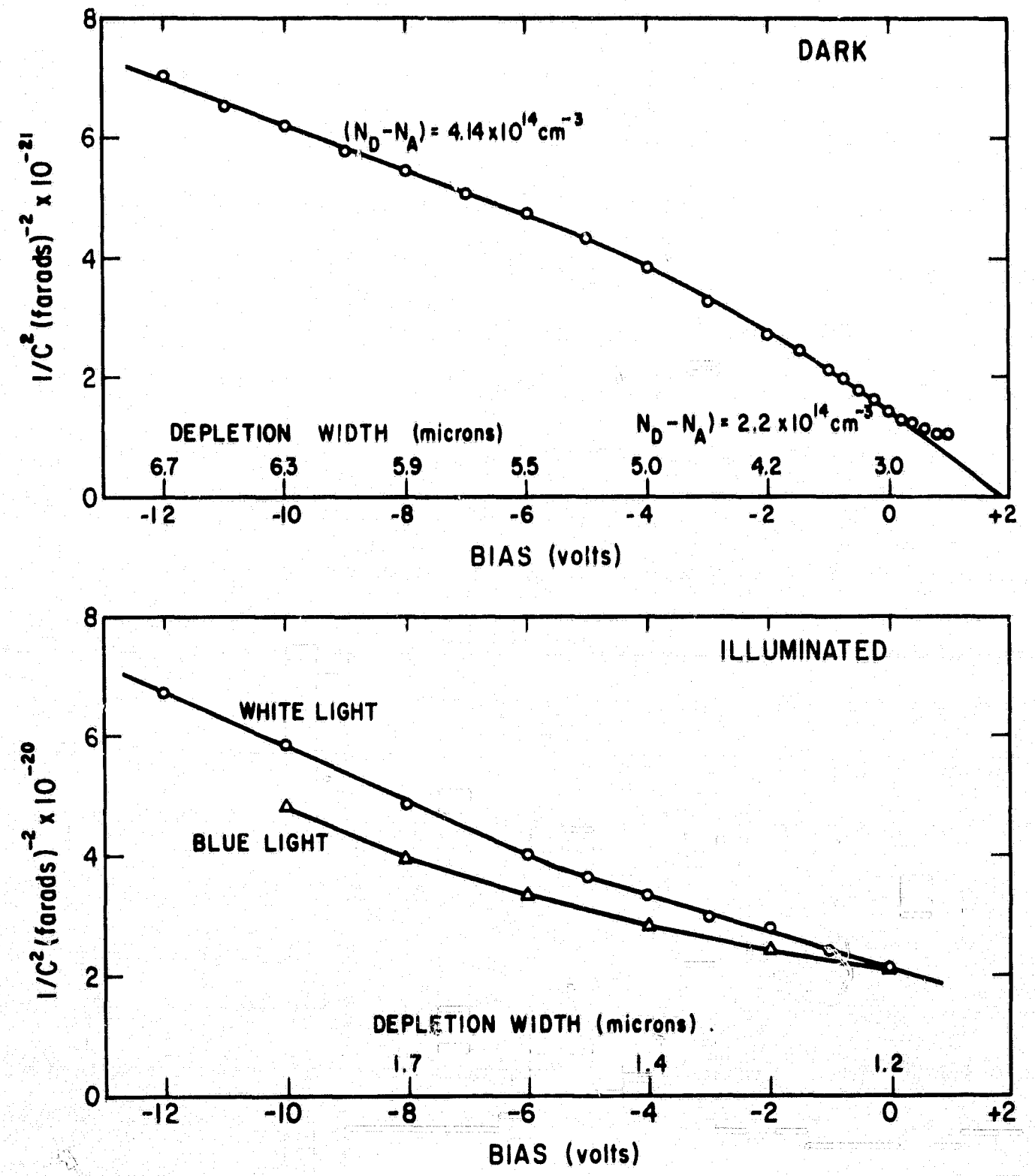

FIGURE 4.11: $1/C^2$ VERSUS BIAS VOLTAGE IN THE DARK AND UNDER ILLUMINATION FOR CELL #4 AFTER 2.5min. AT 250°C IN AIR. THE WHITE LIGHT WAS AN INTENSE TUNGSTEN SOURSE WITH A CORNING 1-69 FILTER. FOR THE BLUE LIGHT A CORNING 4-96 FILTER WAS INSERTED IN ADDITION TO THE 1-69 FILTER.

carrier density calculated from bulk resistivity measurements on the CdS crystal. Unlike many other linear $1/C^2$ vs V plots which have been measured, no appreciable deviation from linearity was observed at small bias voltages. For this reason, the extrapolation in the forward direction to give an effective barrier of 1.1 volts is thought to be valid.

In figure 4.10, the $1/C^2$ vs V curves are plotted for cell #1 before and after heat treatment. Before heat treatment a linear plot was obtained resulting in a value of $(N_D - N_A)$ in good agreement with that obtained from resistivity measurements assuming the electron mobility to be 200 $cm^2/V\text{-}sec$. However, at small bias voltage, deviation from linearity was observed indicating the presence of an insulating layer about 0.1 microns thick. Plots similar to this were typical of results on most cells before heat treatment. Extrapolation in the forward direction to obtain the barrier height is no longer reliable.

After heat treatment the capacitance of all cells decreases drastically due to the diffusion of copper acceptors into the CdS from the Cu_2S. Figure 4.10 shows the results for cell #1. No significant change was seen in the net donor density at large distances from the junction, but the insulating layer appears to have increased in width to about 0.5 microns. Similar results obtained on other cells indicate that heat treatment causes formation of a narrow i-layer in the CdS with an abrupt transition to n-type CdS at the i-n interface.

Effect of Illumination

Spectral response measurements to be discussed in a later section indicate that depletion widths of heat treated cells are decreased by illumination due to the presence of deep hole traps. Direct evidence for the effect of the proposed trapping process on the depletion width was obtained from capacitance measurements with light on the cell. The data are presented here, with discussion deferred to a later chapter. Figure 4.11 shows the dark $1/C^2$ vs V plot for cell #4 after heat treatment, and the results obtained with two conditions of illumination. Under illumination, the junction capacitance increases due to depletion width narrowing. Illumination with a white light source and a Corning 4-96 filter, which allows only the short wavelength light to pass, causes the capacitance to increase to $1/C^2$ values shown in curve (1). The 4-96 filter was then removed, allowing additional strong long wavelength illumination to fall on the cell. The capacitance now decreased, indicative of depletion layer widening due to a reduction in the net ionized donor density from that observed with only short wavelength light incident on the cell.

Transient Effects

Transient effects are also observed during capacitance measurements of heat treated samples. After illumination with short wavelength light the capacitance of cell #2 remains some 40% higher than the equilibrium value and drifts downward extremely slowly. Illumination with infrared light causes a rapid return to the equilibrium capacitance.

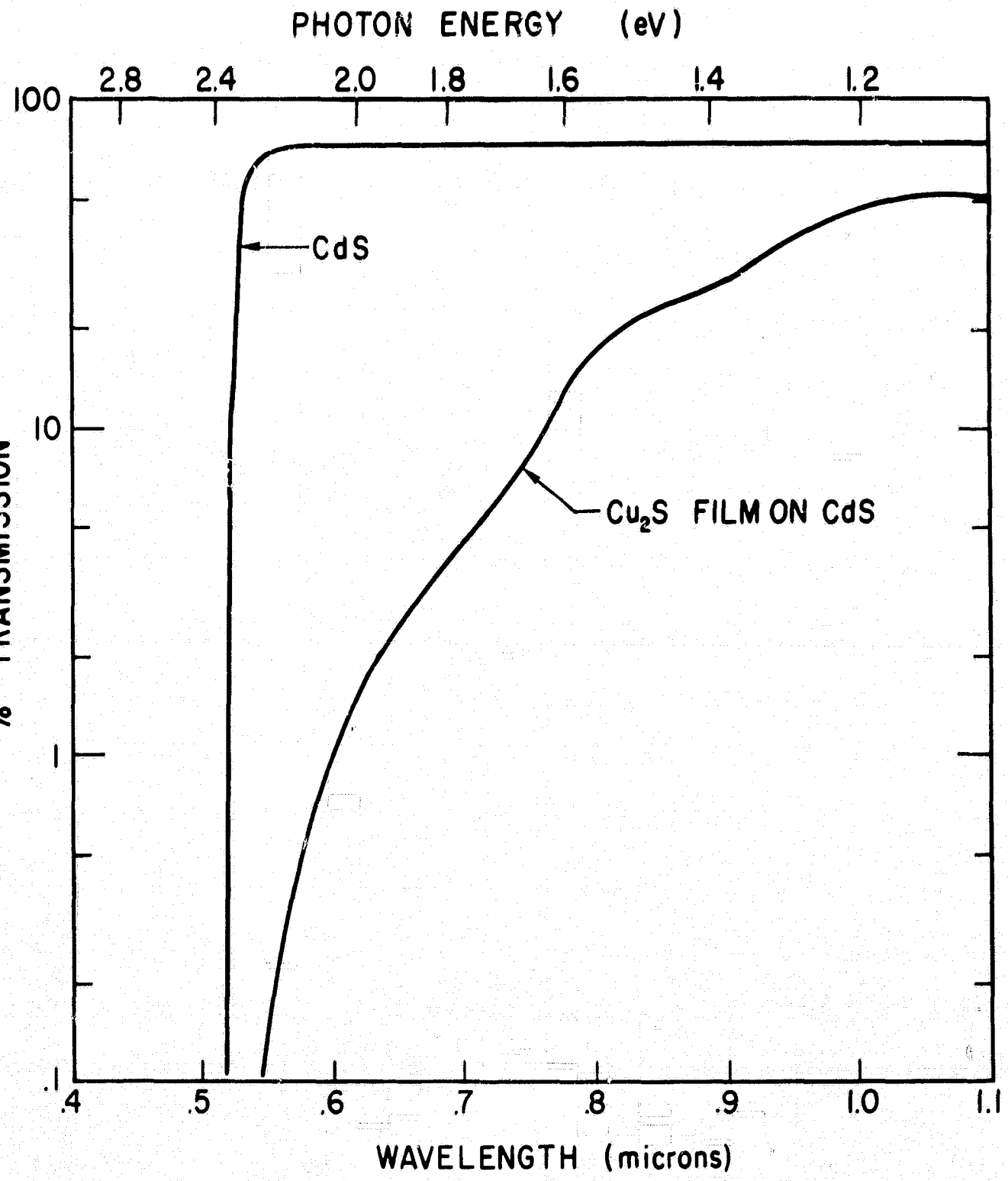

FIGURE 4.12: PERCENT TRANSMISSION OF A THIN Cu_2S LAYER GROWN ON A CdS CRYSTAL.

After forward biasing the junction, the zero-bias capacitance is slightly lowered and slowly increases to reach the equilibrium value. These results are indicative of deep hole-trapping effects in the depletion region of the junctions.

The trap density responsible for the transient effects was estimated for cell #4 from the change in capacitance from the equilibrium value to the value just after short wavelength illumination. The density of deep hole traps was estimated to be 4×10^{14} cm^{-3}. This density can be compared with acceptor density, $N_A = 8 \times 10^{14}$ cm^{-3}, introduced by heat treatment. Therefore, half of these deep acceptors were neutralized for long times due to hole-trapping during the short wavelength illumination.

4.3 Spectral Response

Optical Absorption in the Cu_2S Film

The optical transmission of thin films of Cu_2S grown on CdS crystals was obtained using a Cary 14 scanning spectrophotometer. A thin CdS crystal was polished on both surfaces and the percent transmission obtained. The sample was then dipped to form a thin Cu_2S layer, and another optical transmission curve was taken. The results are shown in figure 4.12. The reduced transmission at $\lambda > 1.0$ microns is probably due to increased reflection losses at the Cu_2S-CdS interface and the high refractive index of Cu_2S.[67] Absorption edges were observed at 1.2 eV, 1.5 eV and 1.8 eV. The edges at 1.2 and 1.8 eV correspond to the structure in the absorption coefficient of Cu_2S (see figure 1.1).

The structure at 1.5 eV is too strong to be an impurity effect and is therefore probably due to another phase in the grown layer.

Non-Heat Treated Cells

The spectral response of cells differs considerably in the long wavelength region. The differences appear to be mostly due to differences in surface treatment of the CdS before dipping. The most consistent results are obtained on crystals with (1) cleaved surfaces, (2) carefully etched surfaces, or (3) mechanically abraded surfaces. Typical frontwall, short-circuit current response for a cleaved surface and an etched surface are shown in the before heat treatment curves of figures 4.13 and 4.14, respectively. On the long wavelength side a rapid increase in photocurrent is observed having a shoulder at 0.9 microns. The response generally peaks at about 0.6 to 0.7 microns and then slowly decreases at shorter wavelengths. A sharp minimum is usually observed at 0.52 microns after which the response rises sharply to a maximum at 0.5 microns due to intrinsic excitation in the CdS. The dip at 0.52 microns is quite generally seen on these heterojunctions being most prominent on cells having thin Cu_2S layers.[68] The dip corresponds exactly to the photoconductivity peak observed in the bulk CdS as can be seen by comparing figures 4.14 and 4.15.

The spectral response of photoconductivity of the CdS crystal used for cell #1 was obtained (figure 4.15) before dipping by chopping the light and using the lock-in amplifier to detect the ac part of the conductivity.

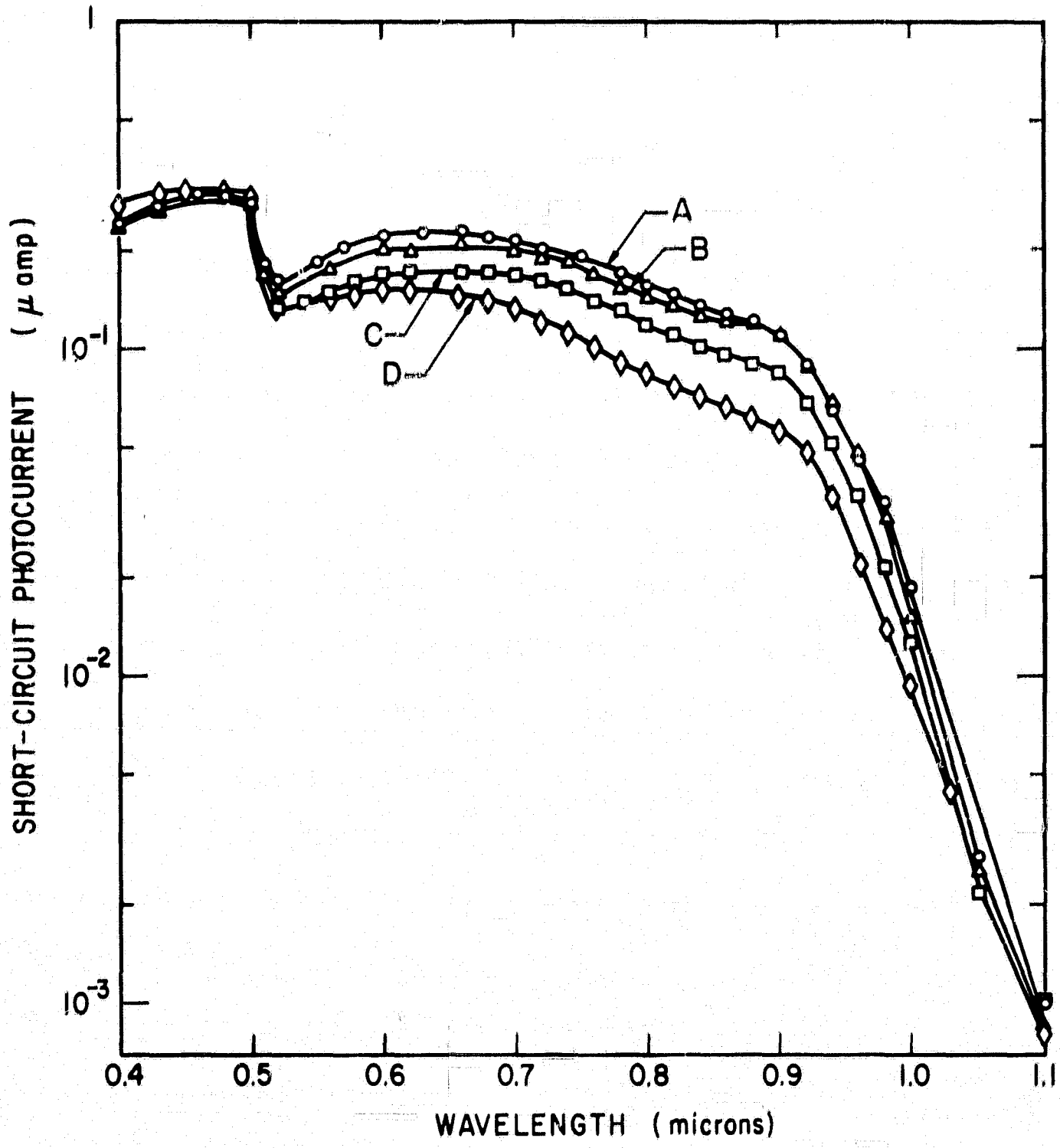

FIGURE 4.13: EFFECT OF HEAT TREATMENT ON THE SHORT-CIRCUIT CURRENT SPECTRAL RESPONSE OF CELL # 2. HEAT TREATMENTS WERE IN AIR AT 250 °C. CURVES A, B, C, AND D ARE FOR NO HEAT TREATMENT, 2 min., 2 + 5 min., 2+5 + 10 min. RESPECTIVELY. LIGHT INTENSITY WAS 100 μwatt/cm^2.

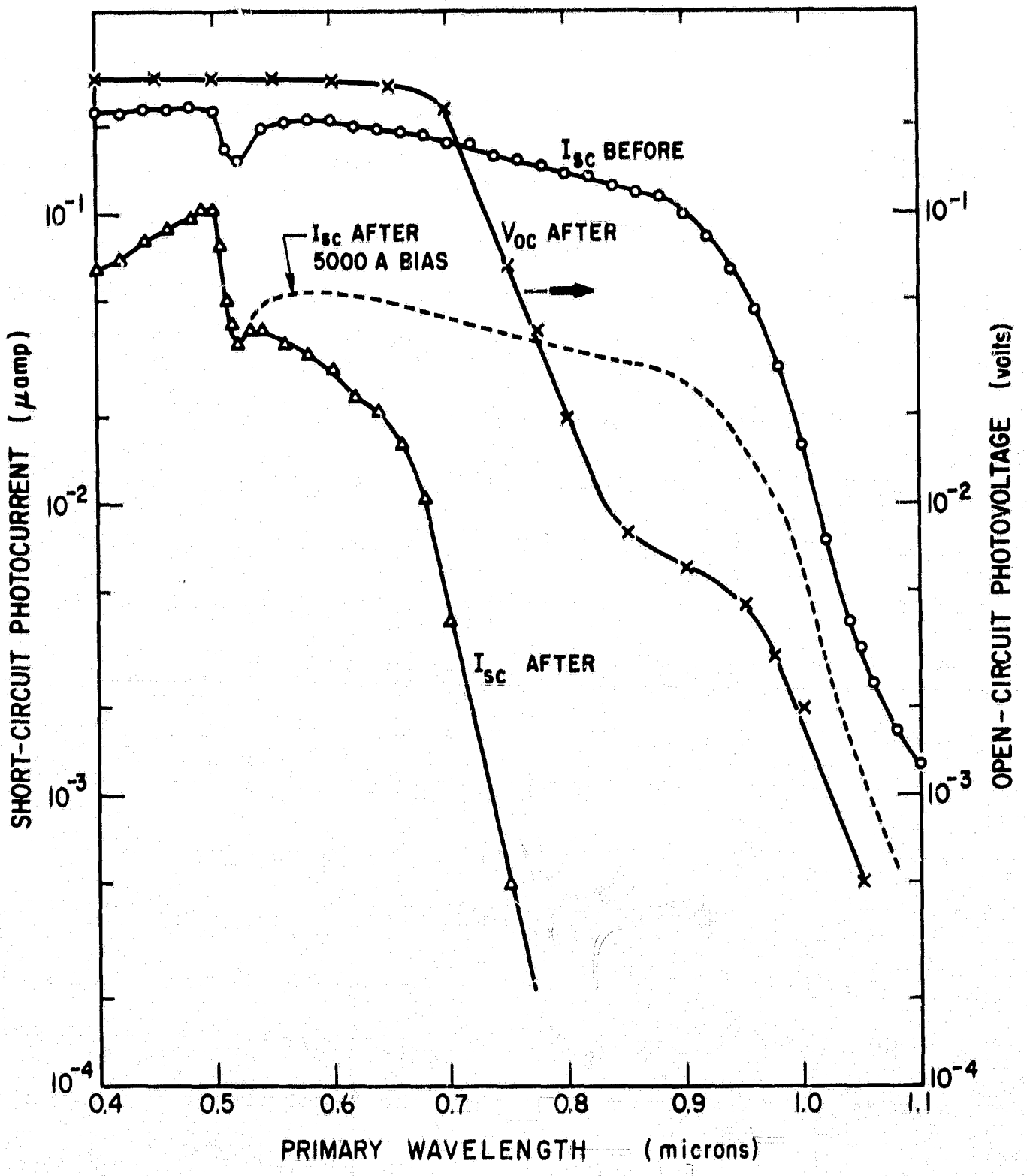

FIGURE 4.14: SPECTRAL RESPONSE CURVES OF CELL #1 BEFORE AND AFTER HEAT TREATMENT FOR 1 MINUTE AT 250 °C IN AIR. THE V_{oc} CURVE WAS TAKEN AFTER THE HEAT TREATMENT AND WITHOUT BIAS ILLUMINATION. THE INTENSITIES OF BOTH PRIMARY AND BIAS SOURCES WERE 300 watts/cm^2.

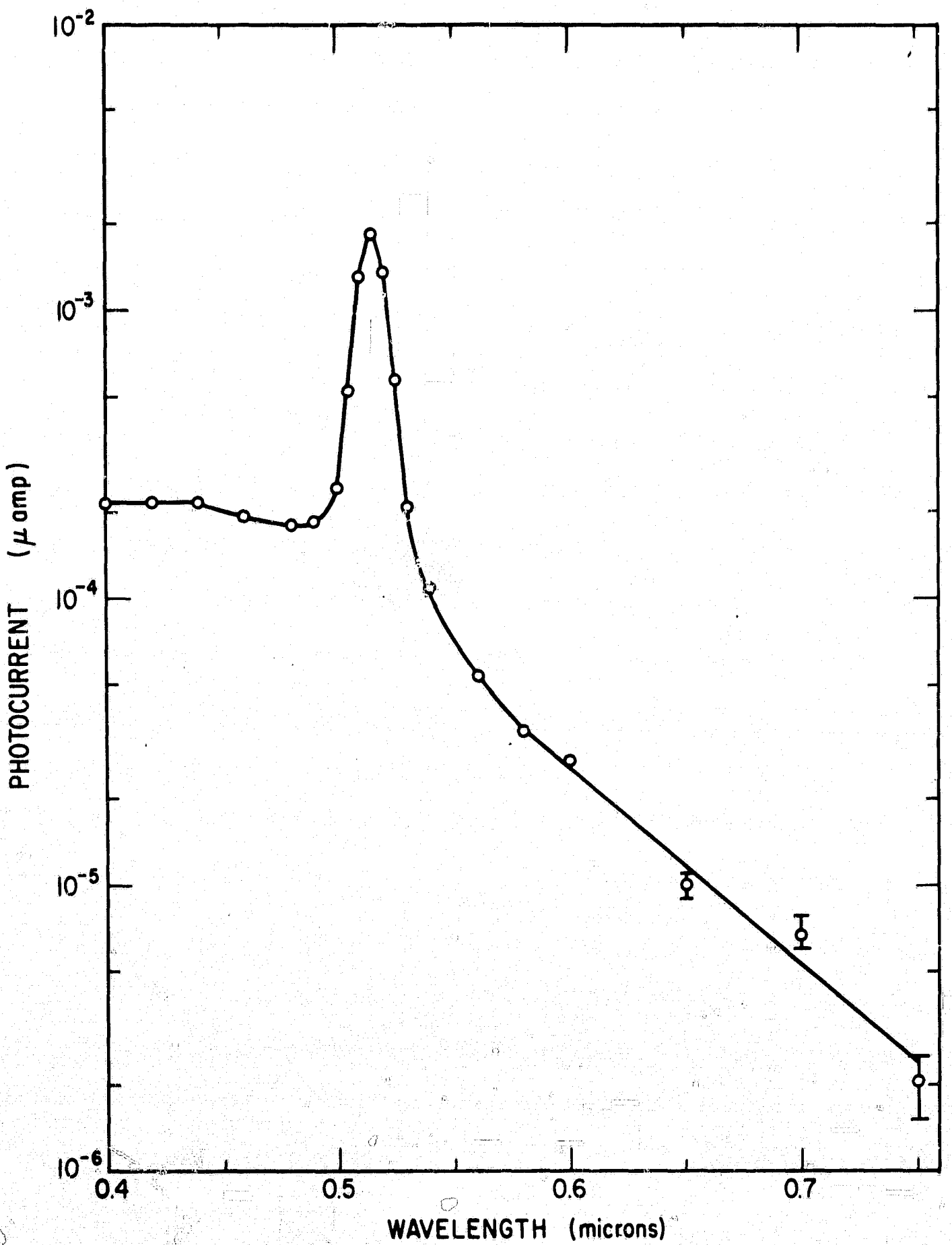

FIGURE 4.15: SPECTRAL RESPONSE OF THE PHOTOCONDUCTIVITY OF A 1 Ω-cm CdS CRYSTAL BEFORE DIPPING TO FORM CELL # 1.

The photoconductivity response was sharply peaked at 5150 A, the band edge of CdS. A long wavelength tail was measured in the photoresponse, but by 6200 A the photosignal was already two orders of magnitude smaller than the peak value. Optical quenching of the photoconductivity was attempted using a weak 5150 A primary source and intense infrared secondary illumination. No quenching was observed except with strong 5150 A secondary illumination probably due to bimolecular recombination at the high injection level. The majority-carrier lifetime, τ_n was calculated from the peak photoconductivity response using the relation[69]

$$\tau_n = \frac{L^2 I}{eF\mu_n V} \quad , \tag{4.2}$$

where L was the distance between electrodes, I was the photocurrent, e was the electronic charge, F was the incident photon flux, μ_n was the electron mobility, and V was the applied voltage. Using a value of $\mu_n = 200$ cm^2/V-sec, the majority-carrier lifetime was 2.5×10^{-6} sec.

After the photoconductivity measurements were completed, the sample was dipped to form a thin ($\approx 5 \times 10^{-5}$ cm) Cu_2S layer. The short-circuit photocurrent response shown in figure 4.14 was then obtained. The quantum efficiency was about 7.5% in the long wavelength region.

Effects of Heat Treatment

In all cases, the effect of heat treatment at 250°C was to degrade the long wavelength spectral response of the cells. No systematic study was made of the effects of varying the duration or temperature of the heat treatment. Similar heat treatments on several different

cells resulted in widely varying degrees of degradation. Since the cells were made from different CdS crystals and the surfaces were not prepared in the same way, variations in the effectiveness of heat treatment were to be expected.

In figure 4.13, the spectral response of cell #2 is shown before and after a series of heat treatments. The relatively small effect of even prolonged (17 min) heat treatment appears to be characteristic of results obtained on cleaved surfaces.

The results of a 1 minute heat treatment of cell #1 are shown in figure 4.14. The degradation from the response before heat treatment to that after heat treatment has been much more rapid than was the case for cell #2. This result was typical for junctions grown on polished surfaces. The results of secondary illumination on the spectral response will be discussed in section 4.4.

The short-circuit current output of a cell having poor long wavelength response is shown in figure 4.16. This cell was a positive bevel-angle sample prepared for diffusion length measurements. Since the Cu_2S layer was 4.5 microns thick, spectral response measurements were made with backwall illumination, i.e., light incident through the CdS crystal. The current response did not decrease to zero on the short wavelength side of the CdS bandgap (0.51 microns) because the bevelled junction was exposed on one end. The effect of successive heat treatments of 30 seconds and 2 minutes at 250°C in air are shown in the figure.

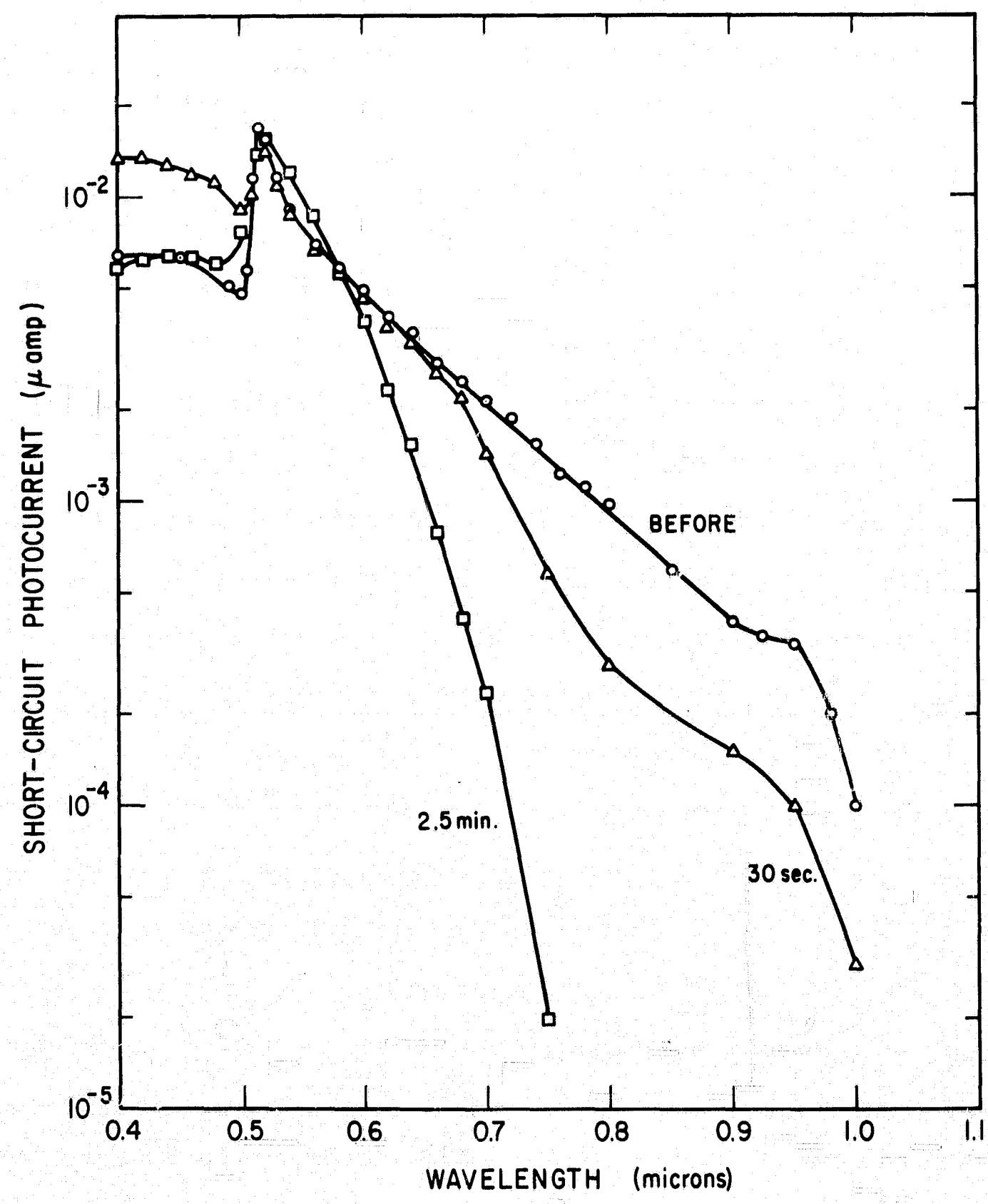

FIGURE 4.16: BACKWALL SPECTRAL RESPONSE CURVES FOR CELL # 4 BEFORE AND AFTER HEAT TREATMENT AT 250 °C IN AIR FOR TIMES INDICATED.

Fast and Slow Components of the Photocurrent

During measurements of the spectral response of many cells, transient behavior with long time constants was observed. Cells which had not been heat treated had fast response to light of all wavelengths to which they were sensitive. After heat treatment, slow downward drift in the short-circuit current response to wavelengths longer than 8500 A and slow upward drift for shorter wavelengths was noted. Typical transients in the long and short wavelength regions are shown in figure 4.17. The time required to reach equilibrium depended on light intensity and wavelength, differing considerably for different cells. The transients were found to be independent of the ambient. Several hours in vacuo or nitrogen ambients with long dark and illuminated intervals caused no change in the effect. Interruption of the slow rise or decay by a dark interval resulted in a rapid decrease of the photocurrent to zero and a rapid rise to the value of photocurrent measured just before switching the light off when the light is switched on again. Return to the initial conditions could be achieved only by holding the sample many hours in the dark or by illumination with strong infrared ($\lambda \geq 9000$ A) for a few seconds.

The fast component of the photocurrent and the steady-state photoresponse plotted as a function of incident light wavelength are shown in figure 4.18 for cell #2. The difference between the steady-state and the fast component gives the magnitude of the slow effects. The slow component enhances the steady-state response at wavelengths

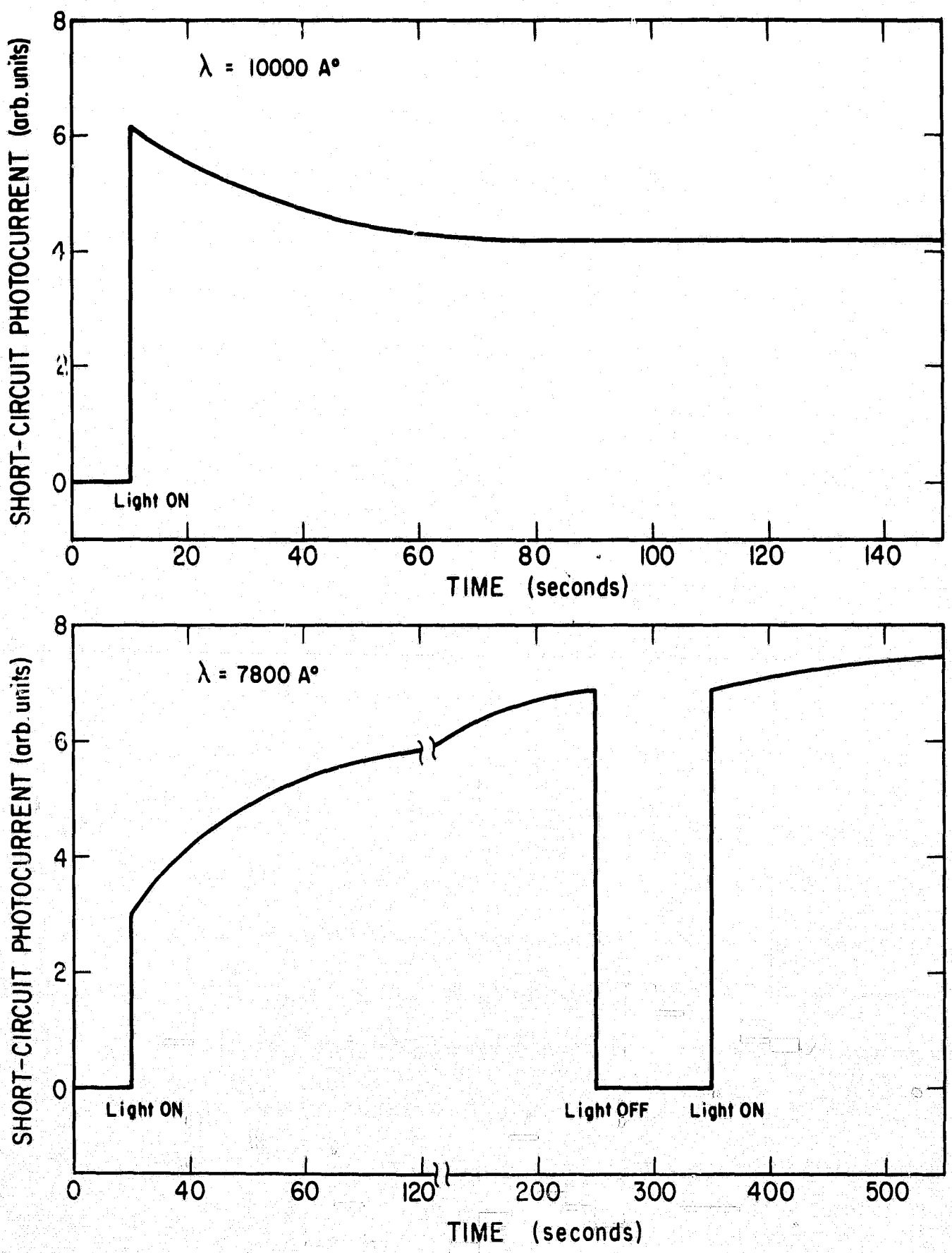

FIGURE 4.17: SHORT CIRCUIT CURRENT VERSUS TIME SHOWING FAST AND SLOW COMPONENTS OF THE RESPONSE.

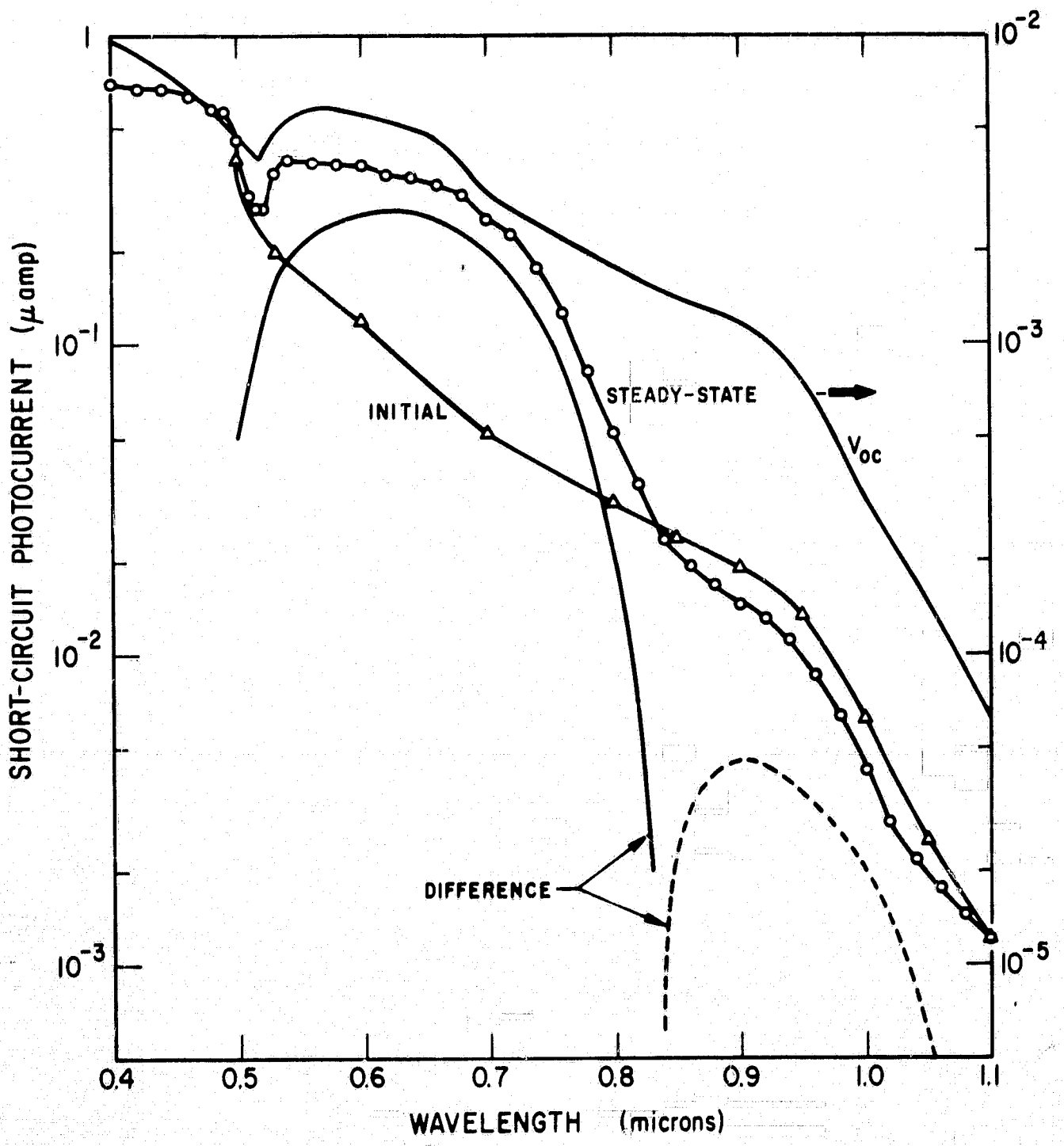

FIGURE 4.18: SPECTRAL RESPONSE OF THE INITIAL FAST AND STEADY-STATE PHOTOCURRENT FOR A HEAT-TREATED CELL (#2). THE DIFFERENCE CURVES REPRESENT THE SLOW COMPONENT OF RESPONSE; SOLID CURVE, ENHANCEMENT, AND DASHED CURVE, QUENCHING. LIGHT INTENSITY WAS 300 μwatt/cm^2. THE V_{oc} CURVE WAS THE NON-SATURATED VALUE OBTAINED WITH 3 μwatt/cm^2 LIGHT INTENSITY.

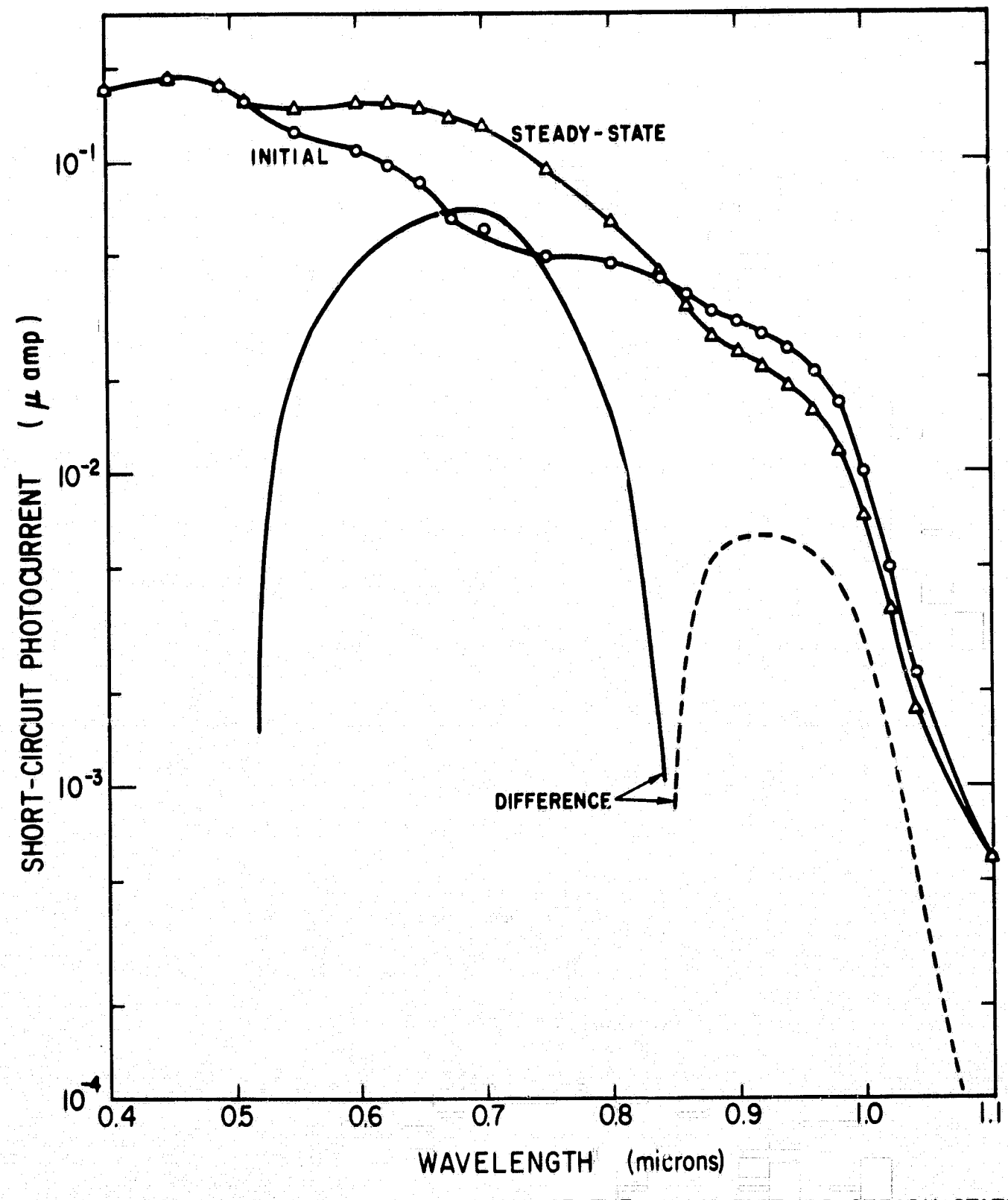

FIGURE 4.19: SPECTRAL RESPONSE OF THE INITIAL FAST AND STEADY-STATE PHOTOCURRENTS FOR THE CLEVITE EVAPORATED CdS CELL. LIGHT INTENSITY WAS 300 μwatts/cm^2. THE ILLUMINATED AREA WAS 0.41 cm^2.

less than 8400 A and quenches the response at longer wavelengths. The steady-state open-circuit photovoltage V_{oc} shown in the figure was the unsaturated value obtained with very weak illumination ($3\mu watt/cm^2$). Figure 4.19 shows similar curves of the spectral response of the fast and steady-state components of the photocurrent obtained with a small section of the Clevite thin film cell. Comparison of the difference curves with the equivalent curves of figure 4.18 shows very similar behavior for the single crystal and evaporated, polycrystalline CdS cells. For both cells, the crossover from quenching to enhancing regions occurs at the same wavelength (8400 A) within experimental error.

4.4 Effects of Secondary Illumination

Simultaneous Primary and Secondary Illumination

The spectral response of non-heat-treated cells was found to be unchanged by simultaneous illumination with an intense secondary light. However, after heat treatment, secondary illumination strongly influences the long wavelength response. In general, the use of white secondary light or monochromatic secondary light with $\lambda \leq 8000$ A results in enhancement of the long wavelength response. Secondary illumination with $\lambda \geq 8500$ A causes quenching of the long wavelength response. The use of steady illumination with both the primary and secondary sources requires great care in correct interpretation of apparent enhancement or quenching of the primary signal. Figure 4.20 illustrates schematically some of the possibilities when dc primary and secondary

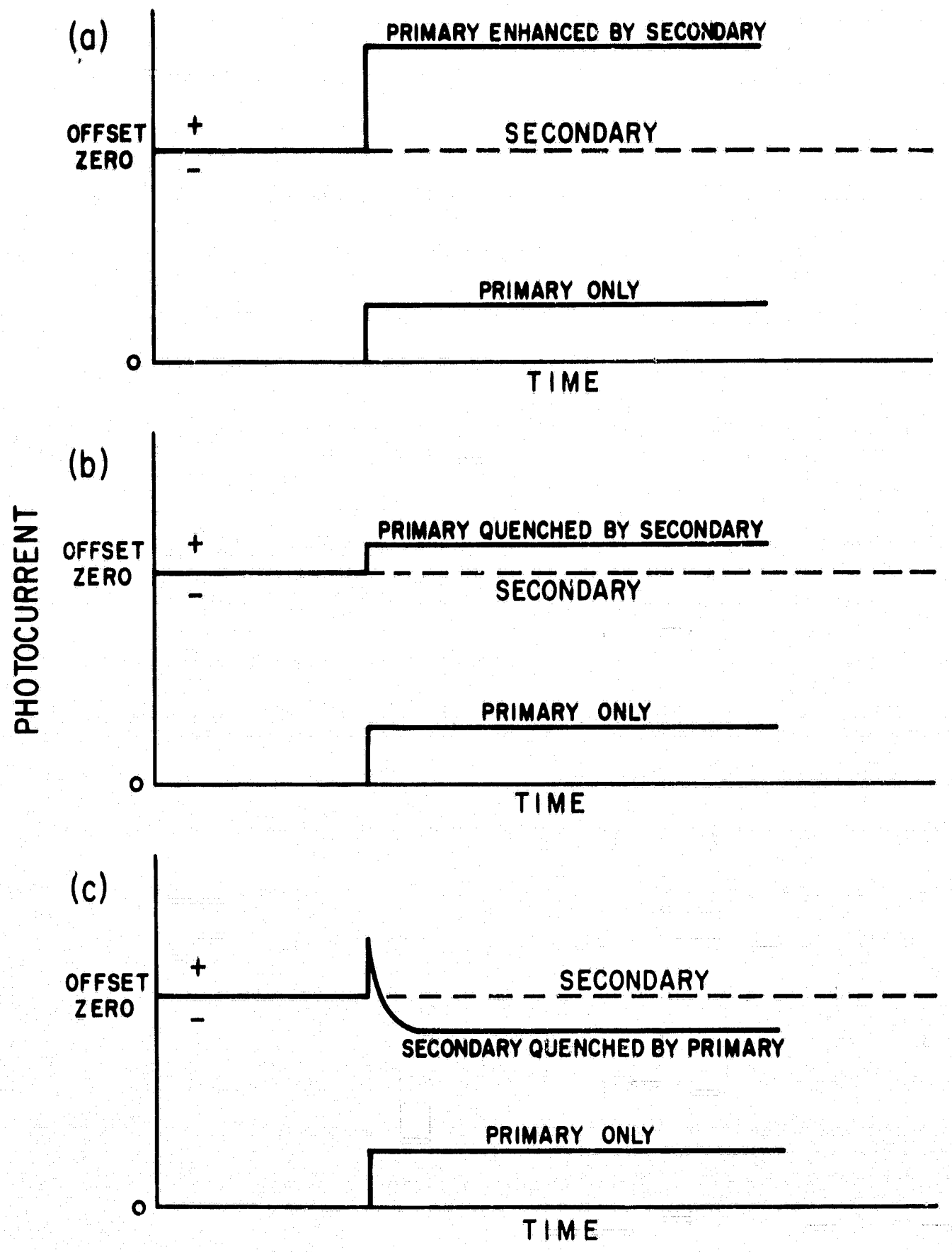

FIGURE 4.20: DIAGRAM SHOWING POSSIBLE EFFECTS WHEN DC PRIMARY AND SECONDARY SOURCES ARE USED. SOLID LINES REPRESENT THE MEASURED CURRENTS.

light source are used. Parts (a) and (b) show enhancement and quenching of the primary signal respectively by the secondary light. Part (c) shows quenching of the secondary signal by the primary light resulting in negative signals rel[illegible]e to the offset zero level. Enhancement of the secondary signal by the primary light is another possibility not illustrated in the figure. Since enhancement and quenching processes are slow compared to the photovoltaic response, the transient behavior when the primary light is turned on helps distinguish these effects. However, slow self-enhancement or self-quenching by the primary light (see figures 4.17 to 4.19) is a further complication making analysis of the transients difficult. The use of a chopped primary light simplifies the interpretation of enhancing and quenching experiments.

Figure 4.21 shows the effect of white secondary illumination on the photocurrent of cell #4. At short wavelengths enhancement was observed. At longer wavelengths the initial response indicated large enhancement, but the measured steady-state photosignal went negative. Since zero suppression had been used to offset the secondary light photosignal, the negative photocurrent represented very strong quenching of the secondary signal by the primary radiation (see figure 4.20(c)). The wavelength (8000 A) where the steady-state signal changed sign may be compared with the changeover from enhancement to quenching at 8400 A in figures 4.18 and 4.19.

Strong 9000 A secondary illumination had the effect shown in figure 4.22. The long wavelength primary response is quenched by the 9000 A light. At wavelengths shorter than 8000 A the primary signal

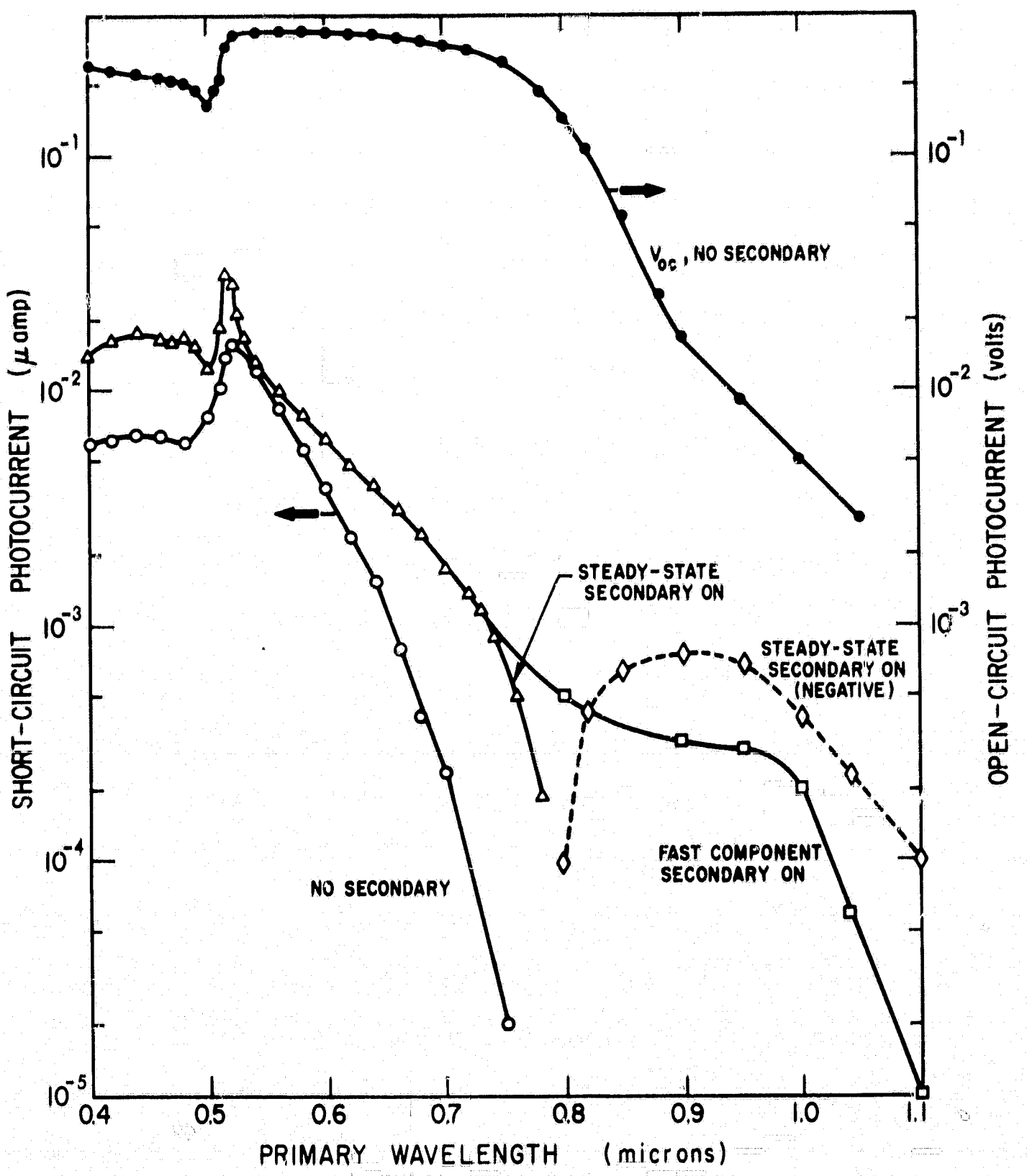

FIGURE 4.21: PHOTORESPONSE OF CELL # 4 AFTER HEAT TREATMENT WITH AND WITHOUT SECONDARY ILLUMINATION (10 mwatt/cm^2, 3000A < λ 10000A). PRIMARY INTENSITY = 300 μwatt/cm^2. THE DASHED CURVE WAS NEGATIVE CURRENT RELATIVE TO THE SECONDARY PHOTOCURRENT LEVEL.

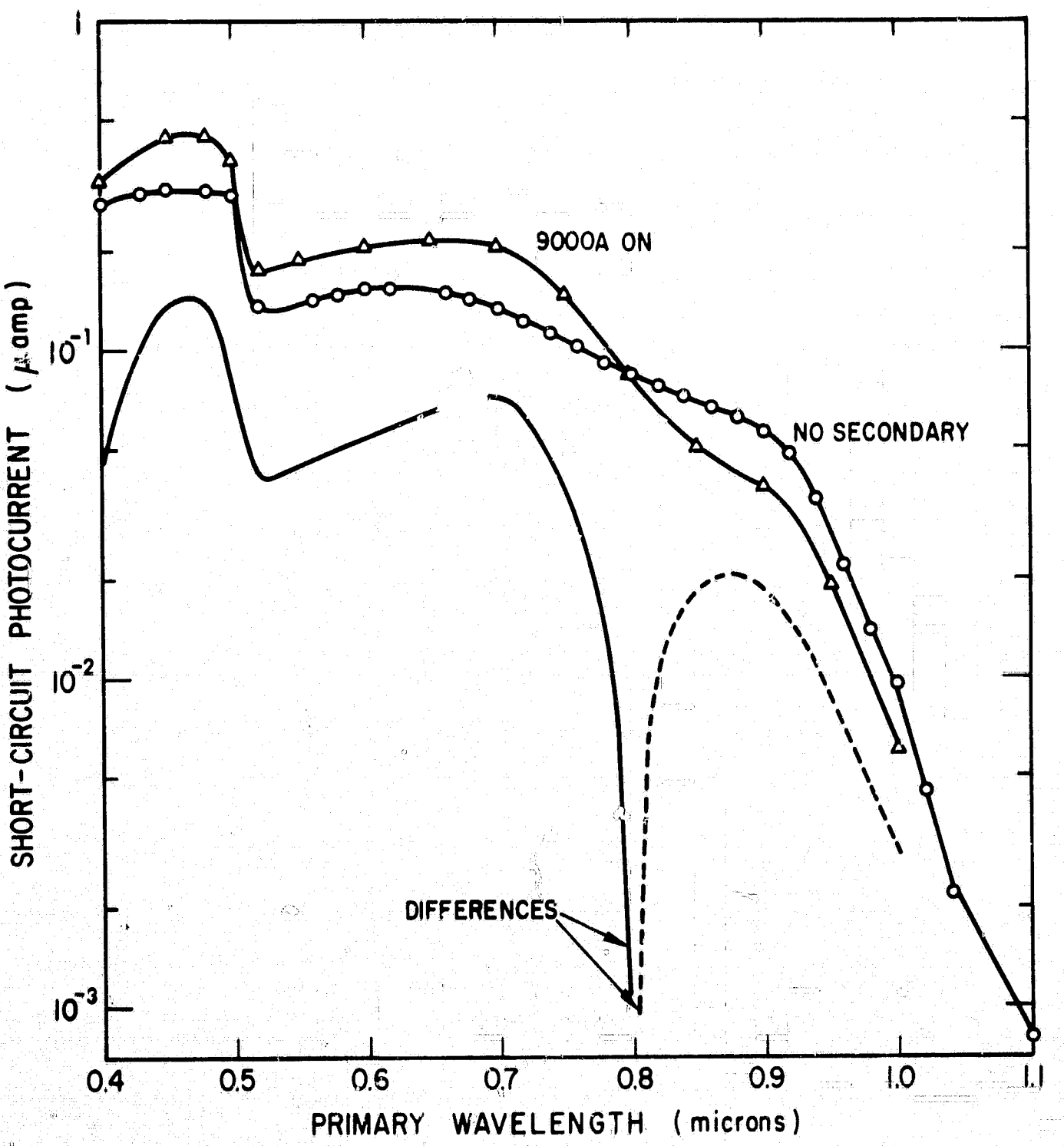

FIGURE 4.22: SHORT-CIRCUIT PHOTORESPONSE OF CELL # 2 AFTER HEAT TREATMENT (2 + 5 + 10 MINUTES) WITH AND WITHOUT 9000A SECONDARY ILLUMINATION (1600 μwatt/cm^2). PRIMARY INTENSITY = 100 μwatt/cm^2.

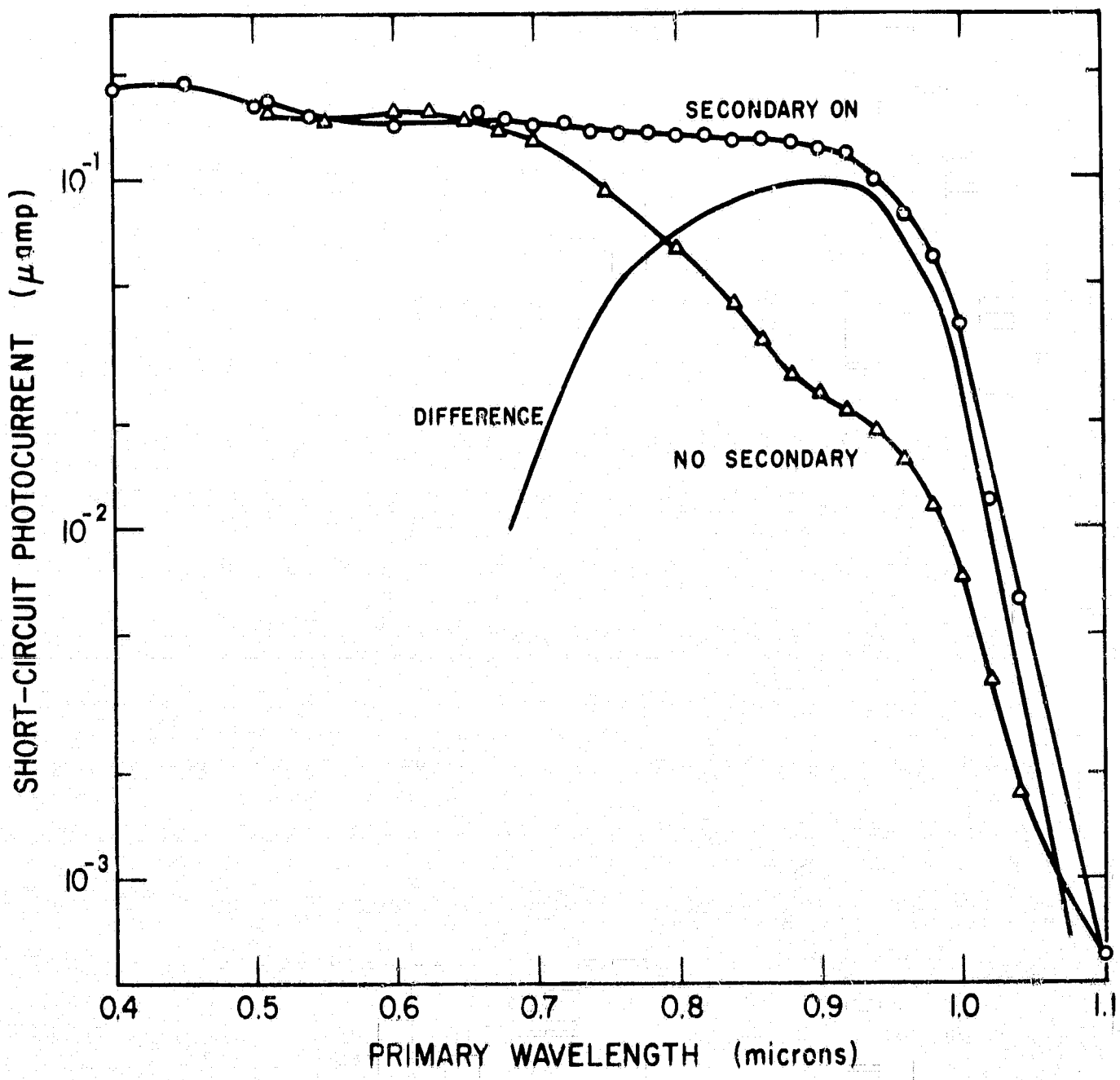

FIGURE 4.23: PHOTORESPONSE OF THE EVAPORATED CdS CELL WITH AND WITHOUT SECONDARY ILLUMINATION (3μwatt/cm^2, 3000 A < λ < 10000 A) PRIMARY INTENSITY = 300μwatt/cm^2.

is apparently enhanced by the secondary light. Actually, the process at shorter wavelengths was enhancement of the secondary light photocurrent by the short wavelength primary light. Once again the cross-over was at 8000 A, but this is probably fortuitous, since competition between enhancement and quenching will generally be dependent on the relative intensities of the two wavelengths concerned. Effects very similar to those observed in figure 4.22 were observed on another cell when secondary light of wavelength greater than 8000 A was used. However, the cross-over occurred at 7000 A on the latter sample, indicating more efficient quenching.

Usually the quenching effect of long wavelength secondary illumination is not as pronounced as seen in the examples above. More frequently, short wavelength or white secondary light enhances the longer wavelength end of the primary response as seen in figure 4.14 for a single crystal CdS cell, and in figure 4.23 for the thin film evaporated CdS cell. Enhancement effects are more pronounced than quenching because the enhancement involves hole trapping in normally empty centers while quenching is the inverse process of emptying the traps of holes. Quenching can only occur in situations where self-enhancement by the primary radiation takes place. When enhancing and quenching effects compete a net enhancement must always result. These effects and the trapping levels causing them will be more fully discussed in the following subsection and in Chapter VI.

Secondary Light Effects with a Chopped Primary Source

Use of dc primary and secondary light sources, as described in

the previous section, most closely simulates the operational conditions of solar cells. However, in order to avoid the confusion of the primary source affecting the secondary signal, a method of distinguishing between the primary and secondary photoresponse is essential. Since for the light intensities used in these experiments the effects of secondary illumination have been slow, relative to the effects of primary illumination, use of a chopped primary source and steady secondary light provides a simple means of separating the signals.

The effect of secondary illumination wavelength on the primary photocurrent due to chopped 6550 A light is shown in figures 4.24 and 4.25 for cell #4 and cell #1, respectively. In each case two quenching bands were seen at long wavelengths, while at short wavelengths the signal was enhanced. The cutoff in the enhancement region of figure 4.24 at 5200 A was due to absorption of the secondary light by the CdS crystal. The arrows on figure 4.25 show the wavelengths at which optical quenching of photoconductivity begins in sensitive CdS crystals.[70,71]

Since quenching and enhancement are competing processes in the region of the crossover near 6500 A, an accurate determination of the wavelength for onset of the enhancement mechanism requires that the quenching be suppressed. This was accomplished by changing the primary light wavelength to 9200 A. The reason that such a wavelength change eliminates quenching is that the primary light is no longer in the self-enhancing region and therefore quenching which is the inverse of the enhancement mechanism cannot occur. This mechanism will be discussed fully in Chapter VI. Figure 4.26 shows the effect of varying the

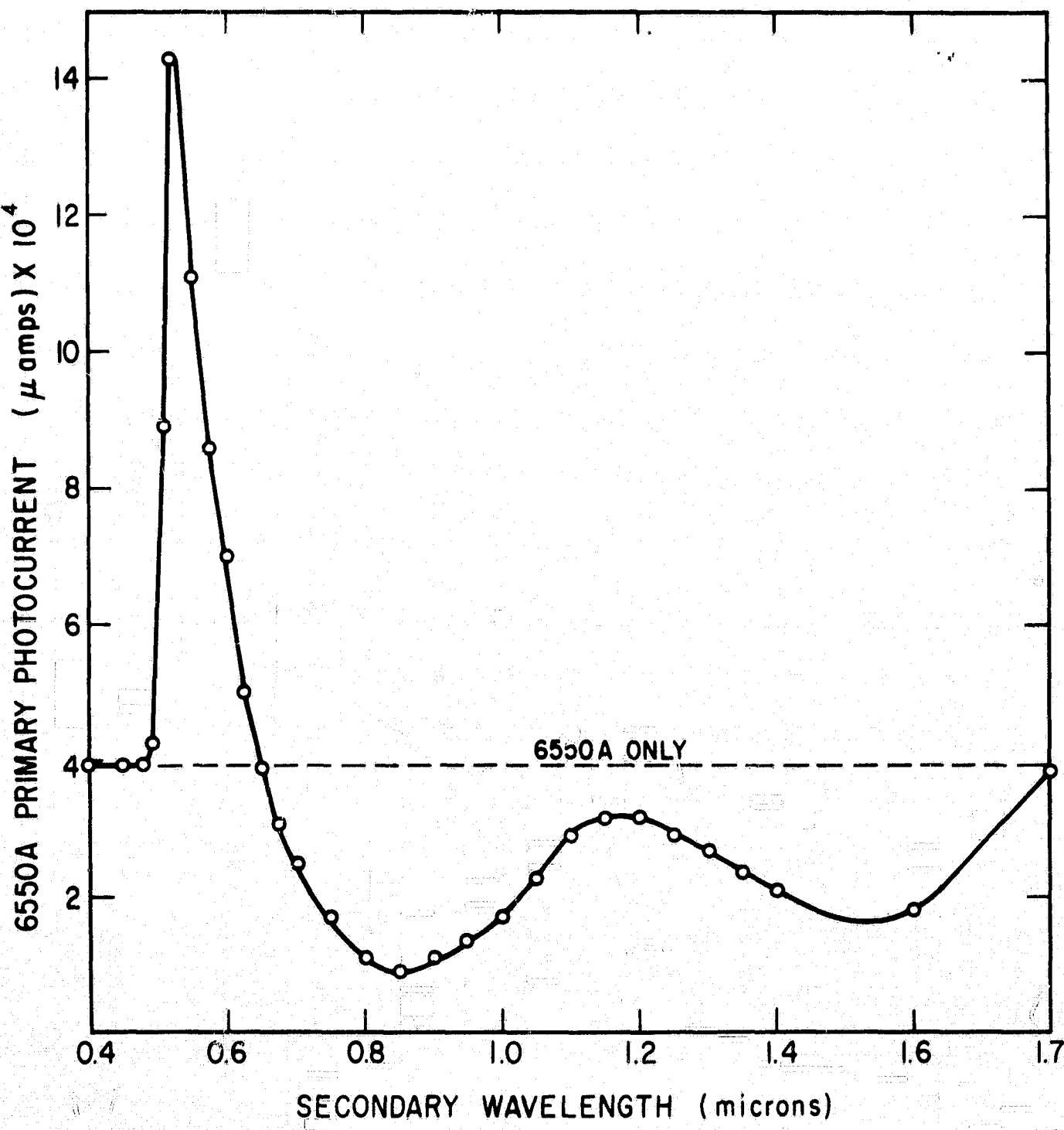

FIGURE 4.24: EFFECT OF SECONDARY ILLUMINATION ON THE CHOPPED PRIMARY (6550A) PHOTOCURRENT OF CELL # 4. PRIMARY INTENSITY = 125 μ watt/cm^2, SECONDARY INTENSITY = 300 μ watt/cm^2. BACKWALL ILLUMINATION

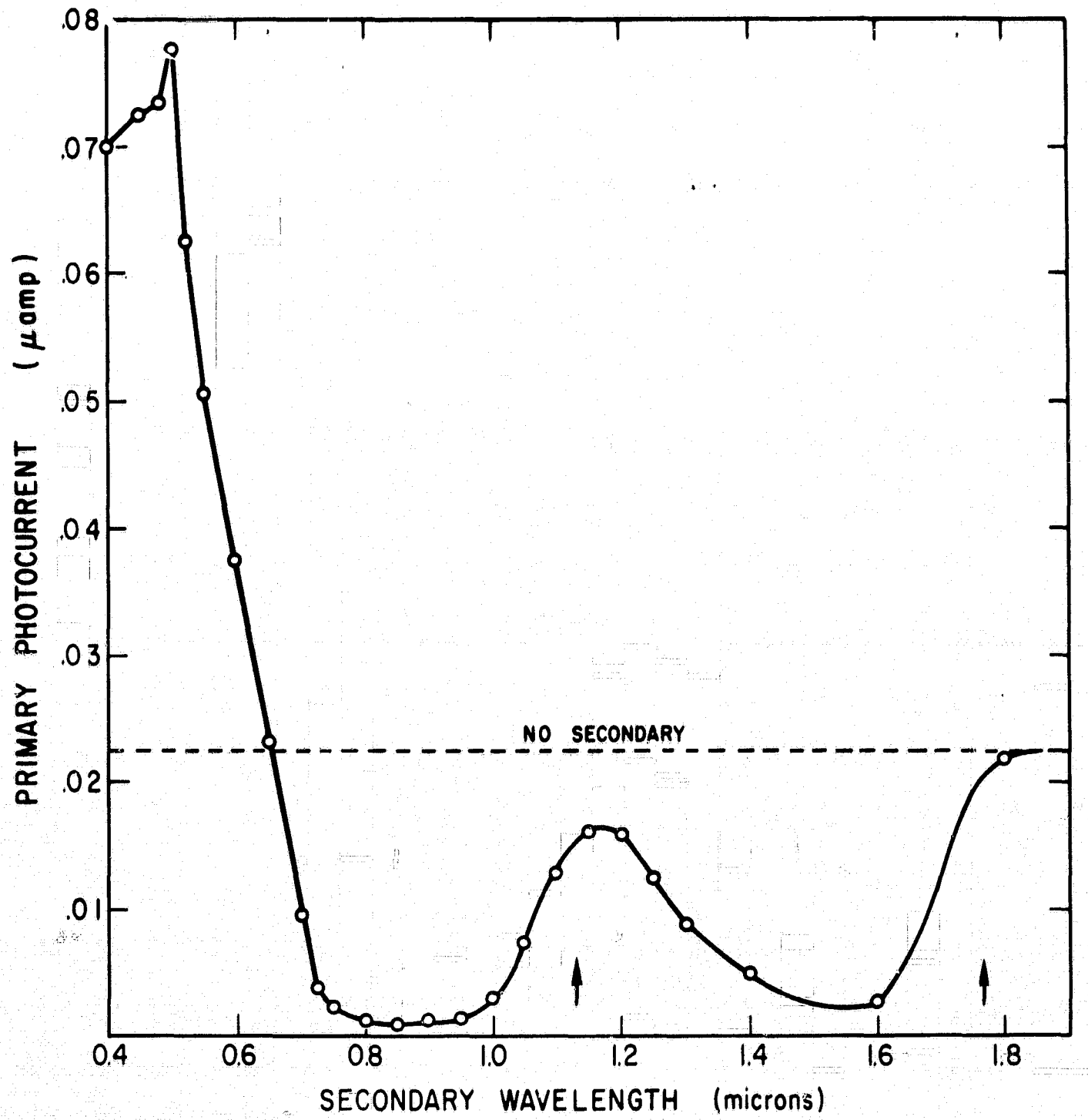

FIGURE 4.25: ENHANCEMENT AND QUENCHING OF PHOTOCURRENT ON CELL # 1. ARROWS INDICATE WHERE THE ONSET OF OPTICAL QUENCHING OCCURS IN SENSITIVE CdS CRYSTALS. BOTH 6550 A° PRIMARY AND THE SECONDARY INTENSITY WERE 300 μwatt/cm^2.

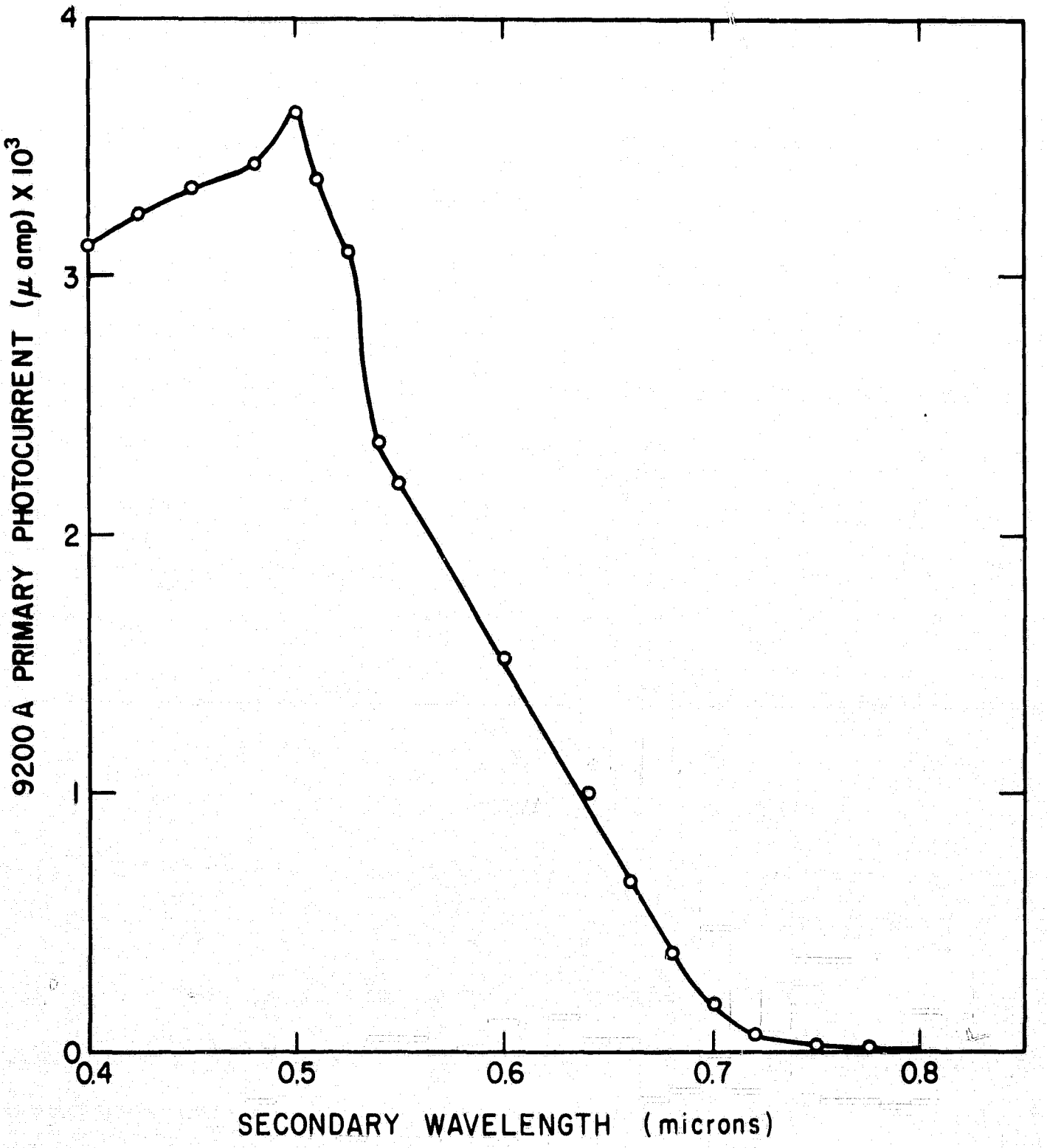

FIGURE 4.26: ENHANCEMENT OF CHOPPED 9200A RESPONSE OF CELL #1 BY SECONDARY ILLUMINATION. PRIMARY INTENSITY = 60 μ watt/cm^2 , SECONDARY INTENSITY = 300 μ watt/cm^2. WITHOUT SECONDARY ILLUMINATION 9200A RESPONSE WAS ZERO.

secondary illumination wavelength on the response to 9200 A primary light. For this cell no photoresponse was measurable at 9200 A in the absence of secondary light. Onset of the enhancement effect occurs near 8000 A.

Figures 4.27 and 4.28 are plots of enhancement and quenching seen on the evaporated CdS cell. Only the higher energy quenching band was observed in this cell. Onset of enhancement was observed at 8400 A, in excellent agreement with the changeover from quenching to enhancement seen in the transient response to one light source shown in figure 4.19.

Intensity Dependence of Enhancement and Quenching

Enhancement of the photocurrent is plotted in figure 4.29 as a function of the secondary light intensity. All the intensity measurements were made at the wavelength corresponding to maximum enhancement of the primary signal. The enhancement saturates at very low secondary illumination intensity. For example, cell #1 required only 3.5μwatt/cm^2 of 5000 A secondary light to triple the primary signal. Even in the case of longer wavelength secondary illumination, the thin film cell required only 10μwatts/cm^2 of 6000 A bias light to reach 2.5 times the base primary signal due to 300μwatt/cm^2.

Percent quenching as a function of the square root of the quenching light intensity is plotted in figure 4.30. The square root dependence fits the data for all three samples up to about 60% quenching.

The response time of the enhancement and quenching effects was dependent on the secondary light intensity. At the lower light

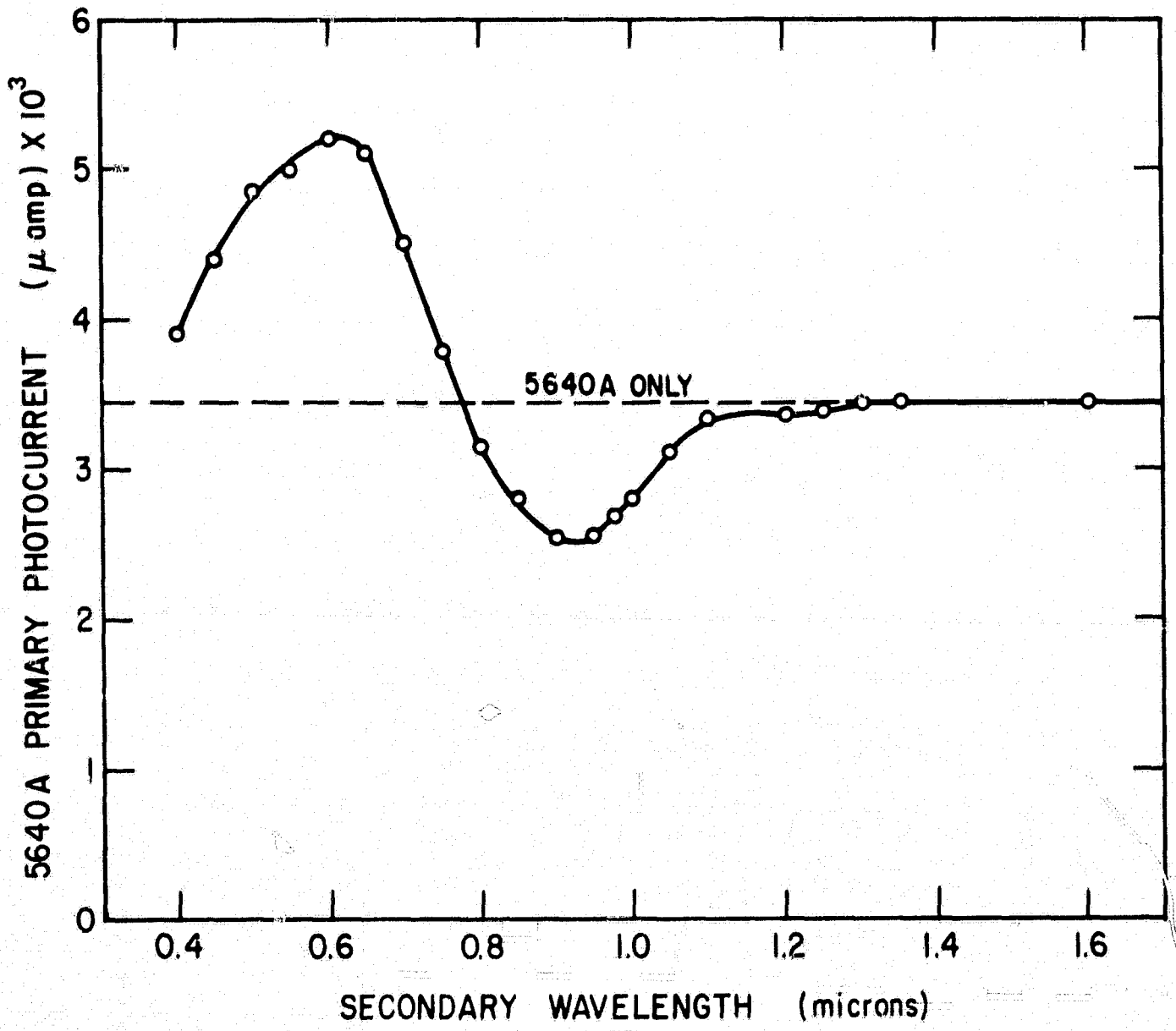

FIGURE 4.27: EFFECT OF SECONDARY ILLUMINATION ON THE CHOPPED 5640A RESPONSE OF THE EVAPORATED CdS CELL. PRIMARY INTENSITY = 6.6 μwatt/cm^2, SECONDARY INTENSITY = 300 μwatt/cm^2.

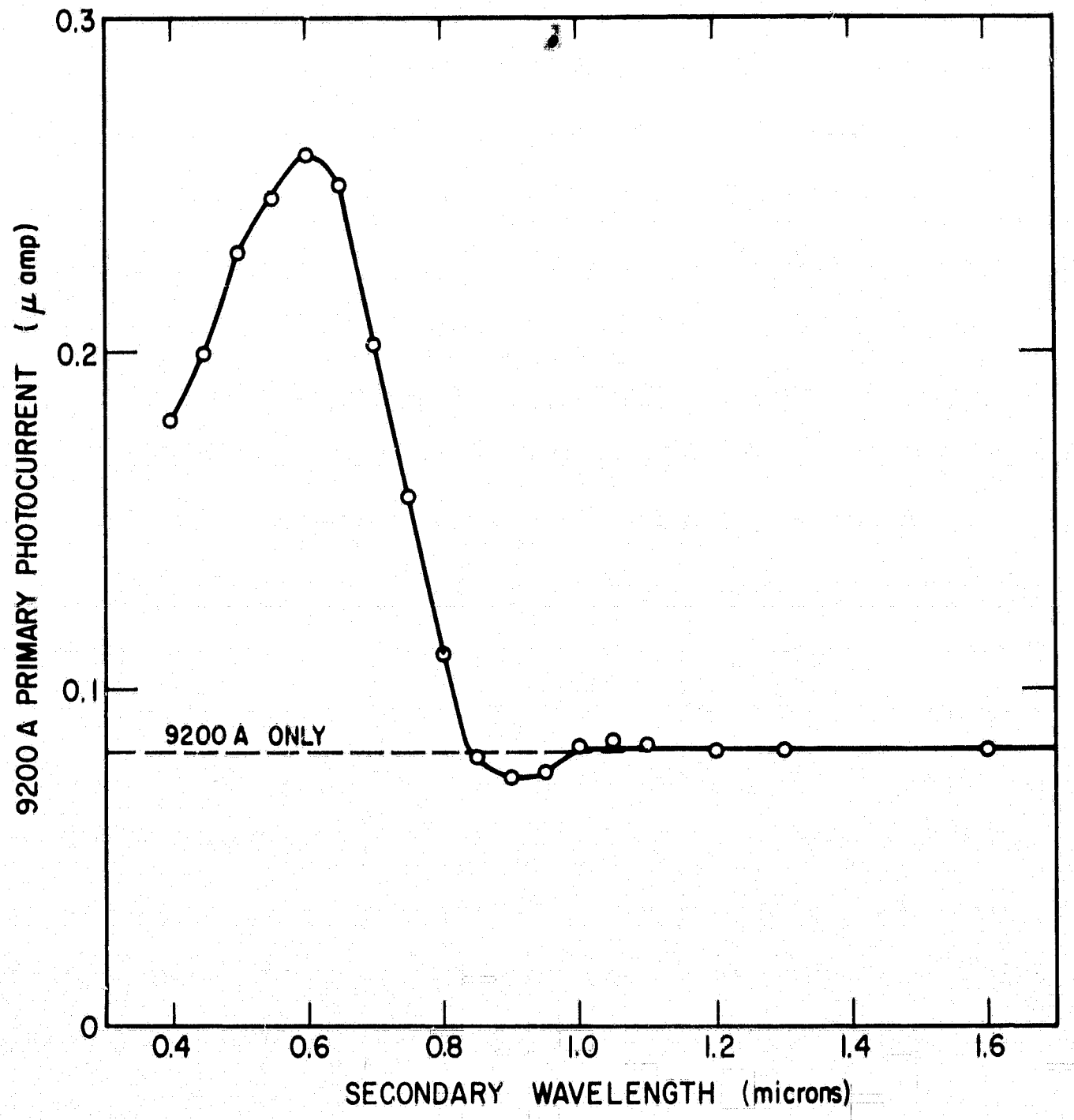

FIGURE 4.28: ENHANCEMENT OF CHOPPED 9200A RESPONSE OF THE EVAPORATED CdS CELL BY SECONDARY ILLUMINATION. PRIMARY AND SECONDARY INTENSITIES = 300 μwatt/cm^2.

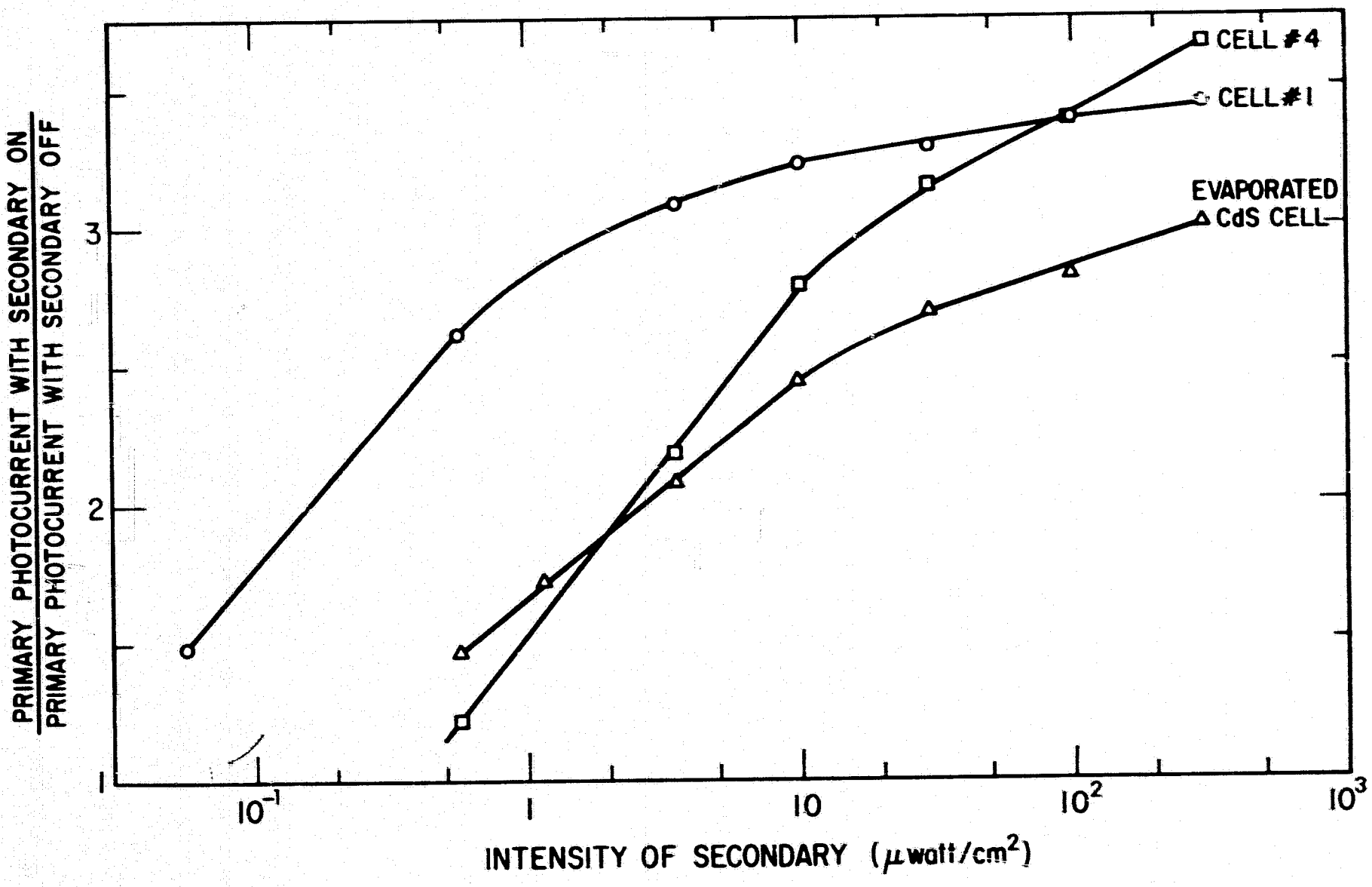

FIGURE 4.29: DEPENDENCE OF PRIMARY PHOTOCURRENT ENHANCEMENT ON THE SECONDARY INTENSITY. FOR CELLS # 1 AND # 4 PRIMARY (6550A) INTENSITY WAS 300 μwatt/cm^2 AND 125 μwatt/cm^2 RESPECTIVELY. SECONDARY WAVELENGTH WAS 5200A. FOR THE EVAPORATED CdS CELL PRIMARY (9200A) INTENSITY = 300 μwatt/cm^2 AND SECONDARY WAVELENGTH WAS 6000 A.

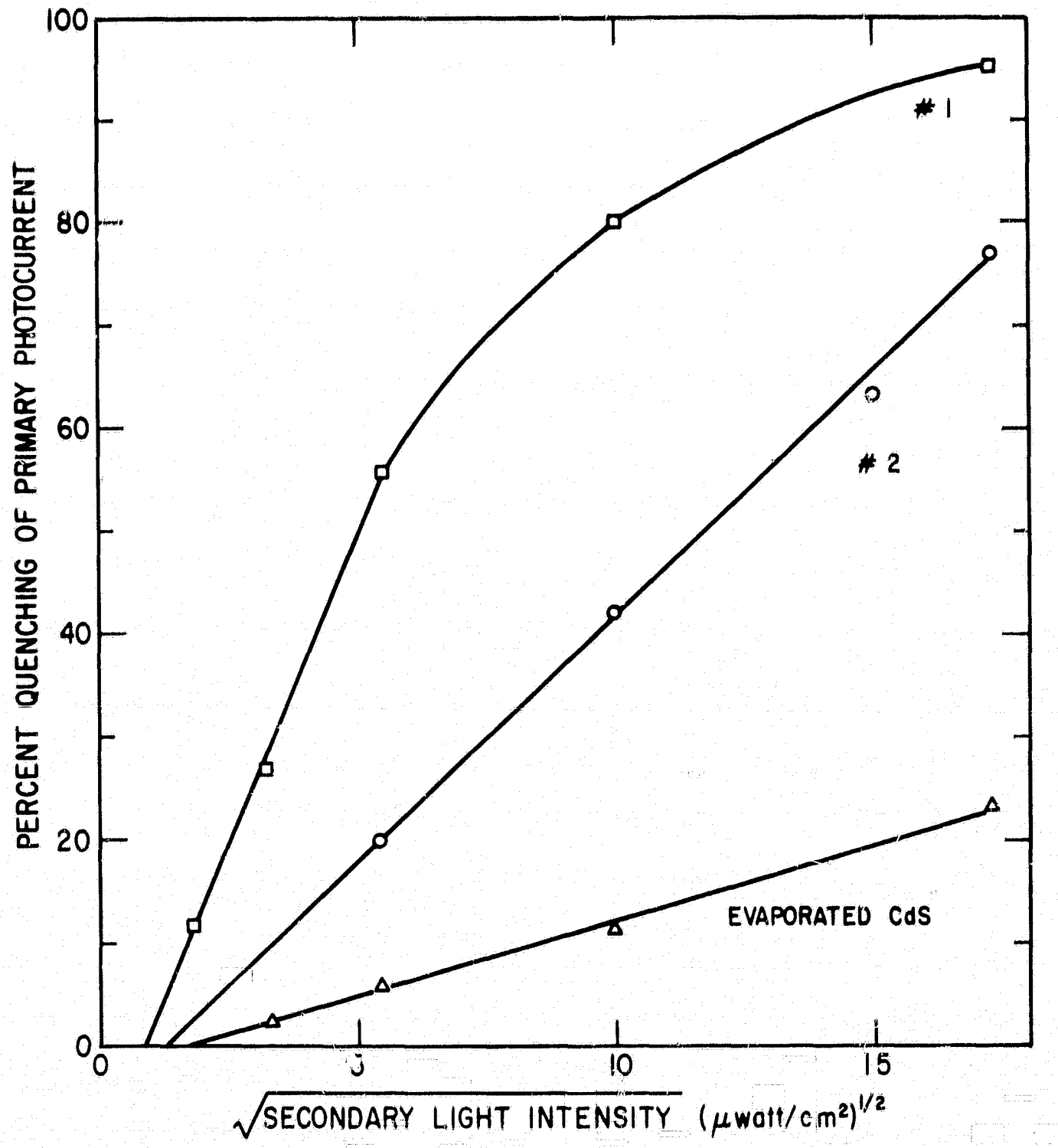

FIGURE 4.30: DEPENDENCE OF QUENCHING OF PRIMARY RESPONSE ON THE INTENSITY OF THE SECONDARY LIGHT. CELL # 1, PRIMARY (5640 A) = 125 μwatt/cm^2, SECONDARY 8500 A. CELL # 2, PRIMARY (5640 A) = 6.6 μwatt/cm^2, SECONDARY 9500 A. EVAPORATED CdS CELL, PRIMARY (6550 A) = 300 μwatt/cm^2, SECONDARY 9000 A.

intensities 15 to 20 minutes was required to obtain a steady state value of enhanced or quenched primary photocurrent. At the higher light intensities enhancement was usually not significantly greater than for a lower bias intensity, but the time required to reach the steady-state value was much shorter.

4.5 Persistence of the Enhancement Effect

The previous section described the results of simultaneous primary and secondary illumination. This section deals with the effects of a dark interval between secondary illumination and the primary illumination. Evidence for persistence of the enhancement effect was seen in figure 4.17 where interruption of the illumination resulted in no appreciable decrease in signal level when the light was turned back on. The dark decay of enhanced photocurrent was investigated by measuring the transient response to primary illumination as a function of a variable dark interval between secondary and primary illumination. The observed transient for a 15 sec delay is shown in figure 4.31. Duration of the secondary illumination was made sufficiently long that the enhancement was saturated. This was checked by measuring the initial 9000 A response for a fixed short dark delay while varying the duration of the secondary illumination interval. At the wavelength and intensity being used, 1 second of secondary illumination was sufficient to saturate the enhancement effect. The observed decay of the primary response depends on the intensity of the primary light source. Interruption of the primary signal was made to show the fast response of the primary photosignal and the negligible decay of the enhancement

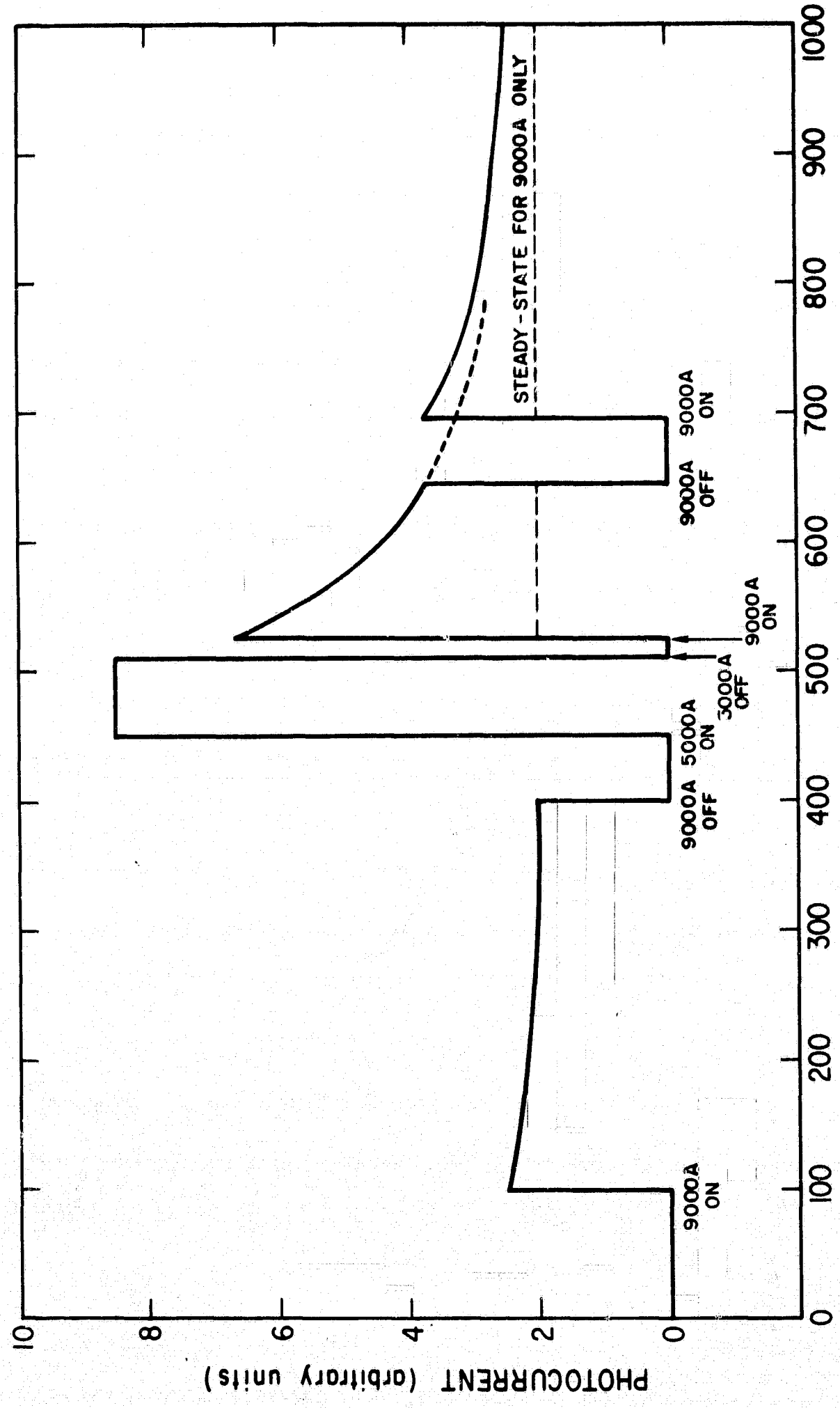

FIGURE 4.31: PHOTOCURRENT TRANSIENTS SHOWING THE EFFECT OF 5000 A PRE-ILLUMINATION ON THE 9000 A RESPONSE. CLEVITE EVAPORATED CdS CELL.

in the dark.

Measurement of the initial primary photocurrent as a function of the dark delay interval is shown in figure 4.32 for cell #2. The steady-state primary photocurrent with no secondary illumination and with simultaneous secondary illumination are indicated on the figure. The initial enhanced photocurrent fits an equation of the form

$$I = A - B \ln(t+t_o) \tag{4.3}$$

where I is the primary photocurrent, t is the dark delay interval, A, B and t_o are constants. For the data shown in figure 4.32 a value of t_o = 10 sec fits all the experimental points to the dashed line. Equation (4.3) has the same form as the Elovich equation used to describe photochemisorption processes on many semiconductors.[72,73] For this reason, the effect of the ambient on the enhancement process and its decay was investigated. The sample was subjected to long illumination in both vacuum and nitrogen ambient with no change in the magnitudes or rates of the observed effects.

The temperature dependence of the dark decay of the enhancement was measured for cell #1. The results of measurements taken between T = 295°K and 372°K are shown in figures 4.33 and 4.34. In figure 4.33, the initial enhanced response after one minute of strong short wavelength bias illumination is plotted for three dark delay intervals. The point at 120 seconds delay on the 372°K curve was higher than expected from the initial decay rate because the unenhanced 8000 A photoresponse at this temperature was only slightly less than the decayed signal,

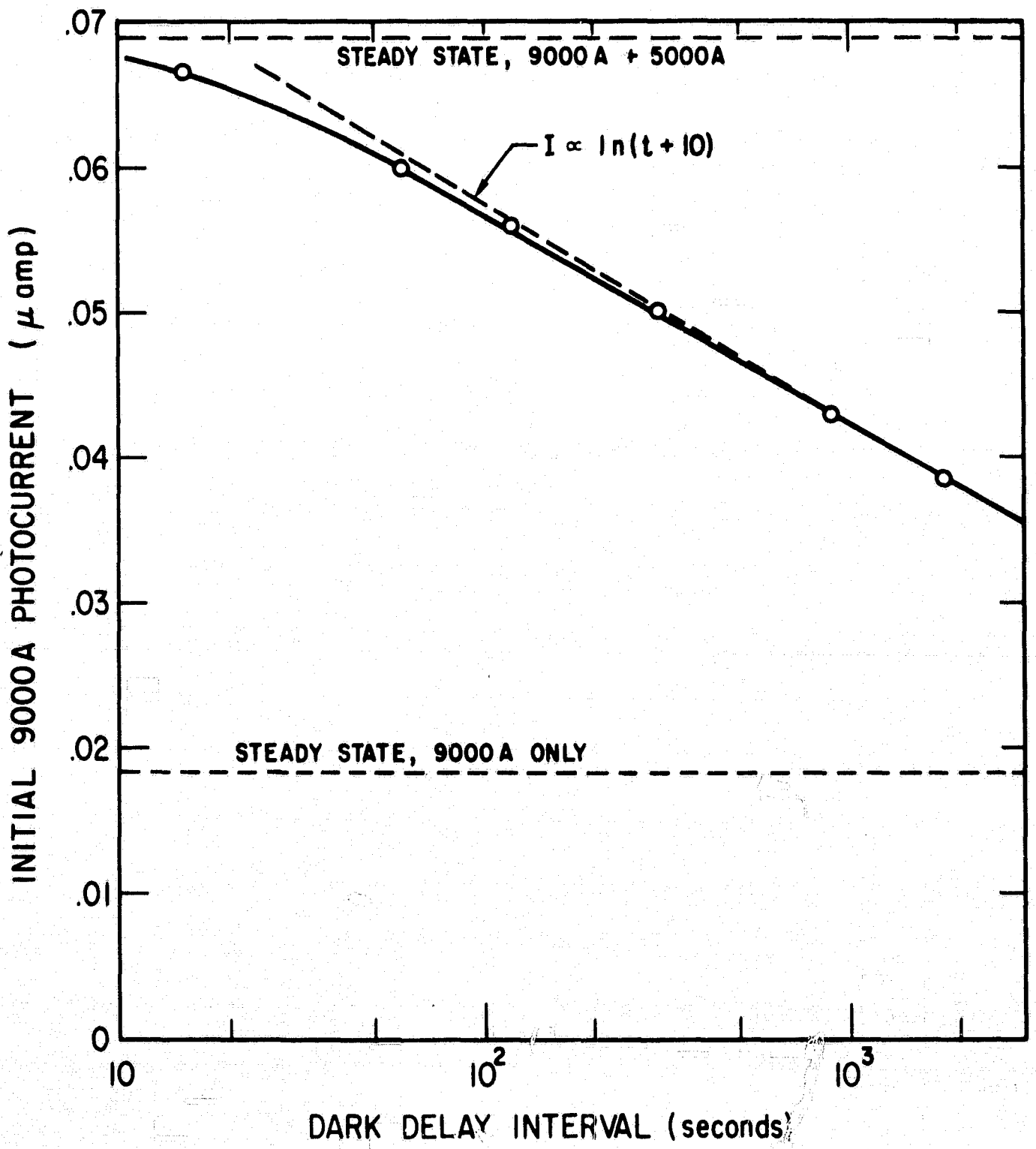

FIGURE 4.32: INITIAL 9000 A RESPONSE VERSUS DARK DELAY TIME AFTER SWITCHING OFF 5000 A ENHANCING RADIATION.

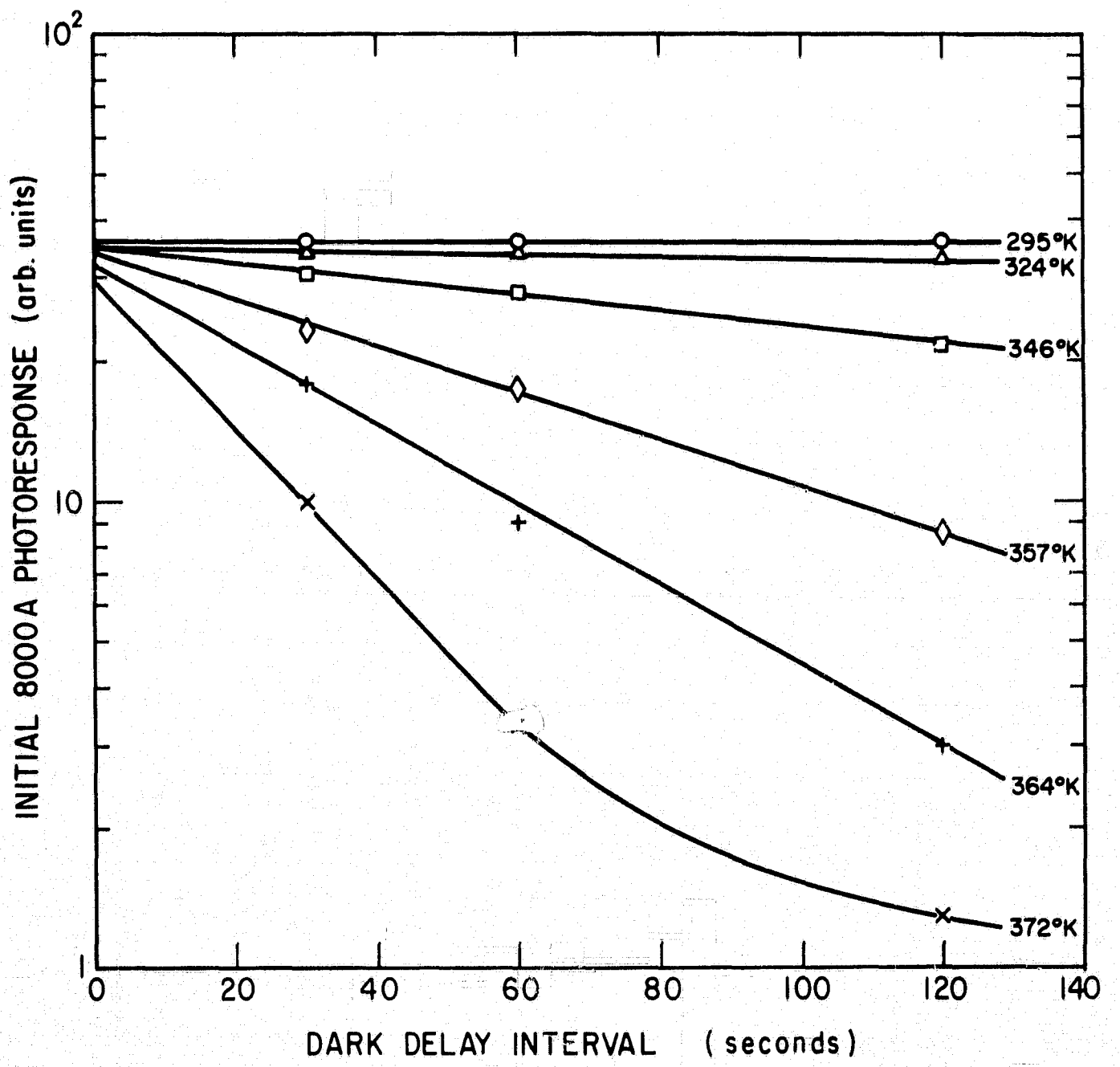

FIGURE 4.33: INITIAL 8000 A PHOTORESPONSE OF CELL # 1 VERSUS DARK DELAY TIME AFTER ILLUMINATION WITH ENHANCING RADIATION.

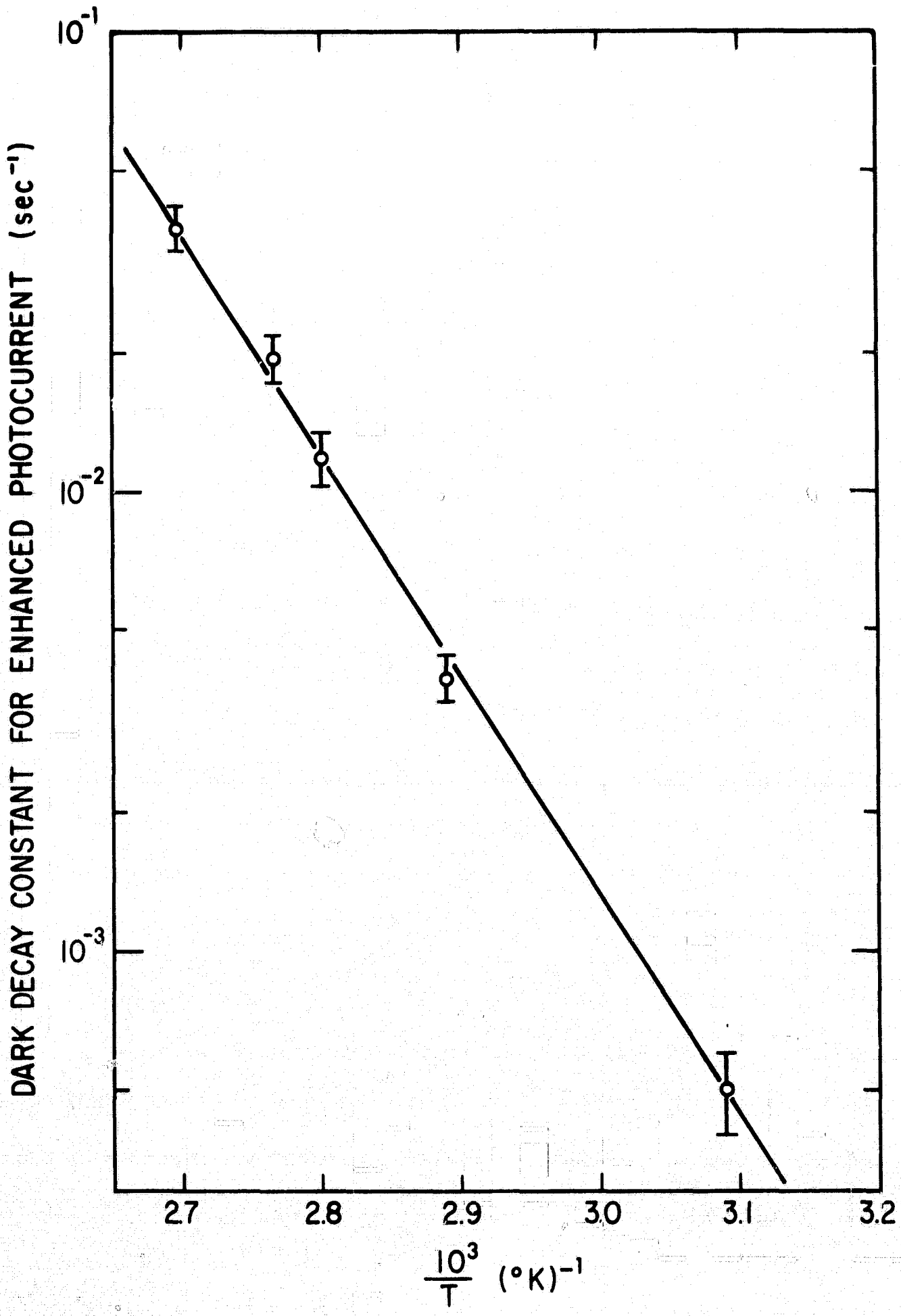

FIGURE 4.34: TEMPERATURE DEPENDENCE OF THE DARK DECAY CONSTANT FOR THE ENHANCED 8000A PHOTORESPONSE OF CELL # 1.

i.e. after about 100 seconds the decay is virtually complete at this temperature. In figure 4.34 the exponential decay constant taken from figure 4.33 is plotted against reciprocal temperature. The exponential nature of this plot suggests an activated process with a characteristic energy of 0.95 eV. The measurement of dark decay rate as a function of temperature is a measure of the thermal quenching of the enhanced photoresponse. The 0.95 eV activation energy should be a measure of the energy required to thermally excite trapped holes from the neutralized acceptor states to the valence band of the CdS. This energy is to be compared with the 1.1 eV energy required for optical quenching of the photoresponse.

An estimate of the capture cross-section for free holes of the level responsible for enhancement is possible from the data of figure 4.34. The rate constant for thermal emptying of the level is[74]

$$\text{rate constant} = N_v S_p v \exp[-E/kT) \ , \qquad (4.4)$$

where N_v is the valence band effective density of states, S_p is the capture cross-section for free holes, v is the thermal velocity of a hole in the valence band, and E is the energy of the level above the valence band edge. If the dark decay constant of figure 4.34 is assumed to be equal to the rate constant of equation (4.4), S_p can be determined from the intercept at $T = \infty$ which has the value $N_v S_p v = 2.5 \times 10^{11}$ sec^{-1}. Putting $N_v = 10^{19}$ cm^{-3} and $v = 10^7$ cm/sec, results in a value $S_p = 2.5 \times 10^{-15}$ cm^2 for the hole capture cross-section.

V. LIGHT MICROPROBE RESULTS

5.1 Minority Carrier Diffusion Lengths

The hole diffusion length in CdS and the electron diffusion length in Cu_2S were measured directly using the light microprobe to inject the minority carriers. Because of the short diffusion lengths expected for both materials, angle-lapped junction techniques were used in all but one sample where a cleaved surface perpendicular to the junction plane was examined. The measurement technique was described in section 3.6. The solutions appropriate to the geometries of these samples were given in section 2.2. Figure 3.4 showed the geometries of samples for both positive and negative bevel angles.

Figure 5.1 shows the result of a light microprobe scan across a junction bevelled to -5°. The solid lines represent the data corrected for the photosignal caused by scattered light. On the Cu_2S side of the interface the minority carriers diffuse through the 5° wedge of Cu_2S to the collector junction. The diffusion length is obtained from the expression

$$L_n = - \frac{\sin \theta}{d(\ln I)/dx} . \qquad (5.1)$$

From the slope of the solid line on the Cu_2S side of figure 5.1, L_n is found to be 3×10^{-5} cm. On the CdS side of the junction, the

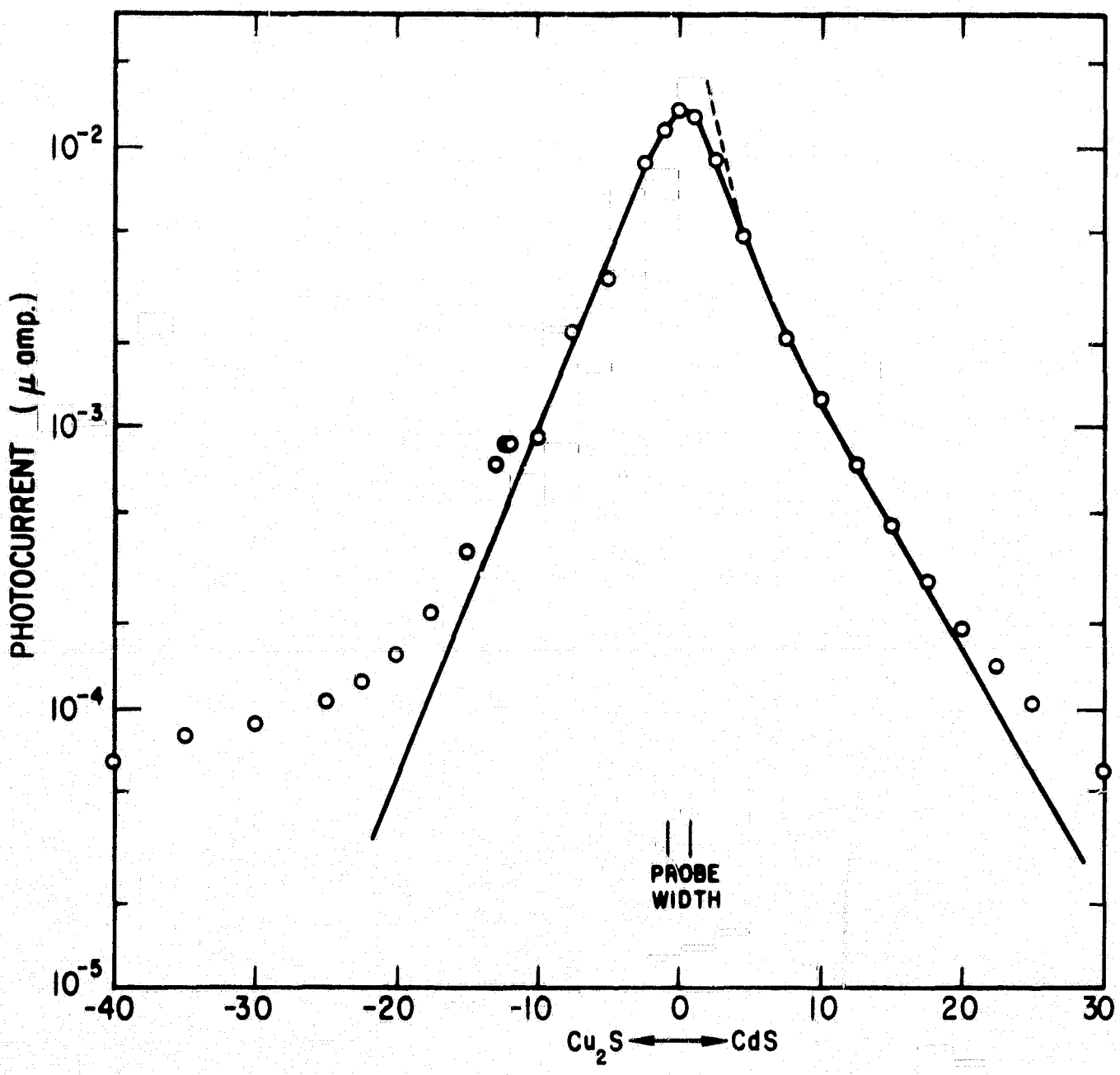

FIGURE 5.1: PHOTOCURRENT VERSUS LIGHT PROBE POSITION ACROSS A -5° ANGLE-LAPPED JUNCTION (CELL # 5). THE SOLID LINES ARE DATA CORRECTED FOR SCATTERED LIGHT. THE DASHED LINE IS THE THEORETICAL CURVE GIVEN BY EQUATION 5.3.

geometry for light injected hole diffusion is quite different from the Cu_2S side. In the CdS, the collected carriers must diffuse parallel to the surface to the intersection of the junction plane and the surface. The diffusion away from the line source has cylindrical symmetry resulting in an expression for the hole diffusion in terms of Hankel functions with imaginary arguments,

$$L_p = \frac{H_1^{(1)}(ix/L_p)}{iH_o^{(1)}(ix/L_p)} \frac{1}{\frac{d(\ln I)}{dx}} \tag{5.2}$$

where x is the light probe distance from the junction, and I is the photocurrent. The diffusion length is obtained from the measurement of the slope of the experimental curve at some distance x from the interface. The value of the Hankel function is obtained from tables using an estimated value of L_p obtained by assuming the photocurrent decreases exponentially. One or two iterations are sufficient to obtain a self-consistent value of L_p. A value of 6.0×10^{-4} cm was obtained for this sample. Using this value of L_p, a theoretical curve for the photocurrent J_p can be fitted to the experimental curve. The dashed curve in figure 5.1 is the theoretical curve given by

$$J_p = A\, H_1^{(1)}\,(ix/L_p)\ , \tag{5.3}$$

where A is a coefficient independent of x (see equation (2.23)). The discrepancy between theory and experiment is expected at short distances due to the finite width of the light line.

The results obtained on cell #6 with a -2° bevel angle are shown in figure 5.2. Using the same analysis discussed above an upper limit on the electron diffusion length in Cu_2S was found to be 1×10^{-5} cm. The hole diffusion length on the CdS side was found to be 5.5×10^{-4} cm. On the Cu_2S side the diffusion length was less than the lower limit for use of this microprobe system since both the width of the light line and the depth of penetration of light become comparable to the diffusion length.

Figure 5.3 shows the results of a light microprobe scan across a junction bevelled to +5°. The diffusion length on the Cu_2S side is not measurable for positive bevel angle samples. The photocurrent increased rapidly in a distance equal to the width of the light line as the interface was approached from the p-side. A slowly increasing or almost constant photocurrent was then measured as the spot was moved away from the interface on the CdS side. Beyond about 40 microns, the photocurrent decreased exponentially. The presence of the 40 micron wide constant current region makes analysis of the diffusion length difficult. The bulk depletion width for this sample was 0.2 microns which would result in a flat response for only 6 microns. The wide constant current region is thought to be due to surface damage caused by the bevelling, resulting in a widened space charge region near the surface. Since the edge of the space charge region is considered to be the collector for diffused minority carriers, widening at the surface has the effect of increasing the angle between the surface and the current collector. The collected diffusion current will therefore be very sensitive to the nature of the transition from

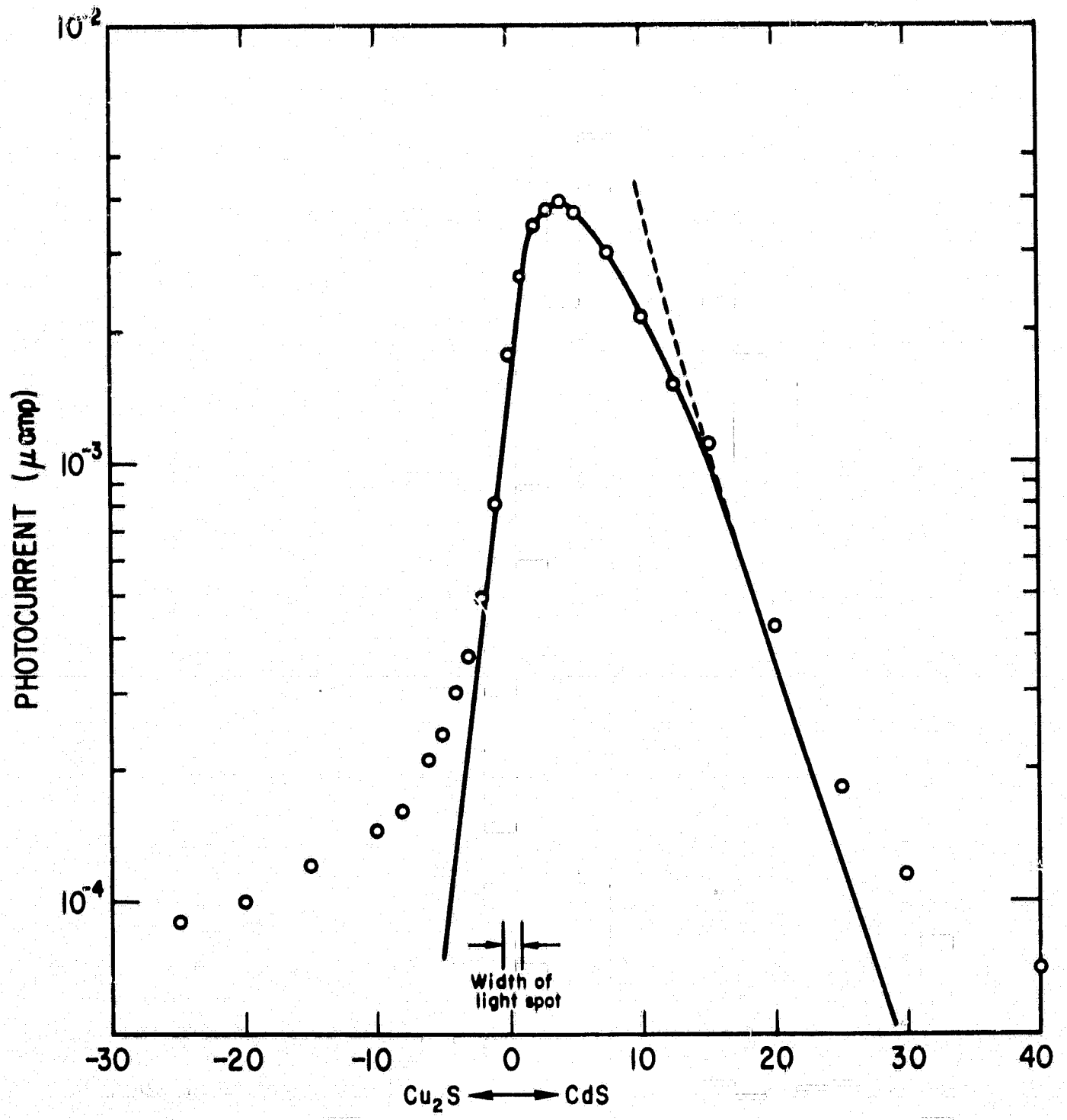

FIGURE 5.2: PHOTOCURRENT VERSUS LIGHT PROBE POSITION ACROSS A -2° ANGLE-LAPPED JUNCTION. (CELL # 6). THE SOLID LINES ARE DATA CORRECTED FOR SCATTERED LIGHT. THE DASHED LINE IS THE THEORETICAL CURVE GIVEN BY EQUATION 5.3.

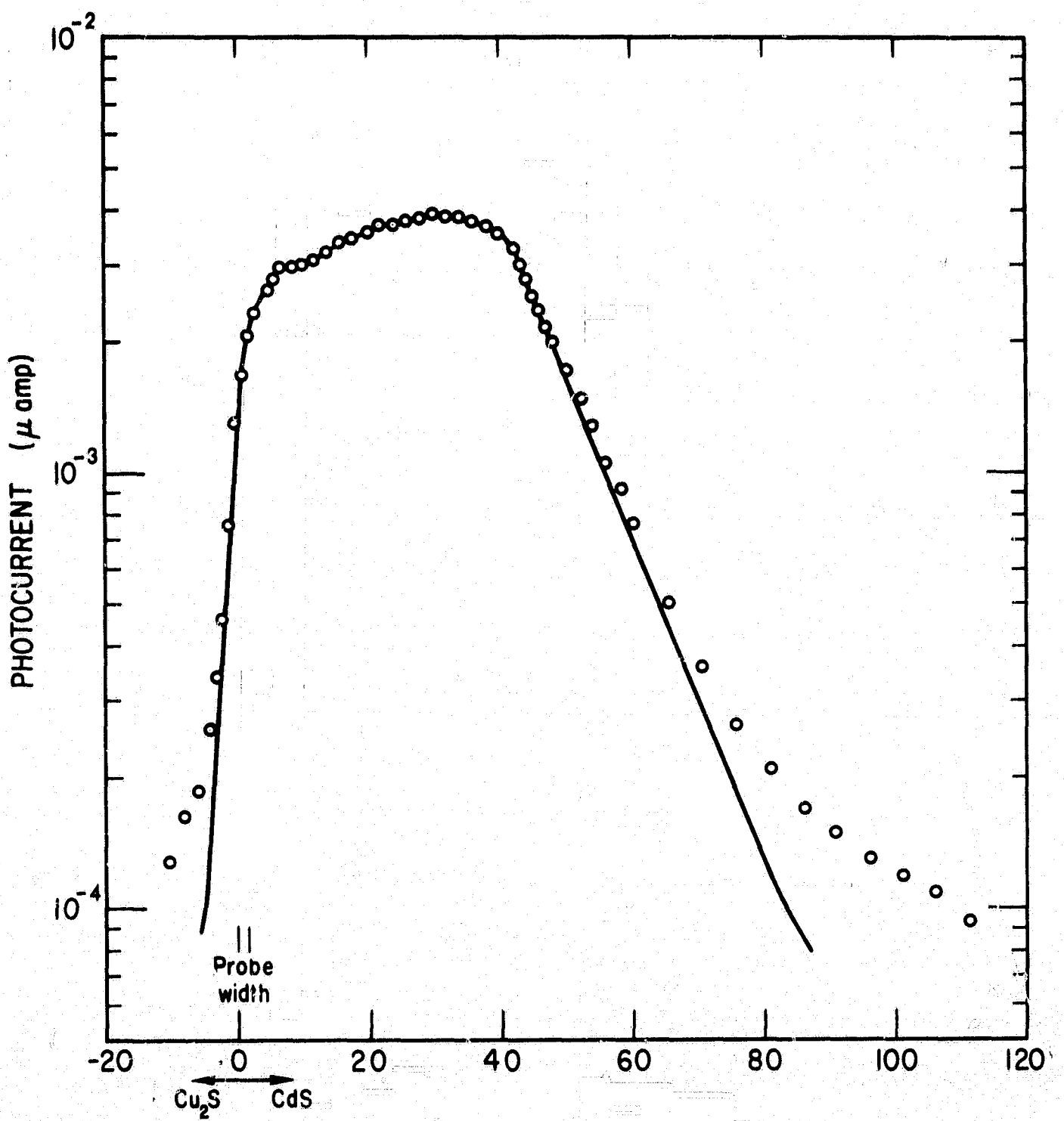

FIGURE 5.3: PHOTOCURRENT VERSUS LIGHT PROBE POSITION ACROSS A +5° ANGLE-LAPPED JUNCTION (CELL # 9). THE SOLID LINES ARE DATA CORRECTED FOR SCATTERED LIGHT.

bulk to surface width of the space charge region. The angle θ to be used in calculating L_p can have any value between 5° and 90°. If $\theta = 5°$ is used, $L_p = 1.0 \times 10^{-4}$ cm is the diffusion length. If diffusion is along the surface to the edge of the surface depletion region ($\theta = 90°$) then $L_p = 1.2 \times 10^{-3}$ cm. The true result is probably between these extremes, a possibility made more plausible by the results obtained on other crystals where the geometry was well-defined. These crystals all have measured hole diffusion lengths in the range 3×10^{-4} to 6×10^{-4} cm.

As will be discussed in the following section, most of the bevelled samples (both positive and negative angles) had wide regions across which the photocurrent remained approximately constant before decreasing sharply far away from the junction on the CdS side. A measurement of the hole diffusion length in CdS on a sample free from the surface damage due to bevelling was desirable. Since a suitable etchant capable of removing the damaged layer without creating a step at the interface could not be found, it was decided to attempt measurements on a cleaved surface. For the hexagonal CdS structure the prismatic planes are known to be good cleavage planes. A crystal was cleaved to expose a $(12\bar{1}0)$ plane. The sample was dipped to form a thin (1μ) Cu_2S layer on the cleaved surface. The cell was then cleaved again along a $(10\bar{1}0)$ plane which was at 90° to the first cleavage. A photograph of the cleaved surface on which diffusion length measurements were made is shown in figure 5.4. The result of a light microprobe scan perpendicular to the dipped surface is shown in figure 5.5. The inset is a sketch showing the region of the crystal scanned and may

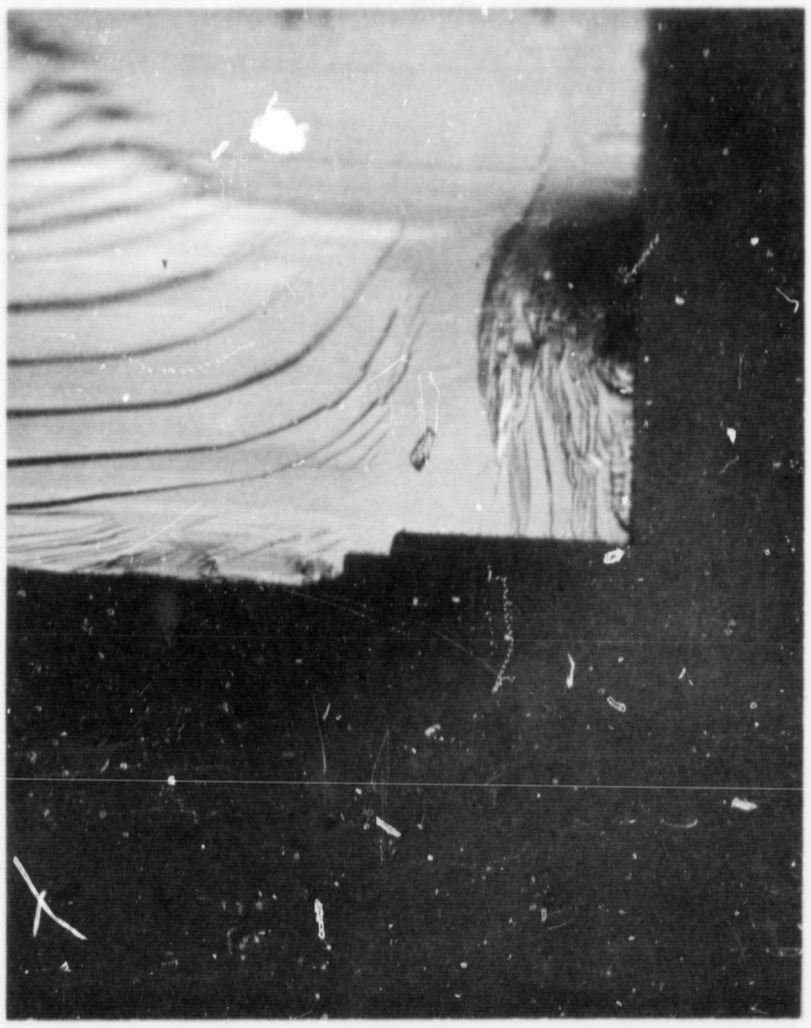

FIGURE 5.4: PHOTOGRAPH OF THE CLEAVED SURFACE OF CELL # 7. THE JUNCTION PLANE IS PERPENDICULAR TO THE PLANE OF THE PAPER AT THE HORIZONTAL EDGE OF THE CRYSTAL. MAGNIFICATION WAS X 200.

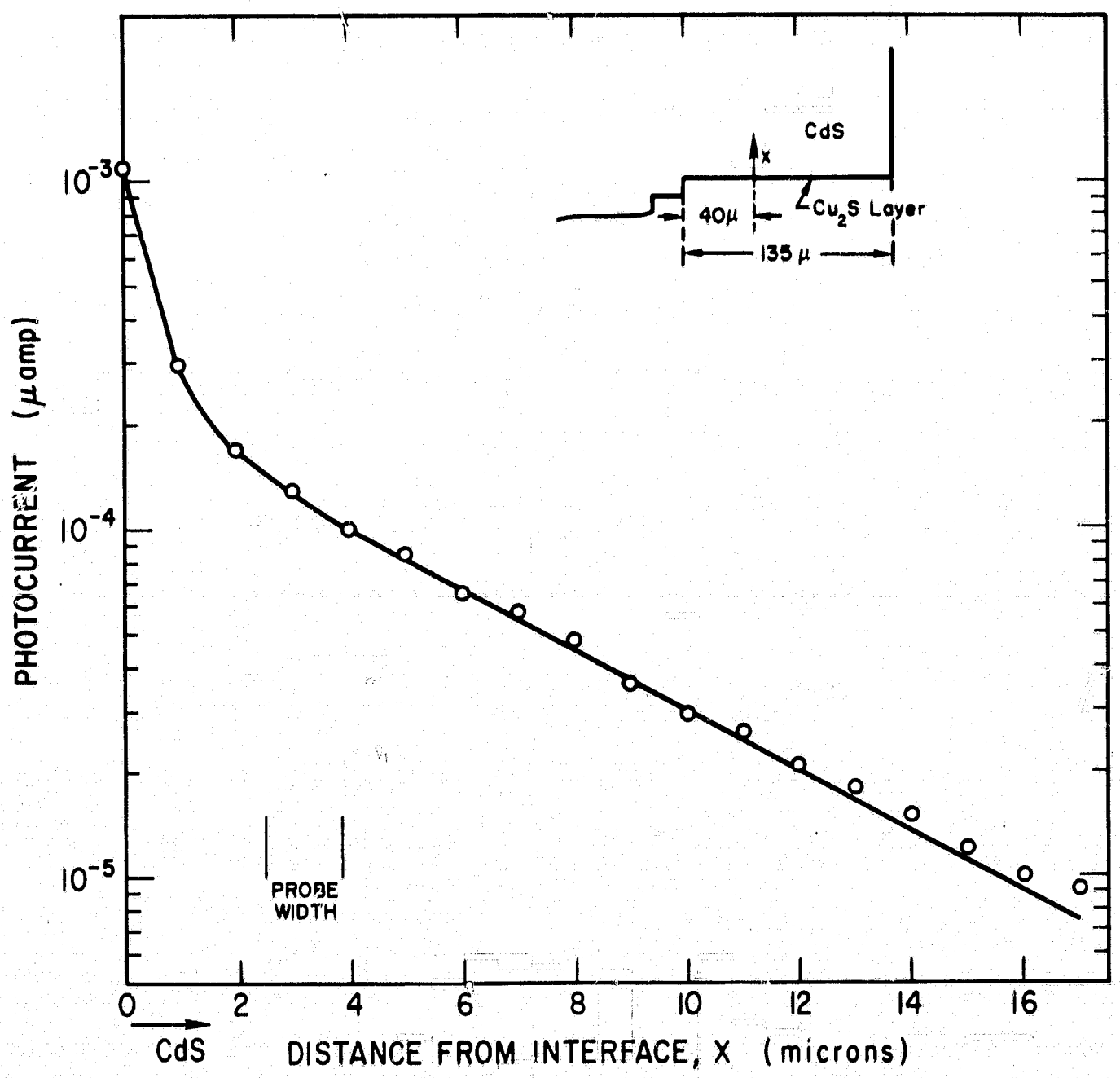

FIGURE 5.5: PHOTOCURRENT VERSUS LIGHT PROBE POSITION ON CELL # 7. THE SOLID LINE IS DATA CORRECTED FOR SCATTERED LIGHT.

be compared with figure 5.4. For the 90° angle between surface and junction, the collector is a semi-infinite plane, and the diffusion length can be quite accurately obtained from the reciprocal of the slope of the ln photocurrent vs distance plot. A value of $L_p = 5 \times 10^{-4}$ cm is measured. The deviation from linearity at very small distances from the junction is due to departure from the exponential approximation which is good at distances greater than the diffusion length, and presumably due to decreased surface recombination losses for carrier injection in the space charge region at the interface. An upper limit on the surface recombination velocity of 10^3 cm/sec is obtained by comparison of the experimental results with the theoretical curves of van Roosbroeck[52] calculated for this geometry. Using the measured diffusion lengths, minority carrier lifetimes may be calculated from $\tau = L^2/D$. For Cu_2S, the appropriate diffusion coefficient D_n or the electron mobility from which it can be calculated are unknown. Hence the lifetime cannot be determined. The hole mobility is known from Hall measurements to be about 20 cm^2/V-sec.[26] If the electron mobility is assumed to be comparable, an order of magnitude estimate of the electron lifetime can be obtained. This crude estimate gives a value of 10^{-9} seconds for the electron lifetime in Cu_2S. On the CdS side, the diffusion coefficient for holes is known to be 0.4 cm^2/sec from mobility measurements.[75] Using the value of $L_p = 5.0 \times 10^{-4}$ cm from cell #7, the hole lifetime is 6.2×10^{-7} seconds.

The results of diffusion length measurements on six cells are given in Table 5.1.

Table 5.1

Results of Diffusion Length Measurements

Cell	Geometry	L_p (cm)	τ_p (μsec)	L_n (cm)
#3	-5° bevel	4×10^{-4}	0.4	2×10^{-5}
#5	-5° bevel	6×10^{-4}	0.9	3×10^{-5}
#6	-2° bevel	5.5×10^{-4}	0.76	$\leq 1 \times 10^{-5}$
#7	90° cleaved	5.0×10^{-4}	0.62	--
#8	-5° bevel	$\simeq 6 \times 10^{-4}$	0.9	--
#10	-5° bevel	3×10^{-4}	0.22	2×10^{-5}

The minority carrier diffusion lengths and lifetimes measured in the CdS may be compared with the values found in the literature. Diffusion lengths between 1×10^{-4} and 2×10^{-3} cm have been measured using the diffusion of photoconductivity.[76] Cathodoconductivity measurements by Bleil et al.[77] have resulted in hole diffusion lengths as high as 10^{-3} cm in very pure crystals. Spear and Mort[75] measured the hole lifetime and drift mobility from which a diffusion length of 4×10^{-4} cm is calculated. Using the photoelectromagnetic (PEM) effect on insulating crystals Sommers et al.[78] measured diffusion lengths of about 5×10^{-4} cm. Analysis of photoconductivity under strong excitation and measurements of the PEM effect by Maeda and Kasami[79] result in values of hole diffusion length equal to 3×10^{-4} cm in undoped insulating crystals. A review of other measurements given by Broser[80] show a range from 10^{-5} to 10^{-3} cm for the hole diffusion length in pure CdS crystals. Palz and Ruppel[81] determined hole lifetimes to be between 10^{-8} and 10^{-14} seconds from analysis of the photovoltaic effect at metal-CdS contacts. However, these measurements were made on Cu-doped and In-doped crystals. The results shown in Table 5.1 are in good agreement with the values obtained by other methods on undoped CdS crystals.

Reliability of the Diffusion Length Measurements

The direct measurement of diffusion lengths less than about 10 microns is difficult because the techniques used introduce many possible errors. Carrier diffusion takes place very near the surface for any sample geometry and may be expected to be very sensitive to

surface damage. Surface recombination affects have been neglected in these measurements. If the surface recombination velocity is less than 10^3 cm/sec as indicated by the results on cell #7, the measured diffusion lengths will not be seriously affected by this neglect.

Geometric errors in bevel angles, etc., could be quite well controlled except for regions very close to the junction. Here, because of difference in hardness of the two materials comprising the heterojunction, slight steps, chipping at the ends of thin wedges, or other faults with micron dimensions become possible sources of error which are not easily detected.

Scattered light from internal reflections in the optical system, lens aberrations, light scattered at the surface of the sample, and reabsorption of luminescent light, contribute a background signal which is difficult to suppress below a few percent of the maximum signal. Corrections have been made to the data at the larger distances from the junction. In all cases, reasonably long segments of the curves are not significantly affected by scattered light so that the corrections serve mainly to extend the useful portion of the data.

On the Cu_2S side, where $L_p \leq 3 \times 10^{-5}$ cm, the width of the light spot and the depth of penetration of the light both become serious limitations to accurate measurement. That the diffusion length in the Cu_2S must be of about this magnitude is supported by indirect evidence from the efficiency and spectral response of this type of cell. Efficient long wavelength response of these heterojunctions depends on optical absorption in the Cu_2S film. It has been found that a Cu_2S film thickness of about 0.3 microns results in maximum cell

efficiency.[68] If the diffusion length were much shorter than the measured value, it would be difficult to understand the high efficiency of these cells. If the diffusion length were much longer, improved long wavelength response would be expected with somewhat thicker films.

On the CdS side of the junction the advantages of angle-lapped junctions have not been realized because of the wide surface depletion regions. Measurement of a 5×10^{-4} cm diffusion length with a 1.3×10^{-4} cm wide light spot is fairly marginal. The intensity profile of the microprobe line would be useful in evaluating the short diffusion lengths. Fortunately the results obtained on the Cu_2S side of the junction provide an excellent check on the width of the light probe. The asymmetry observed on most scans removes any doubt that the measured diffusion lengths were adversely affected by light spot size effects.

In concluding this section estimates are made of the reliability of the measured diffusion lengths. These estimates are based on possible errors introduced experimentally, through corrections for scattered light, and by approximations in the analysis for each geometry. Possible errors due to neglect of surface recombination effects are not included. For Cu_2S, only three cells yielded a measurable diffusion length. These measurements give values of electron diffusion length between $\leq 1 \times 10^{-5}$ cm and 3×10^{-5} cm ±25%. The efficiency of long wavelength spectral response gives reason to believe that this value is representative of the electron diffusion length of Cu_2S films formed on CdS cells. For CdS the hole diffusion length measured on the cleaved cell #7 is considered the most reliable. A value of

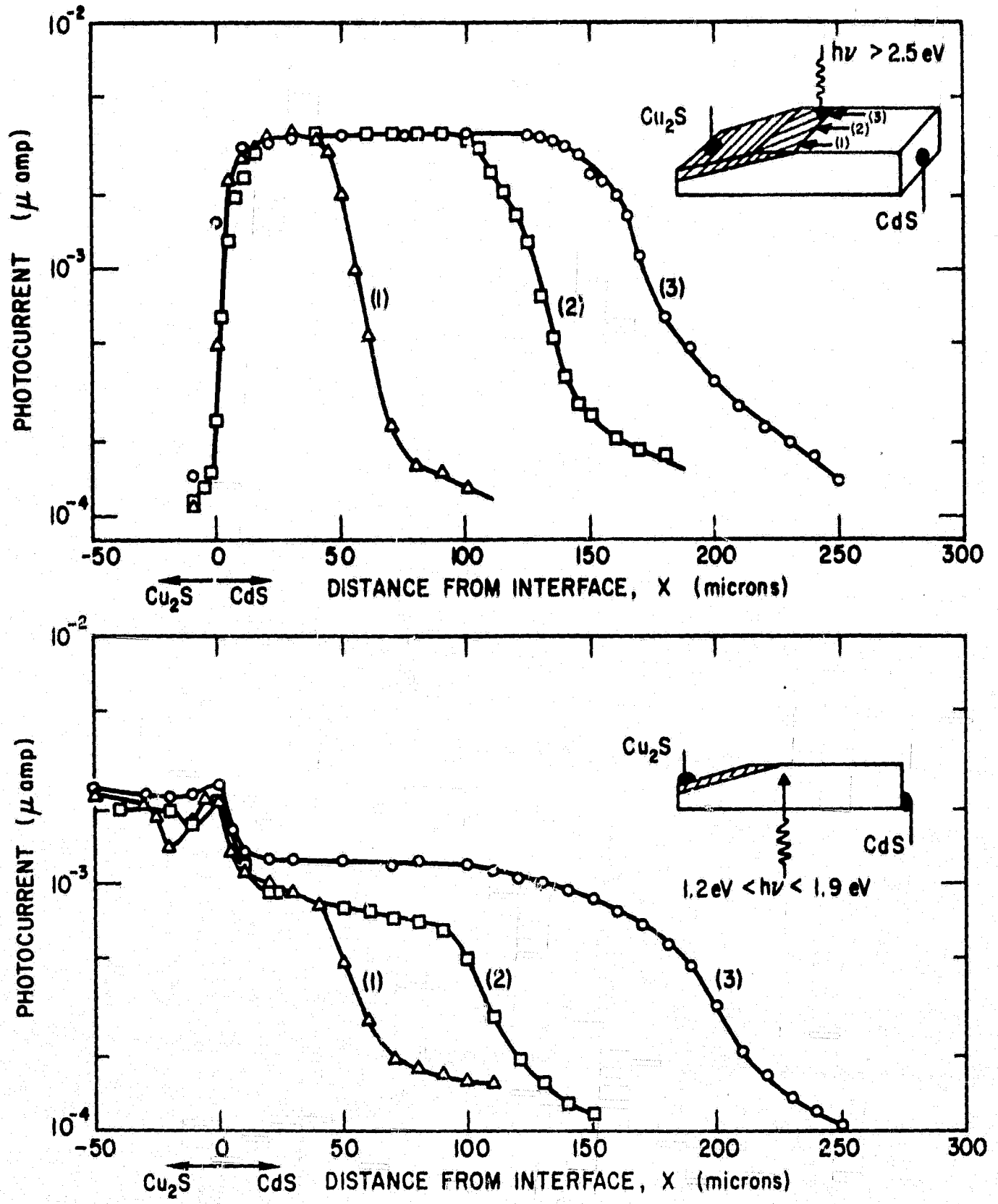

FIGURE 5.6: PHOTOCURRENT VERSUS LIGHT PROBE POSITION ACROSS A -5° ANGLE-LAPPED JUNCTION (CELL # 8).

$L_p = 5.0 \times 10^{-4}$ cm ±10% was obtained. The results of measurements on six cells of undoped, low resistivity CdS were within 40% of this value.

5.2 Wide Depletion Layers

Mention was made in the previous section of the presence of apparent wide depletion layers at the surface of bevelled junctions. In this section, the results of further investigation of these regions are presented and discussed.

Figure 5.3 showed the wide efficient current collection region seen on positive bevel angle samples. In figure 5.6 similar effects are shown on a cell bevelled at -5°. The curves plotted at the top were obtained with highly absorbed light incident on the sample from the Cu_2S side as indicated in the inset. The three curves represent light microprobe scans across the junctions at the three positions indicated on the sketch. The width of the constant current regions of the scan increased approximately linearly in crossing the sample from positions 1 to 3. When corrected for the effects of scattered light the sharp current decrease on the CdS side yielded values of hole diffusion lengths $L_p \simeq 6 \times 10^{-4}$ cm.

The photoconductivity data of Auth and Ridder[76] shows very similar behavior of photocurrent versus distance as that shown in figure 5.6. The low photocurrent region at distances beyond the region of rapidly decreasing current have been interpreted as the reabsorption of luminescent light.[82] Such a process is another mechanism for scattering of light in measurements of this type. Our measurements with the light

probe just off the edge of the crystal indicate that the effects of reabsorption of luminescent light were not as important as light scattered by the microprobe optics. The curves shown in the lower part of figure 5.6 were obtained with light whose energy was less than the CdS bandgap incident on the junction region through the CdS crystal as indicated on the sketch. The light microprobe line was focussed through the CdS on the upper surface at the same three positions used for the upper scans. Passing the long wavelength light through the crystal decreased the amount of reflected light reaching the large junction area away from the bevelled edge. Reduction of reflection effects can be easily seen by considering that long wavelength light incident from below requires two surface reflections to reach the junction plane, while light incident from the top requires only one reflection. Light scattered in passing through the bulk of the CdS crystal is probably about the same for either direction of travel. On the CdS side, long wavelength photoresponse was seen with sharp decreases in collected current observed at the same distances from the interface as were seen with short wavelength light. Near the junction the red response rose to a maximum at the visible interface. The current was then expected to remain constant as the light was moved further from the bevelled edge on the Cu_2S side. The sharp dips in the photocurrent on the Cu_2S side are not understood, but interference effects may be responsible since the Cu_2S wedge is only about 1 micron thick at this distance from the junction.

After microprobe spectral response measurements described in the following section, cell #8 was heat treated for 5 minutes at 250°C

in air. Microprobe scans across the junction with short wavelength light were then repeated. At all three positions across the crystal negligible constant-photocurrent regions existed, implying that the wide depletion layer at the surface had disappeared. The crystal was then very lightly polished to remove a few microns from the surface and another series of microprobe scans were made. This time a constant current region about 6 microns wide was measured. The conclusion from these results is that the wide depletion region measured on the CdS side is very sensitive to surface treatment, accounting for the large variations in this width measured on different crystals.

Removal of surface damage caused by mechanical polishing during bevelling was attempted with chemical etches. A suitable chemical etch is very difficult to find for a heterojunction especially when diffusion lengths in the micron range are to be measured. Different rates of etching of the two materials leads to steps at the junction which can seriously distort the geometry over the short distances being investigated. It was finally decided that a very light etch of the CdS on a positive bevel angle cell might remove the surface damage and permit measurements of the hole diffusion length in the angle-lapped geometry. For this purpose an optical quality etch consisting of 0.3 molar $KMnO_4$ dissolved in concentrated H_2SO_4 was used.[60] The results of a 2 minute etch at room temperature in this solution are shown in the photograph reproduced in figure 5.7. In this figure, part of a bevelled junction is viewed perpendicular to the junction plane from the CdS side of the cell. The bevelled Cu_2S layer, about 3.5 microns thick, appears as the light band (40 microns wide) forming

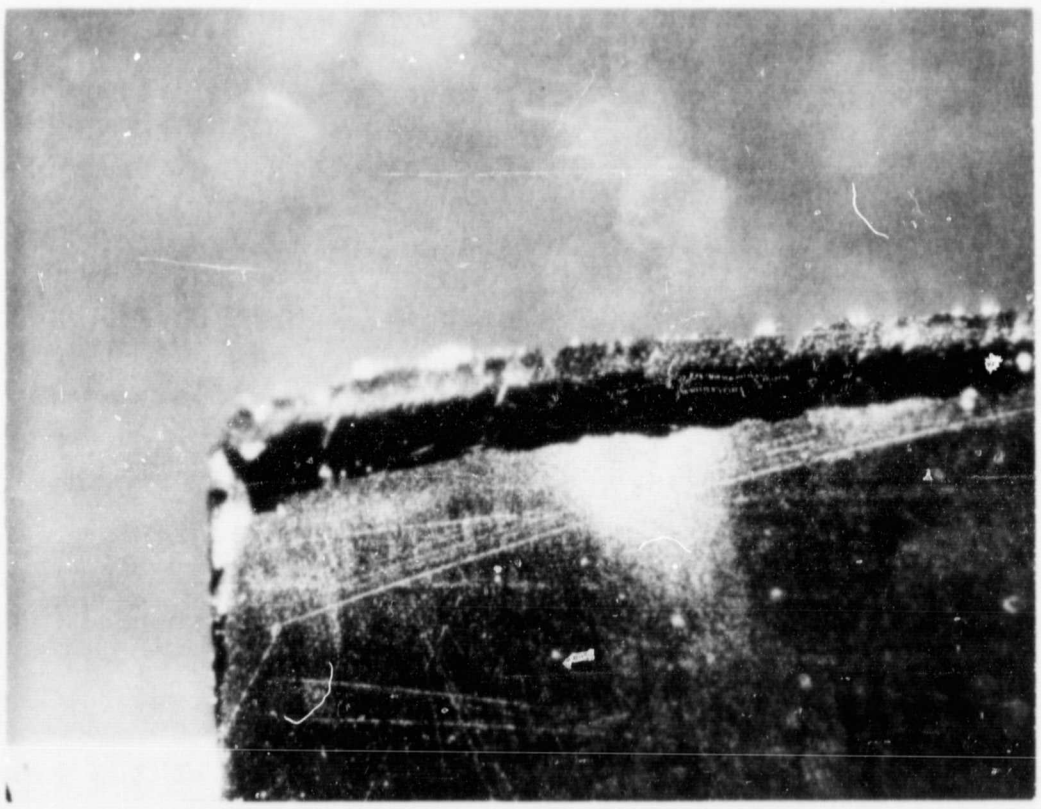

FIGURE 5.7: PHOTOGRAPH OF THE +5° ANGLE-LAPPED JUNCTION REGION OF CELL # 4 AFTER ETCHING IN $H_2SO_4 + KMnO_4$ FOR 2 MINUTES. Cu_2S IS AT THE TOP OF THE SAMPLE, THE DARK BAND IS THE UNETCHED CdS, AND THE ETCHED CdS IS AT THE BOTTOM. MAGNIFICATION X 100.

the top edge of the sample in the photograph. The Cu_2S-CdS interface is at the top edge of the dark band in the photograph. The dark band (100 microns wide) is unetched CdS, the polished surface scattering very little light. Then beginning at an abrupt edge, the rest of the CdS surface is lightly etched developing some surface roughness which scatters the light. A light microprobe scan across this junction (see figure 5.12) shows that the unetched region of CdS corresponds to the constant photocurrent regions associated with wide depletion layers at the surface. The reason for the ineffectiveness of the etchant in this narrow band of CdS is not understood. It would appear that the presence of the built-in field associated with the junction retards the chemical reaction at the surface since etching was found to be equally fast on highly insulating and conducting crystals. The wide depletion width developed by the etching technique and seen with the light microprobe was only a surface effect, since capacitance measurements indicated a bulk depletion width 0.6 microns wide, a value consistent with resistivity measurements on the bulk CdS.

The surface depletion region was investigated by still another technique on one cell. Electron mirror microscope photographs were taken of a junction bevelled at 90°.[83] In the electron mirror microscope a low energy electron beam is deflected by surface fields a few microns outside the solid. The reflected electrons are refocussed to form an image of the electric field distribution at the surface of the solid. A series of such photographs was taken of the Cu_2S-CdS junction with bias voltages ranging from +1.0 to -4.0 volts. Several of these photographs are shown in figure 5.8. The Cu_2S side of the junction is

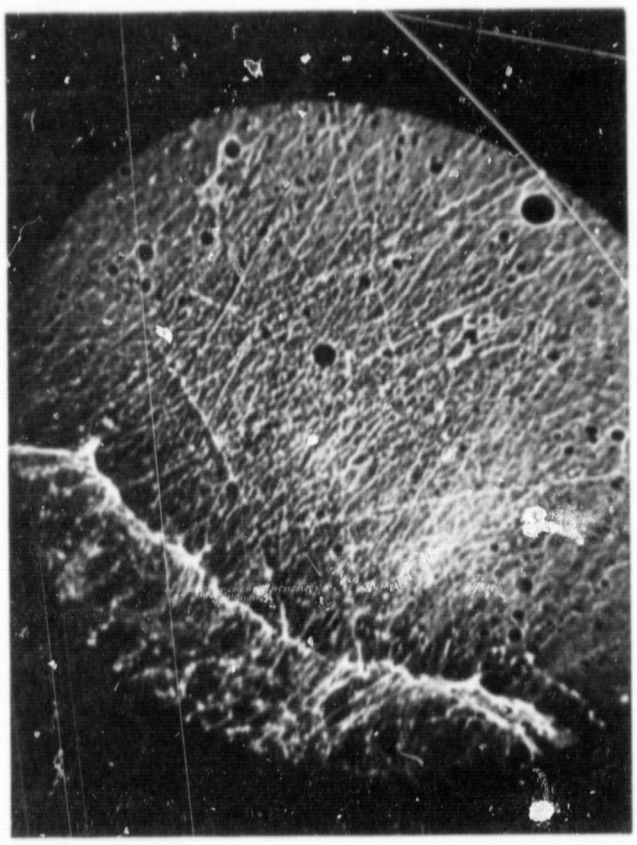

(a) BIAS = 0

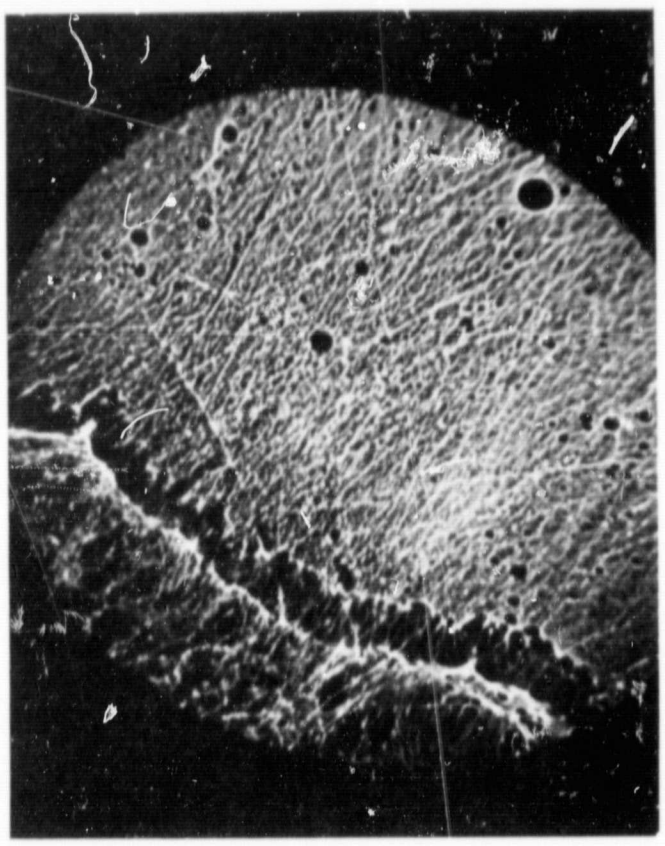

(b) BIAS = – 1 VOLT

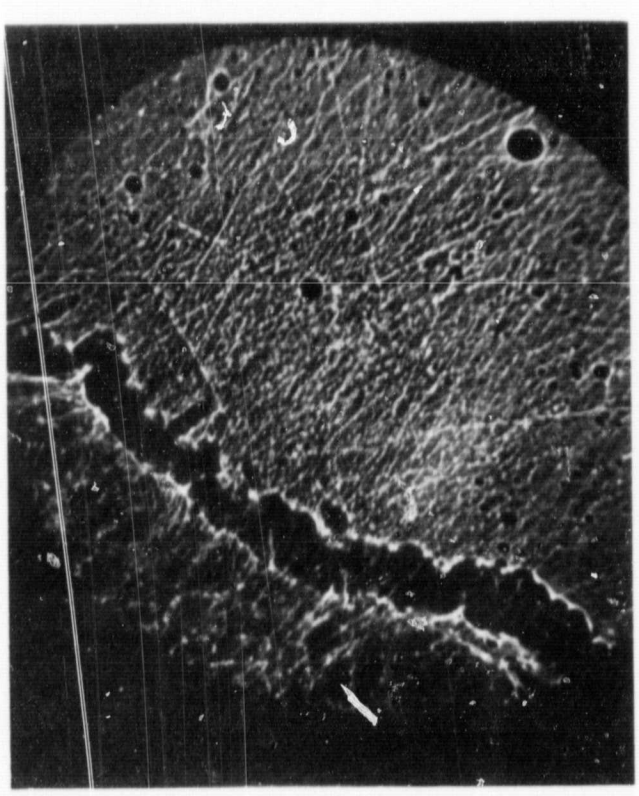

(c) BIAS = – 2 VOLTS

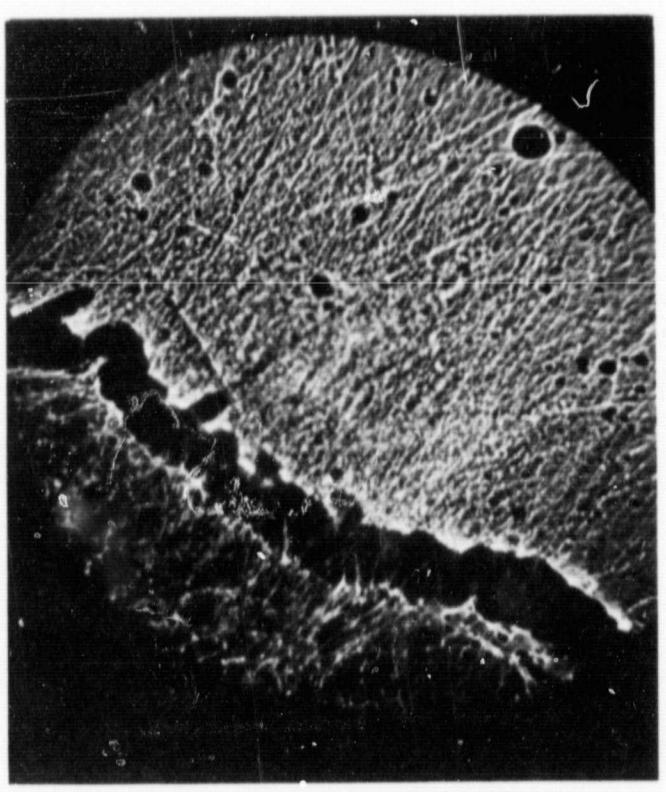

(d) BIAS = –4 VOLTS

FIGURE 5.8: ELECTRON MIRROR MICROSCOPE PHOTOGRAPH OF A Cu_2S-CdS HETEROJUNCTION. THE Cu_2S IS IN THE LOWER LEFT OF THE PHOTOGRAPHS. THE DARK BAND IS THE SPACE CHARGE LAYER IN THE CdS. BEVEL ANGLE IS 90°, MAGNIFICATION X150.

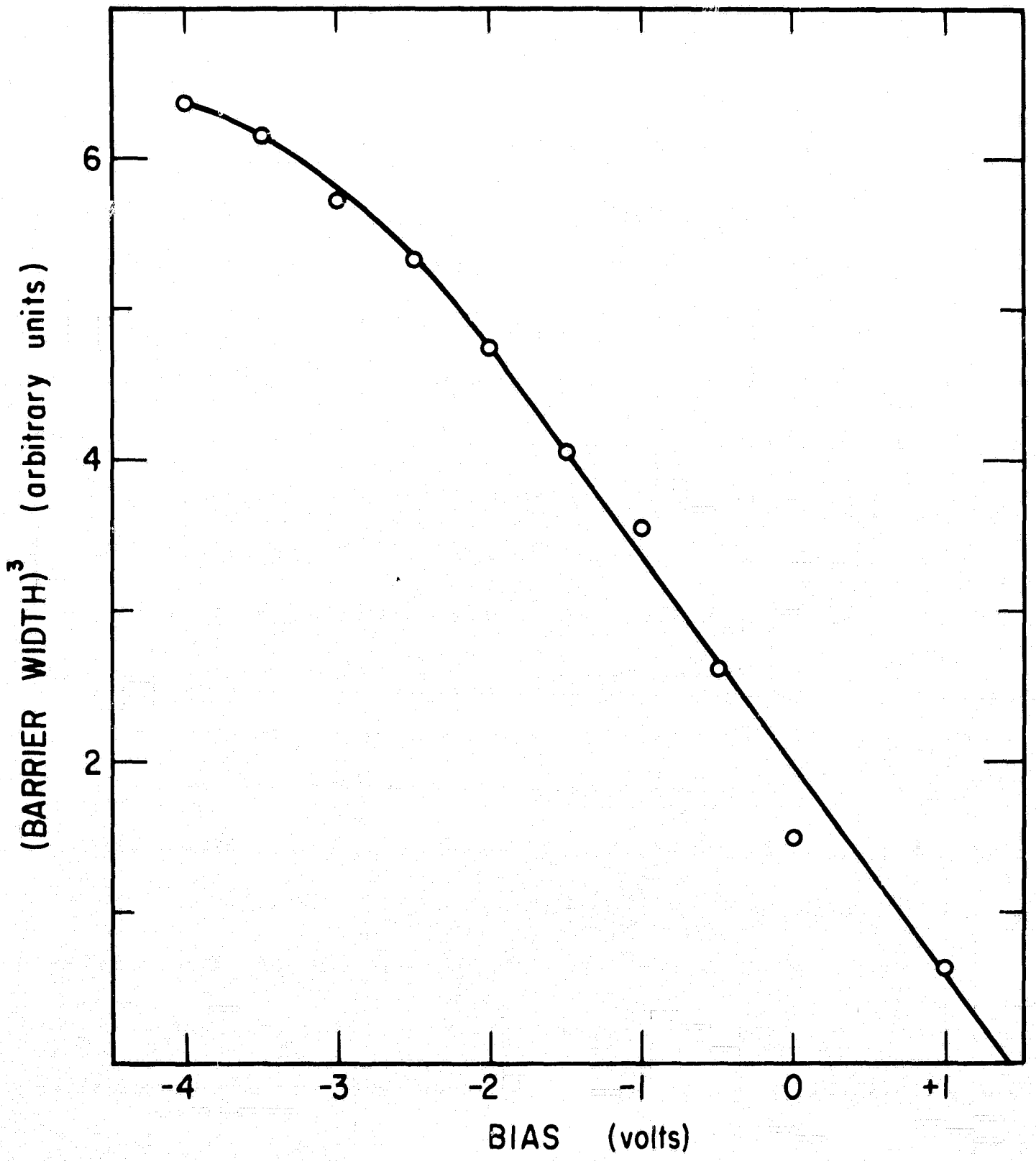

FIGURE 5.9: DEPLETION WIDTH CUBED VERSUS BIAS VOLTAGE TAKEN FROM ELECTRON MIRROR MICROSCOPE RESULTS. BEVEL ANGLE = 90°.

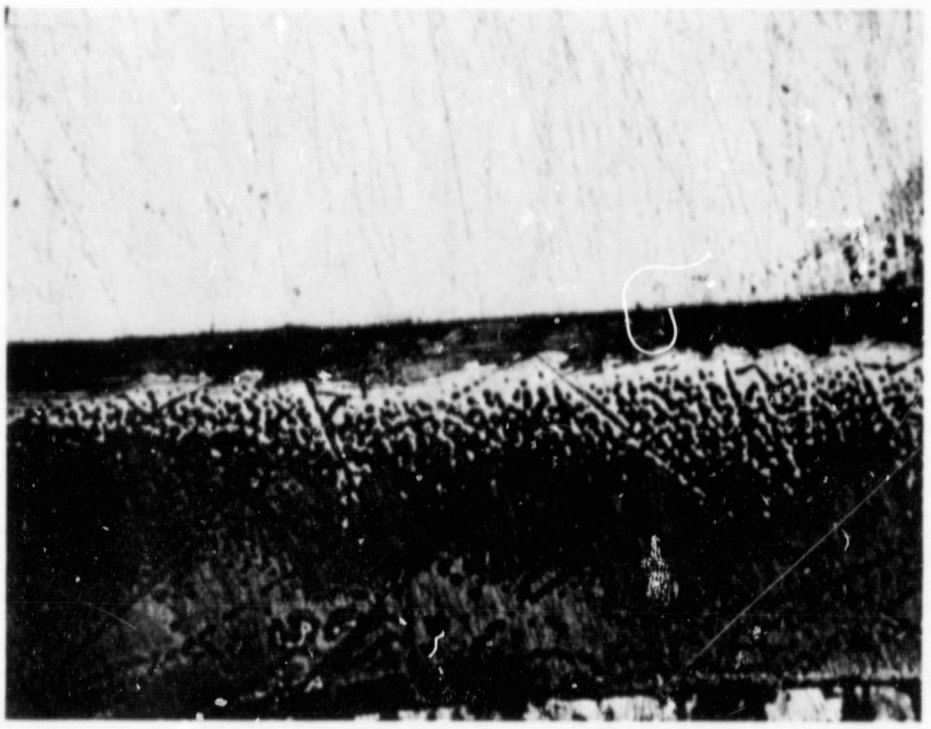

FIGURE 5.10: PHOTOGRAPH OF THE CELL USED FOR ELECTRON MIRROR MICROSCOPE MEASUREMENTS AFTER ETCHING IN $H_2SO_4 + KMnO_4$ FOR 2 MINUTES. UPPER DARK BAND IS Cu_2S LAYER. UNEVEN LIGHT REGION IS UN-ETCHED CdS. DARK AREA AT THE BOTTOM IS ETCHED CdS. MAGNIFICATION X50.

in the lower left of photographs. The depletion layer is the dark band which grows into the CdS side as reverse bias is increased. At zero bias the depletion layer width measured from these photographs was about 30 microns. The variation of the barrier width with applied bias is shown in figure 5.9. For small applied bias the barrier width varied as the 1/3 power of bias voltage and extrapolation in the forward bias direction gives a value of V_b = 1.4 volts for the built-in voltage. Light microprobe scans across this junction yields widths between 10 and 15 microns. The sample was etched in the $KMnO_4$ + H_2SO_4 solution with the result shown in figure 5.10. The Cu_2S layer is the dark band across the middle of the photograph, with the CdS in the lower half of the picture. The Cu_2S layer was very thick (120 microns) resulting in the non-planar interface. The etched CdS appears dark in this photograph. Once again a wide band of unetched CdS is left adjacent to the junction.

Attempts were made to study the widening of the surface depletion layers under reverse bias using light microprobe methods. Very little change was observed on the cells having wide regions, however, since large increases in the photosignal under reverse bias (to be discussed in a later section) tended to mask any widening effects. Those cells having rather narrower depletion layers showed larger increases with reverse bias which approached a cube-root dependence in a few cases.

5.3 Spectral Response Across a Junction

Cell #8 was used to obtain spectral response curves at various positions of the light probe relative to the Cu_2S-CdS interface.

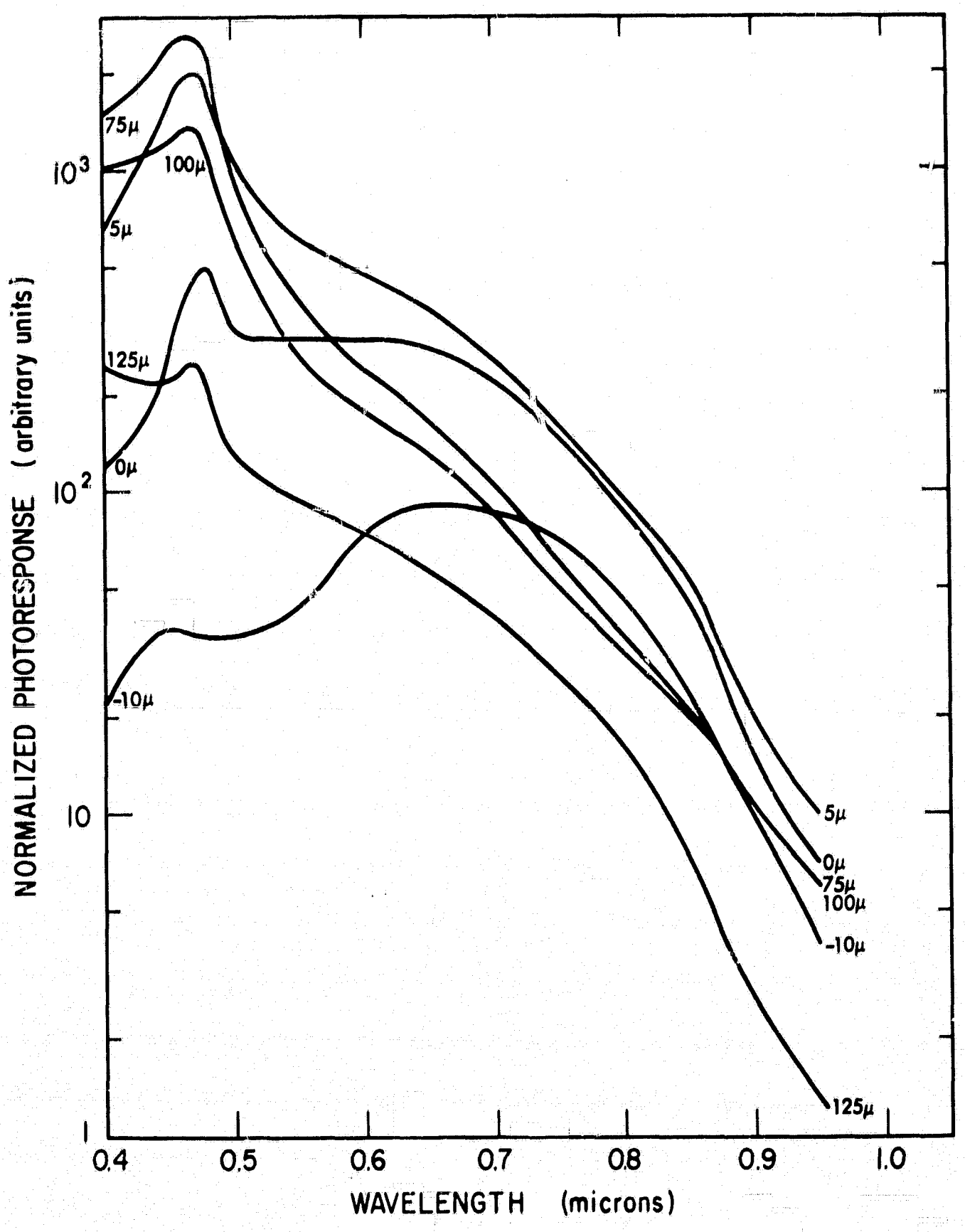

FIGURE 5.11: SPECTRAL RESPONSE CURVES OBTAINED WITH THE LIGHT MICROPROBE AT VARIOUS POSITIONS ACROSS A −5° ANGLE-LAPPED JUNCTION (CELL # 8, POSITION (2) ON FIG. 5.6).

This cell was chosen because the wide surface depletion region resulted in good collection efficiency out to large distances from the junction. The long wavelength response of the cell was poor beyond 7000 A indicating that photoemission from the Cu_2S side was inefficient. Low efficiency of the photoemission process was desirable in order to minimize the background signal due to scattered light reaching the large plane area of the junction. The sharp breaks observed at large distances from the junction in the long wavelength microprobe scans of figure 5.6 are evidence that the long wavelength response was generated near the surface and was not due to scattered light.

Spectral response curves obtained at various distances from the Cu_2S-CdS interface are shown in figure 5.11. The measurements were made at position (2) shown on figure 5.6. The curves have been normalized at 9000 A to the short wavelength curve of figure 5.6 to correct for the variation in collector efficiency as distance from the junction was varied. The curve at -10μ was on the Cu_2S side of the junction and represents a vertical distance of 0.87 microns to the junction. The peak at 4500 A was probably due to scattered light reaching the CdS side of the junction. The increase in the response as wavelength increases is due to the decreasing absorption coefficient (see figure 1.1) allowing more light to be absorbed within an electron diffusion length of the junction. Considerable variation in absorption coefficient data determined by various authors makes estimation of where the peak response should occur difficult. However, assuming the latest data of Shiozawa et al.[23] to be correct, and using $L_n = 2 \times 10^{-5}$ cm, the peak response should occur near 8000 A with about 3% of the

incident light being absorbed within a diffusion length of the junction. The magnitude of the observed response is consistent with these estimates.

Looking next at the curve taken at 0μ, that is with the light probe on the metallurgical interface, the response is seen to have increased at all wavelengths. At short wavelengths the increase is due to bandgap excitation in the CdS, while at longer wavelengths excitation in the Cu_2S is very efficient as the thickness of the Cu_2S at the light probe is less than the electron diffusion length. The response should increase as the Cu_2S absorption coefficient increases with about 35% of the incident light now being usefully absorbed at 6000 A.

As the light probe is moved into the CdS side, the short wavelength component of response is expected to rise and the long wavelength component to decrease. At 5μ on the CdS side, strong short wavelength response is seen. The longer wavelength response is about equal to that seen at the 0μ position. At this position, the CdS at the surface was only 4×10^{-5} cm from the interface before the 5° bevel so that diffused-in impurities could be present. Since the light is no longer highly absorbed as in diffusion length measurements, light scattered from crystal imperfections reaching the junction could also result in this long wavelength response. Light reaching the junction after reflection from the opposite side of the CdS crystal should be the same for the 5μ and 75μ positions. Because capacitance measurements have indicated that the CdS has bulk properties to within 10^{-5} cm of the junction on non-heat-treated cells, the long wavelength response

is believed to be mostly due to scattered light reaching the junction. The shift to shorter wavelengths of the peak attributed to CdS excitation is due to the very thin layer (3×10^{-5} cm) in which excited charge carriers are efficiently collected.

5.4 Photocurrent Gain with Small Reverse Bias

The V-I characteristics taken under short wavelength illumination (figure 4.1) showed that light-induced breakdown was occurring at small values of reverse bias voltage. This effect was investigated with the light microprobe by scanning across the Cu_2S-CdS junctions with reverse bias applied. The result of scans on cell #4 with no bias and 1 volt reverse bias applied is shown in figure 5.12. The effect of reverse bias was to increase the measured photocurrent with the maximum increase being observed at 100 microns from the junction on the CdS side. This position corresponds to the edge of the wide surface depletion region discussed in section 5.2. As indicated on the figure, the maximum also corresponds to the boundary between the etched and not etched regions shown in the photograph of this cell (figure 5.7). The voltage dependence of the increased photosignal observed on cell #8 is shown in figure 5.13. In this figure the five curves were obtained with the light probe at the indicated distances from the Cu_2S-CdS interface (see figure 5.3). Four important features are seen in figure 5.13: (1) the threshold for the onset of photocurrent gain is less than 0.25 volts, (2) saturation of the gain begins at about 1.0 volts, (3) maximum gain occurs when the microprobe is at the edge of the depletion region furthest from the junction, and

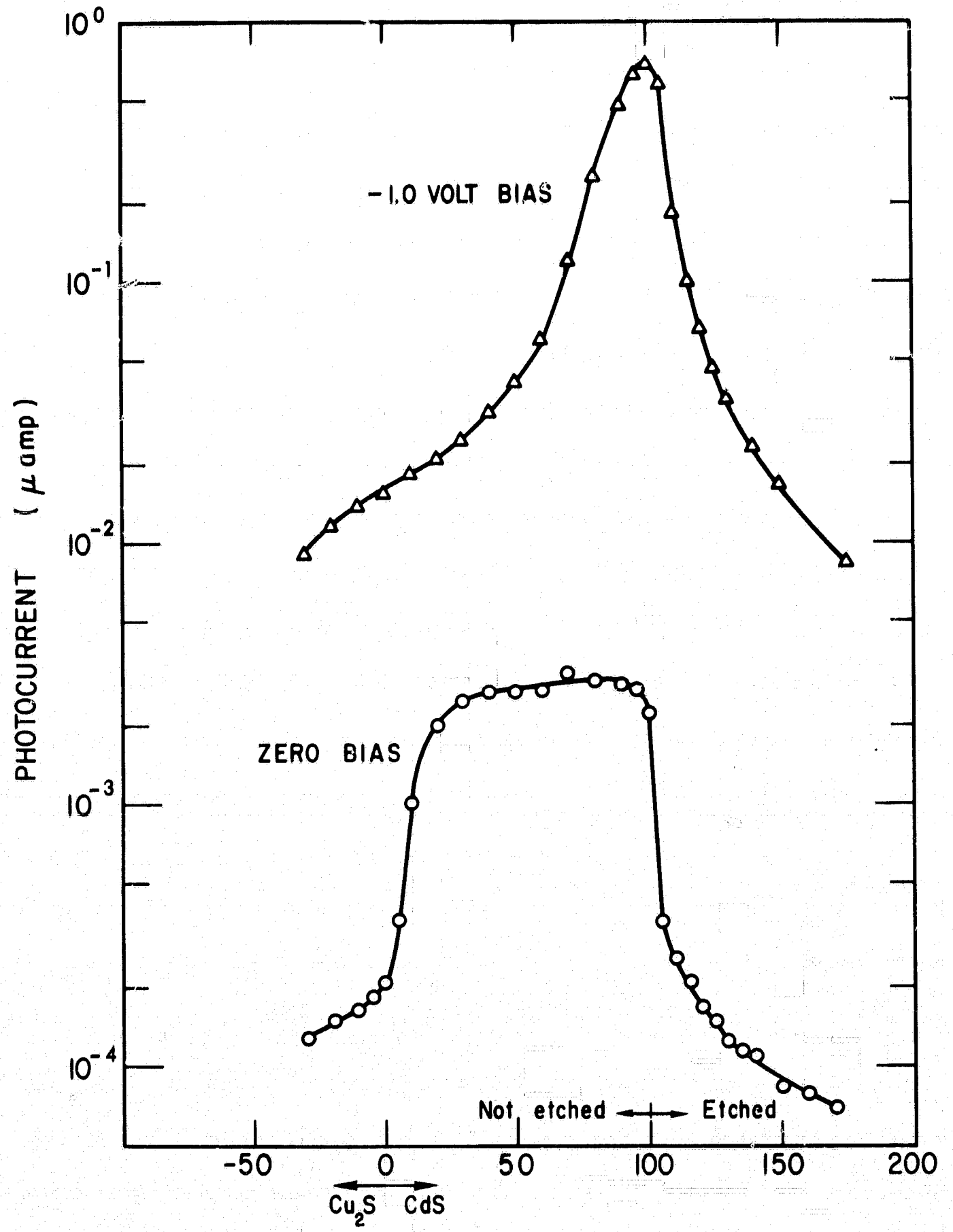

FIGURE 5.12: PHOTOCURRENT VERSUS LIGHT PROBE POSITION ACROSS THE +5° ANGLE-LAPPED JUNCTION OF CELL # 4 WITH AND WITHOUT REVERSE BIAS. ETCHED/NOT ETCHED REFERS TO RESULTS OF ETCHING WITH $KMnO_4$ IN H_2SO_4. (See Fig. 5.7)

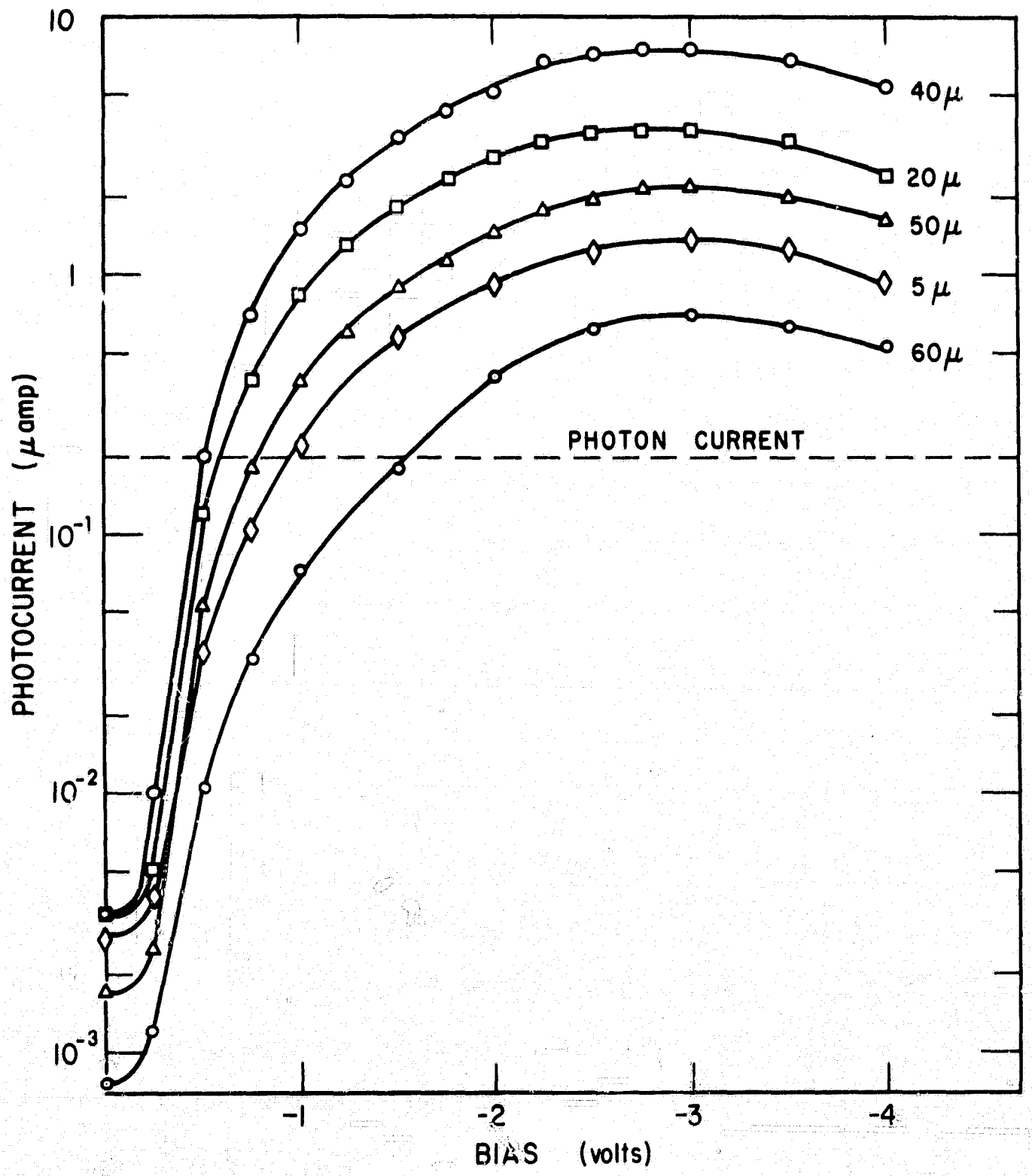

FIGURE 5.13: PHOTOCURRENT AS A FUNCTION OF REVERSE BIAS FOR CELL # 9. THE LIGHT PROBE DISTANCES FROM THE +5° BEVELLED JUNCTION ARE INDICATED ON THE CURVES. SEE FIGURE 5.3 FOR SHORT-CIRCUIT SCAN.

(4) maximum photocurrent is much greater than the number of light injected carriers. Figure 5.14 shows the photocurrent dependence on bias voltage for cell #4. The light probe was at the position of maximum response in figure 5.12. In cell #4 the dark reverse current of the entire junction (area = 10^{-2} cm^2) was measured and is plotted on figure 5.14. The photocurrent due to the microprobe light exceeds the total dark current by more than an order of magnitude. The lines marked 'photon current' in figures 5.13 and 5.14 are the total photon flux incident on the samples from the light microprobe. The light intensity was measured with a calibrated silicon photodiode in the sample position. Assuming that every photon produces a carrier which is collected under reverse bias, the maximum photocurrent should be the indicated photon current. In figures 5.13 and 5.14 the maximum current represents gains of 40 and 150 respectively.

Following is a summary of the major observations from an investigation of the photocurrent gain effect on many samples.

(1) A threshold of 0.2 to 0.4 volts reverse bias for onset of the gain effect was seen for all Cu_2S-CdS junctions. Similar gain observed on electroplated Cu-CdS barrier cells showed no threshold.

(2) Saturation of the photocurrent occurs between 2 and 4 volts reverse bias. Some cells show a slight decrease in photocurrent at higher voltage.

(3) Maximum photocurrent is always observed at some distance from the Cu_2S-CdS interface, usually at or very near where

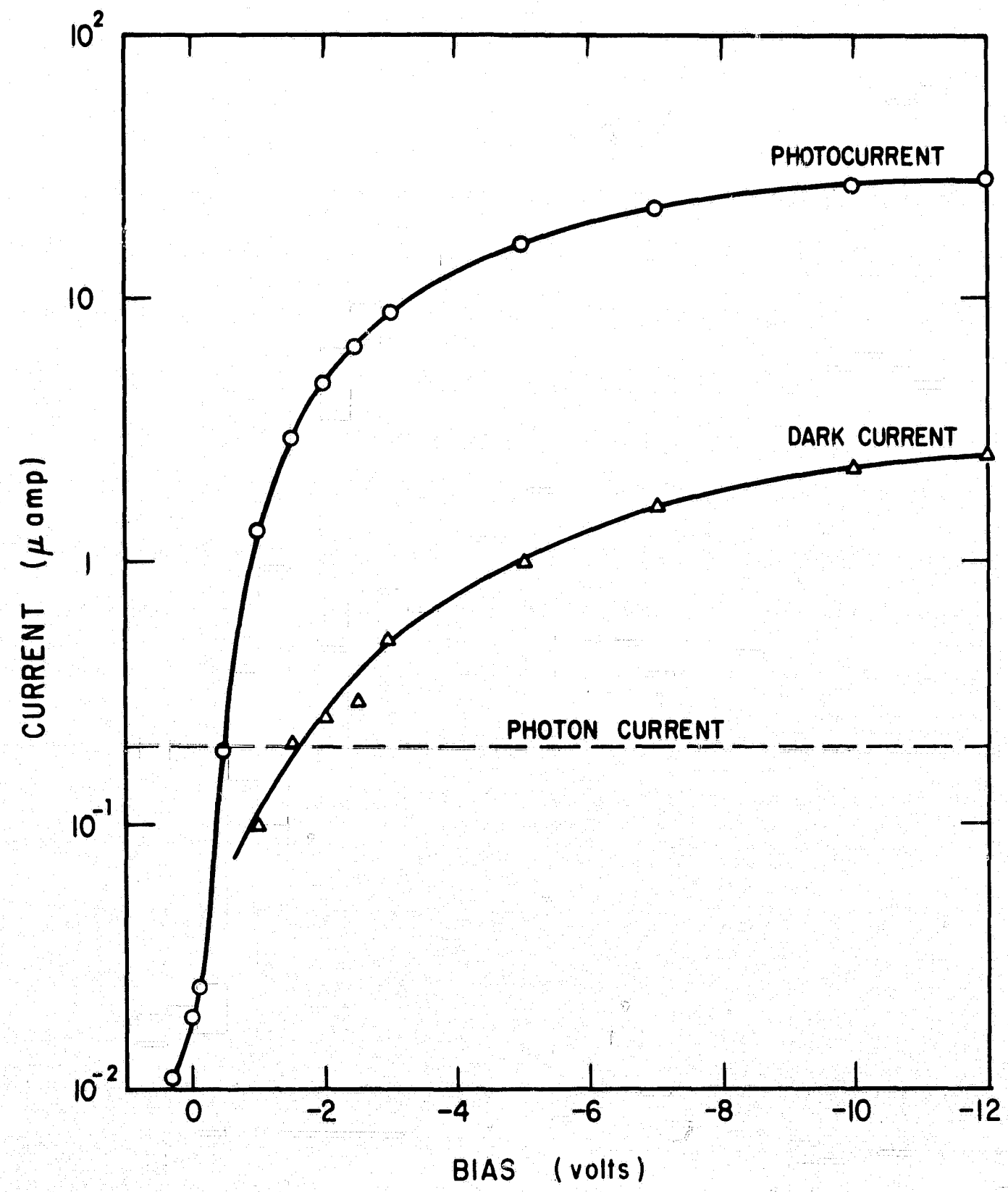

FIGURE 5.14: PHOTOCURRENT AND DARK CURRENT VERSUS REVERSE BIAS VOLTAGE FOR CELL # 4. THE DISTANCE FROM THE LIGHT PROBE TO THE JUNCTION WAS 94 MICRONS. PHOTON CURRENT LINE CORRESPONDS TO THE TOTAL INCIDENT LIGHT FLUX FROM THE MICROPROBE.

the zero bias photocurrent begins to decrease sharply on the CdS side.

(4) Large photocurrent gain effects are only observed for light of energy greater than or equal to the bandgap of CdS. Spectral response measurements of the effect show a very sharp edge at 5200 A.

(5) The response time for the photocurrent gain was 2×10^{-4} sec. Measurements were made using a 600 Hz chopping frequency and observing the shape of the photocurrent pulse on an oscilloscope at various values of reverse bias.

(6) Photocurrent gain in the range of 100 to 200 was seen on most bevelled junctions. Gains between 2 and 5 were seen when light was incident through a thin Cu_2S layer. Gain of 2000 was observed at the junction of cleaved cell #7.

(7) Photocurrent greater than the total dark current has been observed. Magnitude of the dark current does not seem to be related to the photocurrent gain.

(8) Photocurrent gain varies greatly (but reproducibly) as the light probe is scanned parallel to the junction.

(9) Photocurrent gain begins to saturate at high light intensities (see discussion below).

(10) Short heat treatment of the cells at 250°C in air drastically reduces the photocurrent gain.

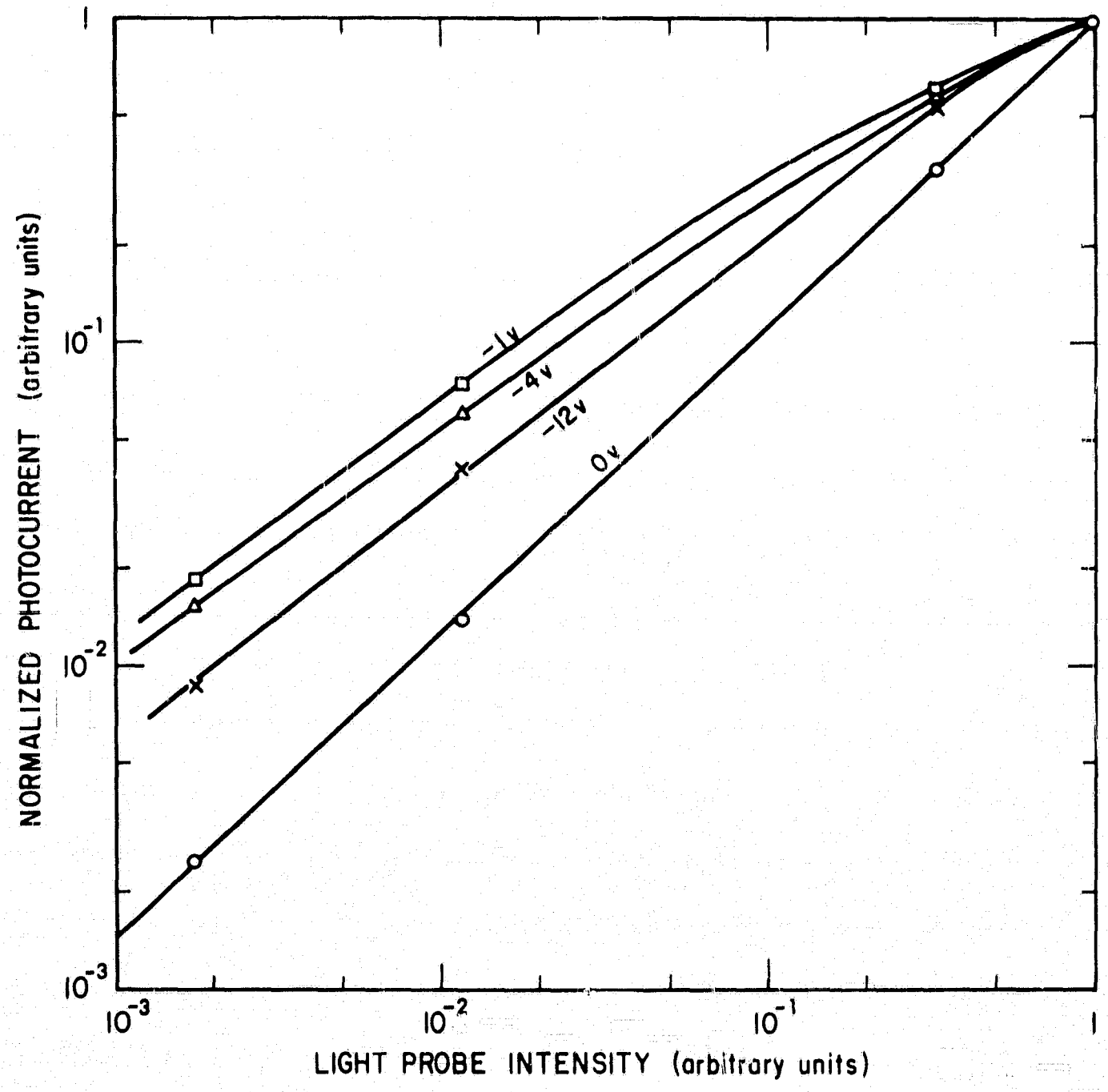

FIGURE 5.15: INTENSITY DEPENDENCE OF THE PHOTOCURRENT AT VARIOUS REVERSE BIAS VOLTAGES. LIGHT MICROPROBE AT THE PEAK RESPONSE POSITION (X = 100μ) ON BEVELLED JUNCTION OF CELL # 4.

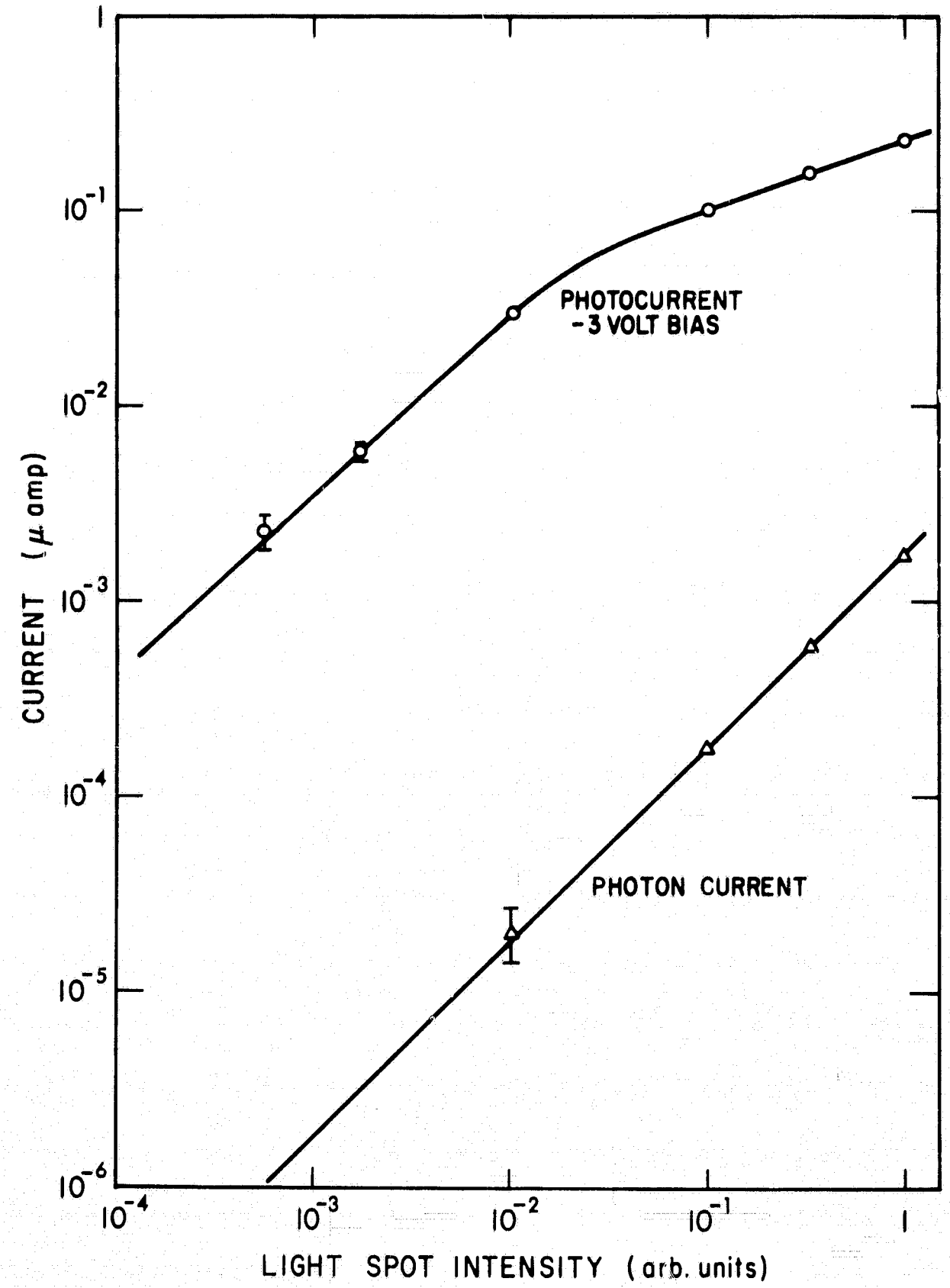

FIGURE 5.16: INTENSITY DEPENDENCE OF THE PHOTOCURRENT UNDER REVERSE BIAS WITH THE LIGHT PROBE AT A MICRO-CRACK ON THE JUNCTION OF CELL # 7. PHOTON CURRENT CURVE IS THE INCIDENT LIGHT FLUX MEASURED WITH A CALIBRATED SILICON PHOTODIODE.

(11) Photocurrent gain between 2 and 5 times the incident photon current was observed on the reverse-biased thin film cell with the microprobe light incident on the Cu_2S side.

The intensity dependence of the photocurrent observed at various bias voltages is shown in figure 5.15 for cell #4. The results were obtained at the position of maximum gain (100 microns from the interface) using neutral density filters to reduce the light probe intensity. At zero bias the photocurrent varied very nearly linearly with light intensity. Departure from linearity was evident for all reverse bias voltages. Figure 5.16 shows the variation with light intensity of the maximum photocurrent observed from cell #7. This current was observed at a visible defect at the junction (see section 5.5). Also plotted in the figure is the photon current measured with the silicon photodiode. At low intensities, a gain of 2000 is observed. At higher light intensity, the photocurrent saturates, decreasing the gain to about 200 at the maximum intensity used.

5.5 Correlation of Photocurrent Gain with Crystal Defects

As mentioned in the previous section, the magnitude of the photocurrent gain under small reverse bias was strongly dependent on the light probe position along the exposed edge of the junction. On bevelled cells, with zero bias across the junction, relatively small variations in photocurrent were observed when the light probe was scanned parallel to the Cu_2S-CdS interface. However, when reverse bias voltage was applied, large photocurrent gain was observed that varied one or two orders of magnitude as the light probe was scanned.

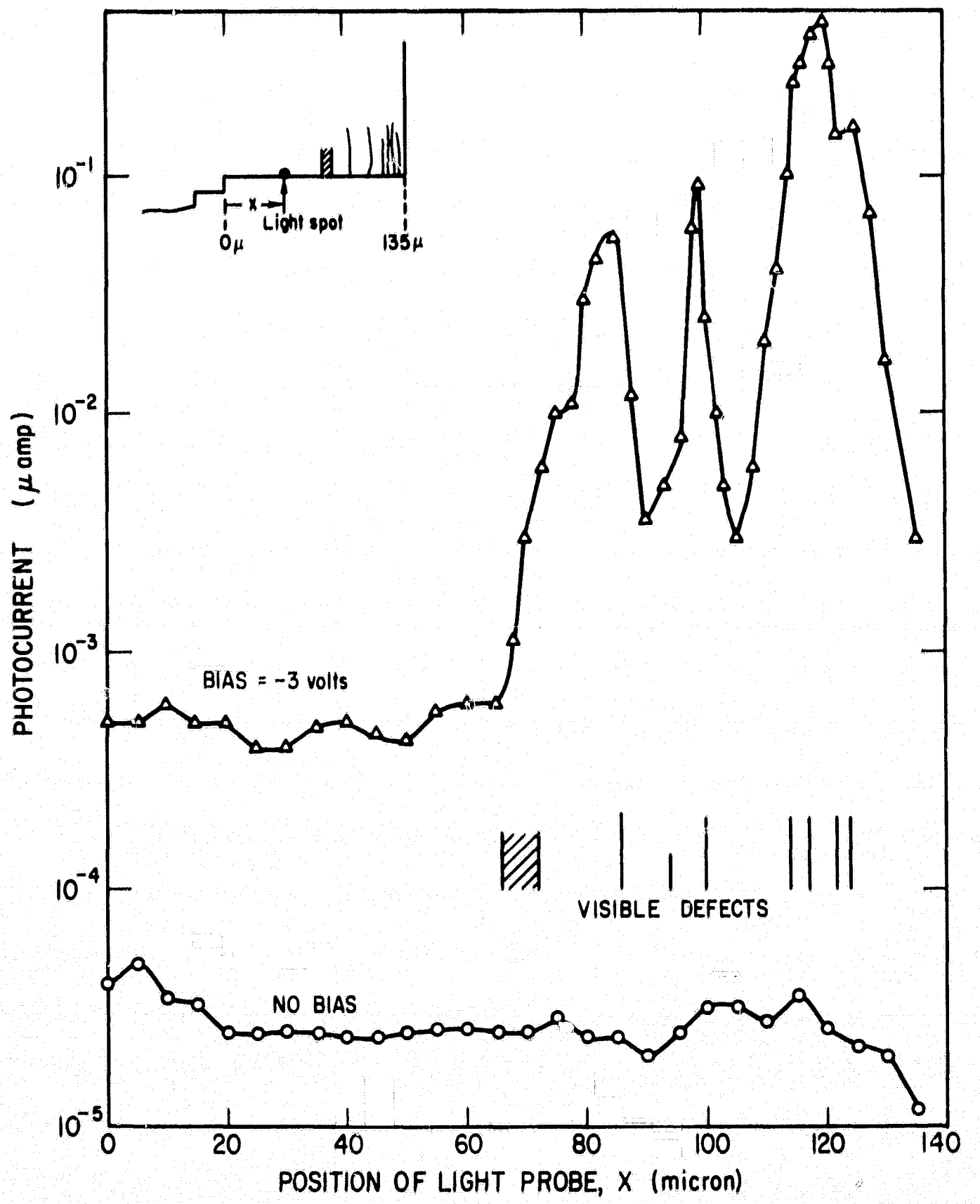

FIGURE 5.17: PHOTOCURRENT VERSUS LIGHT SPOT POSITION SCANNED PARALLEL TO THE INTERFACE.

The separation between adjacent peaks in the photocurrent was between 5 and 20 microns. These observations, and the fact that several carefully prepared cells which were not bevelled showed no low voltage breakdown effects in their V-I characteristics suggested that defects might be responsible for the observed reverse breakdown under short wavelength illumination.

To investigate this possibility, a junction free of polishing damage was necessary. Cell #7 on which both the junction plane and a 90° intersecting plane were cleavage planes, was investigated. A photograph of the surface of this crystal where scans were made has already been shown in figure 5.4 in connection with diffusion length measurements. For these experiments, the light microprobe was reduced to a spot approximately 1.5 microns square. After careful alignment, the spot could be traversed along the very flat portion of the junction edge over a distance of 135 microns.

The results of two such scans; one with, and one without reverse bias, are shown in figure 5.17. Also indicated in the figure are the exact locations of defects intersecting the junction. These defects were examined carefully at magnifications up to 1000X using both reflected and transmitted light. The defects located on figure 5.17 had the appearance of microcracks in the CdS crystal rather than cleavage steps, many of the latter also being visible on this surface. With no bias voltage applied, the photocurrent remains essentially constant over the entire length of junction scanned. Repeating the scan with 3 volts reverse bias applied, an overall increase in photocurrent was measured; but at the locations of the microcracks, an

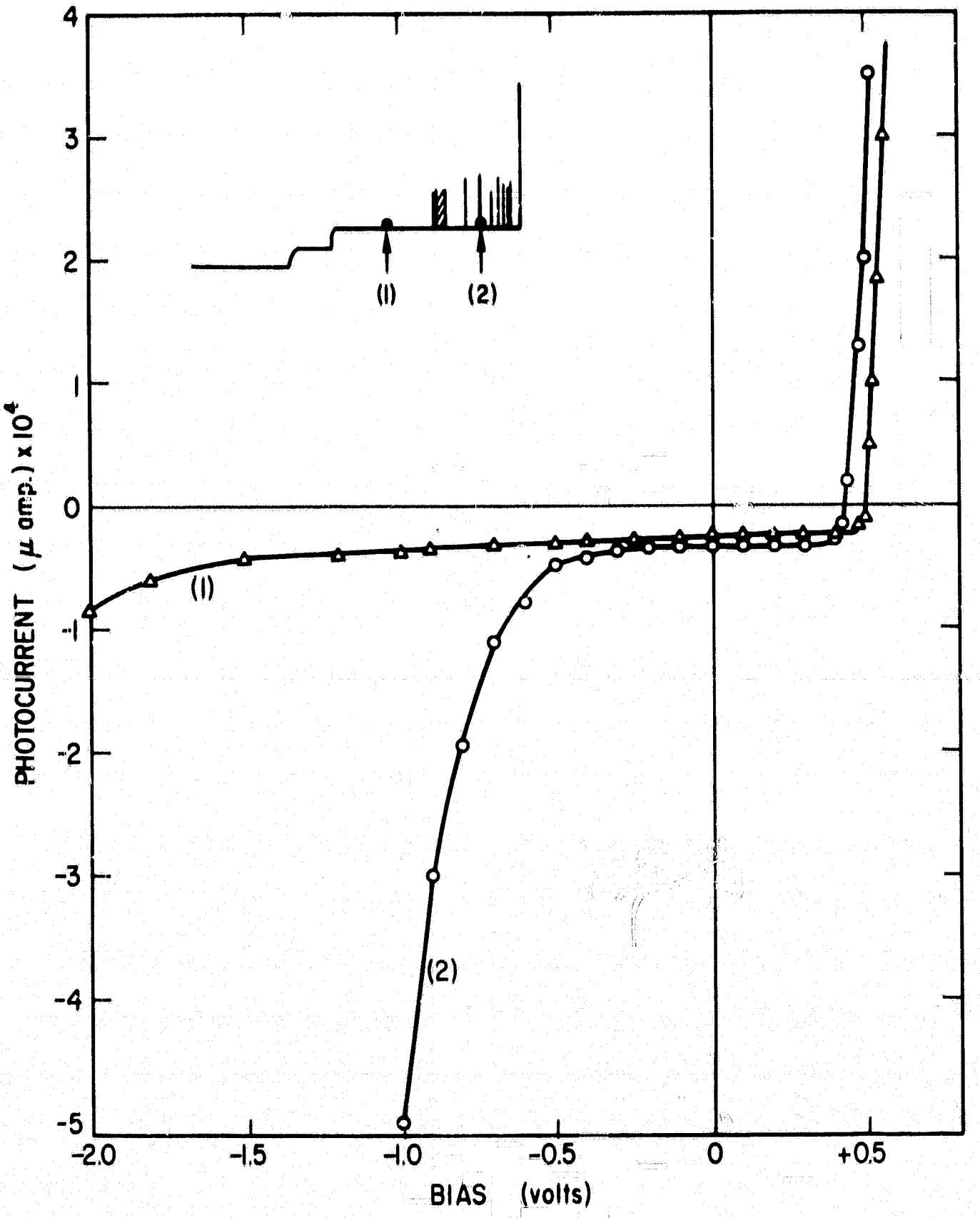

FIGURE 5.18: PHOTOCURRENT VERSUS APPLIED BIAS FOR THE MICROPROBE AT PERFECT (1) AND IMPERFECT (2) POINTS ON THE CLEAVED JUNCTION OF CELL # 7.

additional increase of from 2 to 3 orders of magnitude was seen. Measurements of the total light flux from the light microprobe corresponds to a photon current of 2×10^{-9} amps. Thus, photocurrents with gain of 5 are observed at localized points on this junction. Referring back to figure 5.16, where the intensity dependence of the maximum photocurrent was plotted for this crystal, it can be seen that at lower intensities a gain of 2000 was measured at one of the microcracks. Since no corrections for reflected light have been made, the actual yield per absorbed photon is considerably higher.

The V-I characteristics shown in figure 4.1 showed that short wavelength illumination caused reverse breakdown at small bias voltage. This apparent breakdown is the same phenomenon being discussed as photocurrent gain in this section. The local nature of the breakdown observed in the V-I characteristics under short wavelength illumination could be demonstrated with the light microprobe. Using cell #7, photocurrent versus applied bias characteristics were obtained at two locations on the junction. Figure 5.18 shows the results of these measurements. The wavelength of the incident light was a band between 3500 A and 5000 A. At position (1), the light probe was at a 'perfect' part of the crystal. At position (2), the probe was located on a microcrack. At position (1), the onset of appreciable breakdown current at about -1.5 volts corresponds to the onset of reverse breakdown in the dark for this junction. At position (2), the threshold for breakdown is about 0.2 to 0.3 volts. In the forward direction, the characteristic at position (2) crosses the voltage axis at 0.43 volts, about the same crossing point as is observed for the whole junction

under illumination. At position (1), the crossover is at 0.5 volts, a significant increase in output voltage due to reduced light-modulated forward current.

The results presented here show very clearly the correspondence between defects at the junction and the observed light-induced breakdown or photocurrent gain effects. Defects such as cracks existing in the CdS before dipping to form the Cu_2S layer will result in sharp spikes of Cu_2S penetrating the CdS on an otherwise planar junction. The effects observed at these locations are felt to be due to the high electric fields which will be present at sharp points on the junction. Bevelling produces high field regions due to the bevel edge itself and damage such as scratches, etc. Polycrystalline films contain many potential high field regions at grain boundaries. Further discussion of the breakdown effects is deferred to section 6.6 where a mechanism is proposed for the observed effects.

VI. MODEL FOR THE Cu_2-CdS HETEROJUNCTION

6.1 Introduction

In the preceding two chapters the results from a variety of experiments have been presented. In this chapter a model for the Cu_2S-CdS heterojunction is proposed and the experimental results are discussed in terms of the proposed model.

The major experimental phenomena for which a satisfactory model must account are:

(1) efficient long wavelength response,

(2) loss of long wavelength response after heat treatment,

(3) enhancement of long wavelength response by short wavelength secondary illumination,

(4) existence of fast and slow components in the photoresponse,

(5) optical quenching of the photoresponse,

(6) persistence of enhancement by short wavelength secondary illumination,

(7) V-I characteristics with much greater forward current under illumination than in the dark,

(8) temperature independence of the forward V-I characteristics over a wide temperature range,

(9) quenching of long-wavelength-generated V_{oc} by additional short wavelength illumination,

(10) light-induced breakdown at small reverse bias.

6.2 Origin of Long Wavelength Photoresponse

Several arguments can be made to show that the major part of the long wavelength response of efficient Cu_2S-CdS heterojunctions must be due to photoexcitation in the Cu_2S. The most obvious argument is based on the similarity of the spectral response to the optical absorption spectrum of Cu_2S. The long wavelength edge at 1.2 eV is clearly seen in both optical absorption of Cu_2S and the photoresponse of these cells.

In order to attribute the major contribution to the short-circuit current in the long wavelength region to excitation in the Cu_2S layer, it is necessary to show that the collection efficiency for light generated in this layer is sufficient to account for the observed response. Calculations by van Aerschot et al.,[35] using the optical absorption data of Marshall and Mitra[20] and Eisenmann,[21] have shown that collection efficiencies between 0.1 and 1 are possible for Cu_2S layers less than 0.5 microns thick and having electron diffusion lengths of about 1×10^{-4} cm. Shiozawa et al.[68] have shown that the most efficient cells have Cu_2S layers about 0.3 microns thick. The diffusion length results of the present work (section 5.1) indicate a value of electron diffusion length between 0.1 and 0.3 microns. It is therefore apparent that the observed efficiency of good cells can plausibly be attributed to absorption in the Cu_2S.

Another argument in favor of Cu_2S contributing the major long wavelength response is the inverse of the argument presented above.

One must ask whether it is possible to generate sufficient long wavelength response on the CdS side of the junction. If optical absorption by impurities within a hole diffusion length of the junction cannot account for observed cell efficiency, absorption in the Cu_2S or at interface states must be accepted as the origin of long wavelength response.

Measurements on non-heat-treated single crystal CdS cells show that from 2.5% to 15% of the incident light in the 1.3 eV to 1.8 eV range results in collected carriers contributing to short-circuit current. Capacitance measurements show that the CdS still has bulk properties to within at least 2×10^{-5} cm of the interface. Optical absorption and photoconductivity measurements on the CdS before dipping indicate very small absorption in this photon energy interval. Assuming the collection efficiency is unity within half the hole diffusion length measured in CdS ($L_p = 5 \times 10^{-4}$ cm) and using a value of optical cross-section for impurities $\sigma = 10^{-16}$ cm^2, the density of impurities required to absorb say 10% of the incident photons is estimated to be 10^{20} cm^{-3}. This density is unreasonably high for these crystals even if it were assumed that the impurities or defects were electrically inactive in the capacitance measurements. Since the estimate made here used the total incident light with no corrections for reflection losses, light absorbed in the Cu_2S layer, or recombination losses in the CdS, the value of impurity density obtained in this way is probably a lower limit. It is evident that the high efficiency of these non-heat-treated cells cannot depend on absorption on the CdS side of the junction. Even after heat treatment, capacitance measurements show

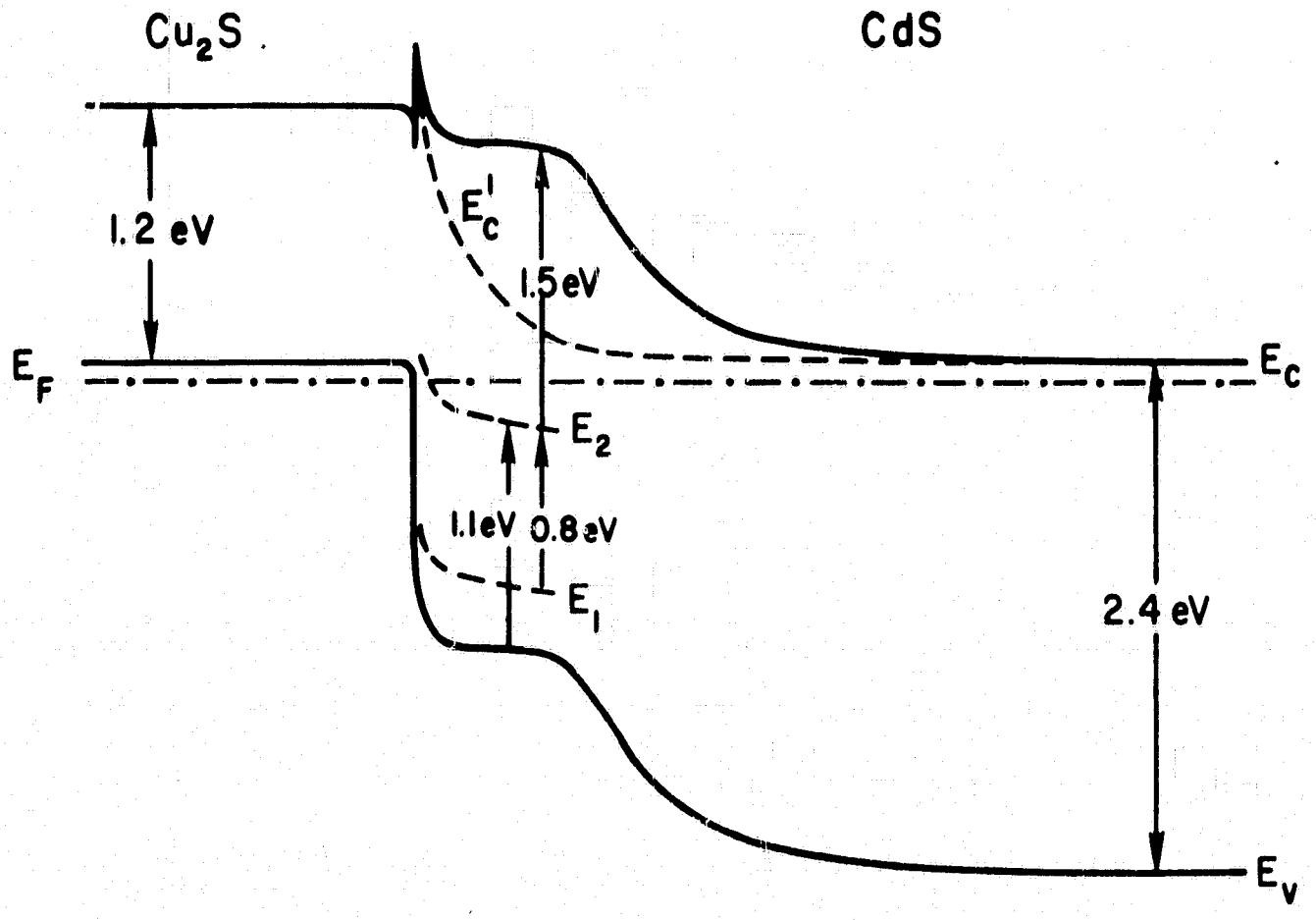

FIGURE 6.1: BAND PROFILE OF THE HETEROJUNCTION AFTER HEAT TREATMENT. E_C' IS THE CONDUCTION BAND PROFILE WHEN LEVELS E_2 ARE FILLED WITH HOLES.

at most a region 5×10^{-5} cm wide in which diffused impurity density may be high, so that optical absorption is again insufficient to support the observed photocurrent.

Measurements by Shiozawa et al.[23] on thin film cells in which the quantum efficiency is about 70% in the response band have shown that 90% of the incident light is absorbed in the Cu_2S layer. It is also observed by these authors and by Mytton[29] that the long wavelength response improves with increasing Cu_2S layer thickness up to about 0.3 micron thick layers. These observations are clearly incompatible with excitation either in the CdS or at interface states.

A model applicable to efficient Cu_2S-CdS cells must require the major part of the optical excitation to take place in the Cu_2S layer. The diffusion length results presented in this thesis and the optimum Cu_2S thickness measured by Shiozawa et al.[23] support this conclusion.

Although the long wavelength response of these cells is due to absorption in the Cu_2S, the effect of secondary illumination in enhancing and quenching this photoresponse is apparently due to light absorbed in the CdS. The model proposed in section 6.3 is introduced to explain the mechanism by which secondary illumination modulates the collection efficiency of the junction for carriers generated in the Cu_2S layer.

6.3 Proposed Band Profile

The proposed band profile for heat-treated Cu_2S-CdS heterojunctions is shown in figure 6.1. The major difference between this profile and the one previously suggested by Shiozawa et al.[23] is the conduction band spike. The bulk properties of the Cu_2S and CdS and the requirement

that the system come to equilibrium (flat Fermi level) fixes the relative location of the valence and conduction bands on both sides of the junction far from the space charge region. The Cu_2S is represented as a degenerate p-type semiconductor. The CdS is a low resistivity (0.1 to 1Ω-cm) n-type semiconductor. Heat treatment has produced a layer a few tenths of a micron thick of partially compensated CdS adjacent to the interface presumably due to copper diffusion from the Cu_2S. At the interface a difference of electron affinity between the Cu_2S and CdS or effects of interface states causes a discontinuity in the bands resulting in a conduction band spike. Because of the large difference in the bandgap of the two semiconductors, the barrier height for holes is about twice that for electrons.

Two energy levels associated with imperfections in the compensated CdS region are located in the forbidden gap at energies E_1 and E_2, approximately 0.3 eV and 1.1 eV respectively above the CdS valence band edge. The occupation of these imperfections controls the depletion width in the CdS. Hole trapping in these levels results in depletion layer narrowing, changing the conduction band profile to that indicated by E_c' in figure 6.1. This modulation of the band profile by extrinsic light absorption in the CdS, or by intrinsic absorption followed by hole trapping, varies the photocurrent by controlling the transparency of the conduction band spike to photoexcited electrons tunnelling from the Cu_2S conduction band into the CdS. This mechanism alone, with its direct corollaries, is sufficient to describe the wide variety of photovoltaic behavior observed for heterojunctions of Cu_2S-CdS.

6.4 Light-Modulated Tunnelling Model - Discussion

Conduction Band Spike

The band profile of figure 6.1 is introduced to explain the spectral response results of heat-treated Cu_2S-CdS cells. Prior to heat treatment no slow component in the response to light was observed, and no quenching or enhancement effects by secondary illumination were seen. The efficient long wavelength response in the cells is due to light absorption in the Cu_2S layer and diffusion of electrons to the junction. Collected electrons must tunnel through the narrow conduction band spike. Using relations developed in section 2.1, the width of the tunnelling barrier and the tunnelling probability through the base of the spike can be calculated. Using a tunnelling barrier height $E' = qV_B = 0.1$ eV, and assuming a step junction with a net donor density of 10^{17} cm^{-3}, the width of the conduction band spike is calculated from equation (2.8) to be 20 A. From equation (2.9) the tunnelling probablity is 0.22 where a diffusion potential $V_D = 1.3$ volts has been used. This is the transparency of the conduction band spike for electrons tunnelling from the Cu_2S to contribute to the photocurrent.

Since the proposed mechanism for enhancement and quenching of photocurrent requires modulation of the transparency of this spike, it must be shown that tunnelling dominates over Schottky emission over the spike. The photogenerated electrons in the Cu_2S conduction band may be represented by a Boltzmann distribution $N(E') = e^{-E'/kT}$. Excitation over the barrier requires a minimum value of $E' = 0.1$ eV. The probability of an electron having this energy at 300°K is 0.02.

comparing this with the tunnelling probability of 0.22, it is seen that tunnelling is about 10 times more effective than Schottky emission at room temperature.

Effect of Heat Treatment

In the proposed model, short heat treatment introduces the impurity levels E_1 and E_2 into a narrow region of CdS at the junction. These levels are acceptors and therefore compensate the n-type CdS by reducing the net donor density near the interface. Because of the reduced net ionized donor density the depletion width must widen to satisfy Poisson's equation for the diffusion potential at the interface. The degree of compensation in this region is not critical to the model being considered, but capacitance data on several cells indicate a fairly abrupt transition from the bulk donor density to a highly compensated region. The effect of any compensation of the CdS at the junction is to widen the conduction band spike, decreasing its transparency to electrons incident from the Cu_2S side. The dependence of the tunnelling probability on the net donor density N_D can be seen from equation (2.9). Because thermalization of photoexcited electrons within the conduction band is very rapid compared to diffusion, all Cu_2S electrons will be equally affected by the spike independent of the exciting photon energy. The narrowness of the region (20 A) in which compensation of CdS need occur to decrease the barrier transparency explains the short heat-treatment times at relatively low temperatures (a few seconds at 250°C) which are often sufficient for significant loss of long wavelength response.

Role of Deep Impurity Levels

The deep impurity levels have an important role in modifying the long wavelength response of the heterojunction. The levels are acceptors in the CdS and therefore widen the depletion region. Widening the conduction band spike decreases its transparency to photoexcited electrons in the Cu_2S; therefore the presence of these levels decreases the photoresponse of the cells especially in the long wavelength region.

The level E_2 can also act as a deep hole-trapping level. Capture of a hole results in a change of the charge state of the center to a less negative value with respect to the lattice. The effect of hole trapping in these centers is to decrease the ionized acceptor density resulting in an increase in the net donor density. The depletion width decreases, narrowing the conduction band spike thereby increasing the barrier transparency for tunnelling. Hole trapping in level E_2 can be due to either optical transitions from the level to the conduction band, or to intrinsic absorption in the CdS creating a hole-electron pair followed by capture of the hole in the center. Since the level is very deep and the free carrier density in the depletion region is extremely small, captured holes will remain trapped for long times at room temperature.

The charge state of the deep impurity levels is the factor controlling the transparency of the conduction band spike proposed in this model. The conduction band spike may be regarded as a photocurrent gate which is controlled by the occupancy of the deep acceptor level E_2.

Level E_1 is introduced into the model to account for the two infrared quenching bands observed experimentally. Quenching of the enhanced photocurrent occurs due to the inverse of the hole-trapping process described above. Optical or thermal emptying of holes from levels E_2 results in decreased transparency of the conduction band spike. Optical quenching occurs by either a 1.1 eV transition from the valence band to an empty (of an electron) level E_2 or by a 0.8 eV transition from levels E_1 to E_2 plus a thermal excitation from the valence band to E_1. Thermal quenching for a level 1.1 eV deep will be very slow at room temperature. The transitions involved in these quenching processes are very similar to those observed in quenching of photoconductivity in sensitive CdS crystals.[70,71]

6.5 Experimental Support for the Light-Modulated Tunnelling Model

In section 6.4, the mechanism of light-modulated tunnelling through the conduction band spike of the proposed band profile was discussed. In this section, the experimental basis for this mechanism will be discussed.

Fast and Slow Components of Spectral Response

Fast and slow components of the spectral response were shown in figures 4.18 and 4.19. The fast component represents tunnelling through the spike with levels E_2 completely filled with electrons. The slow component (difference between steady-state and fast component) is due to some of the incident light penetrating to the CdS causing changes in the band profile by changing the charge state of levels E_2. The

slowness of these effects is a result of the small optical absorption coefficient (α = 1 to 100 cm^{-1}) of these impurities. In figures 4.18 and 4.19, the slow component is seen to enhance the response for energies greater than 1.47 eV (λ < 8400 A). This energy corresponds to the threshold for optical excitation from E_2 to the conduction band. The decrease in the slow component at the band edge of CdS (5200 A) is due to the highly absorbed band gap light creating a high density of free holes some of which are captured in centers E_2. The enhancement process still takes place in the short wavelength region, but because of the much more efficient generation and trapping of holes the response is very rapid. In the short wavelength region a good fraction of the observed photocurrent is due to the carriers generated in the CdS.

At photon energies less than 1.47 eV, the slow component has a small quenching effect on the photocurrent. This effect may be due to the levels E_2 which lie very near the Fermi level close to the interface. Some of these levels will be empty of electrons in the dark. Excitation of electrons from the valence band will ionize these centers making them effective as acceptors. The width of the conduction band spike is very sensitive to the charge state of impurities close to the metallurgical interface. A small increase in acceptor density results in widening of the spike reducing the tunnelling current.

Secondary Illumination Experiments

Spectral response measurements made with secondary illumination

on the cell cause enhancement or quenching of the primary response. Typical results for short wavelength and white secondary illumination were shown in figures 4.15, 4.20 and 4.23. For short wavelength secondary illumination the effect is straightforward enhancement by capture of holes in level E_2 as discussed above. Figure 4.15 shows the results of such illumination on a cell which lost most long wavelength response on heat treatment. It is significant that the long wavelength edge for the heat-treated cell with no secondary illumination is near 1.5 eV and response in this region was found to be slow. For photon energies greater than 1.5 eV hole trapping by excitation from levels E_2 to the conduction band increases the transparency of the conduction band spike to electrons excited by the same wavelengths in the Cu_2S.

Competition between quenching and enhancement effects of different wavelengths in the secondary spectrum results when white secondary illumination is used. Since most of the levels E_2 are normally filled (with electrons) at equilibrium, quenching effects cannot occur (except in a narrow region immediately adjacent to the Cu_2S) until enhancing radiation has trapped holes in the levels. Quenching radiation will decrease the effectiveness of the enhancing radiation but the net effect will usually be enhancement.

Figure 4.23 showing results on a Clevite cell is a good example of the self-enhancement effects of the monochromatic light. With strong secondary illumination very little enhancement is produced for photon energies greater than 1.6 eV. Most of the enhancement effect of secondary illumination is for those wavelengths not

sufficiently energetic to excite electrons from levels E_2 to the conduction band.

The effects of long wavelength secondary illumination require more careful interpretation. As pointed out in section 4.3, the use of steady primary and secondary sources can lead to confusion in interpreting enhancing and quenching data. In figure 4.22 the results of strong 9000 A secondary illumination are shown. At long primary wavelengths the photocurrent was quenched slightly by the effect discussed above in which levels very near the interface can be filled with electrons. Above 1.5 eV apparent enhancement of the primary response was observed. As explained in section 4.3 (see figure 4.20) the effect was actually enhancement of the 9000 A secondary signal by the short wavelength primary. The peak at 2.6 eV shows the effect of intrinsic excitation of the CdS followed by hole trapping. The slight change from 8400 A to 8000 A for the transition from quenching to enhancement is due to the low intensity of the enhancing radiation relative to the quenching radiation.

By using chopped monochromatic primary radiation and steady monochromatic secondary illumination, quenching and enhancement effects of the secondary radiation were studied. Results of these experiments were shown in figures 4.24 through 4.28. On single crystal CdS cells two strong quenching bands were observed (figures 4.24 and 4.25) which are associated with the transitions from E_1 to E_2 (0.8 eV) and from the valence band to E_2 (1.1 eV). The transition at 1.1 eV corresponds to the higher energy quenching peak observed in the photoconductivity of sensitive CdS crystals. The quenching peak at 0.8 eV is slightly

lower in energy than the peak observed in photoconductivity quenching (0.87 eV). However, excitation spectra for IR emission[84] have a lower energy peak at 0.83 eV in better agreement with the present results.

At short wavelengths enhancement of the primary signal was observed. In the transition region from quenching to enhancement the two processes are competitive making it difficult to determine the exact onset of the enhancement. Elimination of strong quenching effects by use of 9200 A primary illumination allowed the onset of enhancement to be determined (see figures 4.26 and 4.28). Agreement is excellent with the energy determined from the transitions from quenching to enhancement seen in the spectral response curves (figures 4.18 and 4.19).

In cell #1 a series of measurements were carried out to determine whether the levels E_1 and E_2 were present before heat treatment of the cell. Before forming the heterojunction, the photoconductivity of the CdS crystal was measured (figure 4.15). Attempts to quench the photoconductivity with infrared illumination showed no quenching. The cell was then dipped to form a heterojunction, and secondary illumination was used in an attempt to enhance or quench the short-circuit photocurrent. The secondary illumination was found to have no effect on the photoresponse. After 1 minute heat treatment at 250°C, the long wavelength response was drastically reduced, but short wavelength secondary illumination enhanced this part of the spectral response (see figure 4.14). Strong quenching of this enhanced response was then observed in two infrared bands associated with transitions involving levels E_1 and E_2 (figure 4.25). The conclusion

drawn from these observations is that heat treatment introduces the levels E_1 and E_2 into a narrow region of the CdS adjacent to the junction.

Dependence on Secondary Light Intensity

The results of measuring the enhancement effect as a function of intensity of the secondary radiation (figure 4.28) were most informative. Saturation of the enhancement is observed at secondary intensities which are very small compared to the primary intensities. As secondary intensity was decreased the time required to reach a steady state enhanced current increased, but eventually enhancement was almost as effective as with the highest intensities. Cell #1 showed almost completely saturated enhancement with secondary radiation whose intensity was 1% of the primary source intensity. For this cell the primary intensity gave rise to an unenhanced photocurrent density of 1μamp/cm^2 corresponding to a flux density of 6 x 10^{12} electron/cm^2-sec. This photocurrent was doubled by a secondary intensity of 1.6 x 10^{-7} watt/cm^2 which corresponds to a photon flux density of 3.8 x 10^{11} photon/cm^2-sec. Thus each secondary photon resulted in 15 additional primary current carriers being collected. This observation clearly demonstrates the gate-like role played by the conduction band spike. Decrease of the width of this spike by a relatively small number of trapped holes opens the gate. Once a steady-state situation is reached the sole function of the secondary radiation is to replenish trapped holes lost by recombination processes.

The dependence of the photocurrent on the intensity of enhancing

radiation can be estimated from equation (2.9). In this equation, net donor density is a function of the intensity of enhancing radiation since this radiation changes the charge state of levels E_2. The number of levels E_2 filled with holes n_T may be calculated from the rate equation

$$\frac{dn_T}{dt} = G - \frac{n_T}{t_2} , \tag{6.1}$$

where G is the hole-trapping rate and t_2 is the time the holes spend in the level E_2. Assuming the hole-trapping rate is proportional to secondary light intensity, the number of trapped holes is given by

$$n_T = \frac{N_T}{1 + \frac{1}{aFt_2}} , \tag{6.2}$$

where N_T is the density of trapping centers, and a is a constant.

The net donor density to be used in equation (2.9) can be expressed as

$$(N_D - N_A)_{eff} = (N_D - N_A) - N_T + n_T , \tag{6.3}$$

From equation (6.2) it is seen that at high light intensities F, and long hole-trapping times t_2, the number of trapped holes tends to its maximum value N_T. This saturation of n_T with enhancing radiation intensity is responsible for the observed saturation of the enhancement effect at low light intensities. Rough estimates of the intensity at

which saturation is expected were made using a value of t_2 determined from the initial decay of the enhancement effect, and assuming a reasonable hole-trapping efficiency. Enhancing radiation intensity in the range of 1 to 10 μwatt/cm^2 is estimated to be enough to reach saturation in these cells in reasonable agreement with the experimental results shown in figure 4.28.

Persistence of Enhancement

Transient behavior of enhanced photocurrent is consistent with the proposed model. In figure 4.17, the 7300 A illumination was turned off (at t = 250 seconds) after the slow increase had considerably enhanced the photocurrent. After a dark interval of 100 seconds, the light was turned on and fast return was observed to the previous enhanced photocurrent level. The persistence of the enhancement effect was investigated by irradiation with short wavelength (enhancing) light followed by a dark interval, after which the transient response to long wavelength light was observed. Figure 4.31 showed a typical experimental sequence. Figure 4.32 showed the initial long wavelength photocurrent as a function of the dark delay interval. Significant enhancement persisted for up to a 1/2 hour delay, a result which can only be explained by deep trapping controlling the long wavelength response. After a 15 second delay the enhanced current is very nearly at the same level as the response with simultaneous primary and secondary illumination. This observation is evidence that free carriers generated in the CdS near the junction have no significant effect on the long wavelength enhancement.

The temperature dependence of the decay constant for enhanced photocurrent shown in figure 4.34 yielded an activation energy of 0.95 eV. This is the thermal energy needed to excite holes trapped in levels E_2 to the valence band and corresponds to thermal quenching of the enhanced photocurrent. The activation energy was somewhat lower than the energy measured by optical quenching (1.1 eV). Energies measured in thermal and optical quenching of photoconductivity show the same discrepancy, thermal activation energies always being somewhat lower than optical energies.[85] Similar discrepancy has been observed in energies determined by thermal and optical quenching of luminescence in ZnS.[86] The similarity of optical and thermal quenching of the enhanced photovoltaic effect to quenching of photoconductivity leaves little doubt that the former are due to processes in the CdS analogous to those seen in photoconductivity. The trapping processes for both photoconductivity and the photovoltaic effect are the same. In the photoconductivity case, hole trapping leads to sensitization by increasing the electron lifetime; for the heterojunction, hole trapping leads to enhancement by narrowing the depletion width which increases the transparency of the conduction band spike at the interface.

V-I Characteristics

The temperature independence of the V-I characteristics (figure 4.4) suggests a tunnelling-limited forward current. Several possible tunnelling processes are indicated on the upper band profile of figure 6.2. Simple tunnelling through a conduction band spike (1) is not consistent with the observed temperature independence since the incident electron

BEFORE HEAT TREATMENT

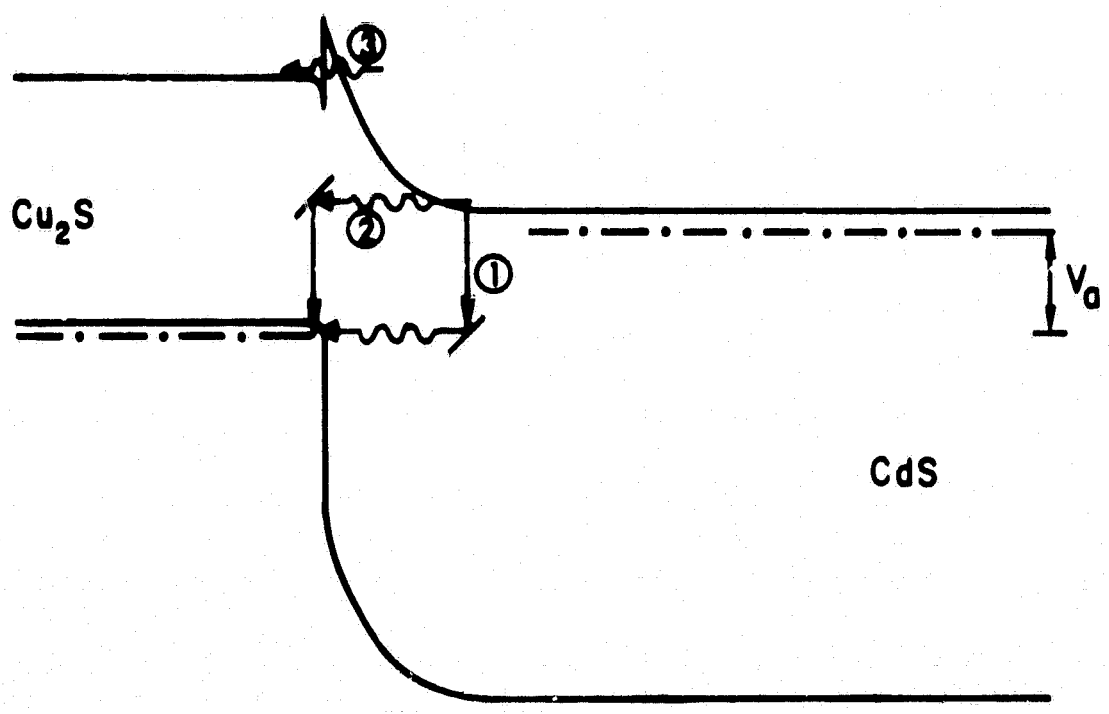

AFTER HEAT TREATMENT

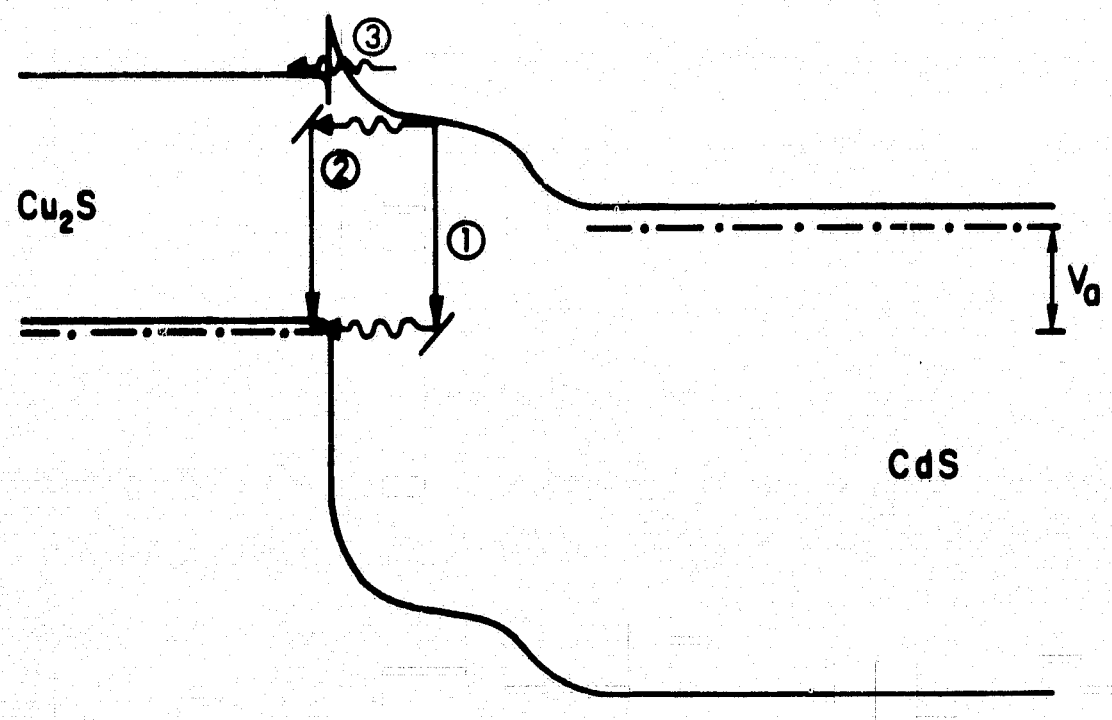

FIGURE 6.2: TUNNELLING MECHANISMS FOR TEMPERATURE INDEPENDENT FORWARD V-I CHARACTERISTICS.

flux on the CdS side of the barrier should be strongly temperature dependent. Processes (2) and (3) involving electron tunnelling via interband states appear to be the only mechanisms that can account for the observations. At sufficiently high forward bias and at the higher temperatures, process (1) may begin to contribute to the current, accounting for the change in slope of the V-I characteristics in figure 4.4. At forward bias greater than 0.4 volts, the 295°K characteristic shows a greater change in slope than the lower temperature curves consistent with this interpretation.

Since the depletion widths in these cells are about 2×10^{-5} cm wide, tunnelling by processes (2) or (3) must occur at high field points on junctions where considerably narrower tunnelling paths are possible.

After heat treatment the situation is shown schematically in the lower band profile of figure 6.2. The increased depletion width due to compensation of the CdS layer adjacent to the interface explains the five order of magnitude decrease in forward current at room temperature (figure 4.5). Below 290°K the characteristics show little temperature dependence. Above 300°K current increases rapidly with temperature (figure 4.6). The coefficient α of equation (2.2) is essentially constant, increasing by only 25% as the temperature decreases from 371°K to 113°K. With the exception of the 288°K characteristic, where a low value of α is obtained, the values of α are between 20 and 25. The decreased current and increased value of α seen after heat treatment are consistent with an intervening compensated CdS layer decreasing the tunnelling probability.

Since appreciable tunnelling can take place only through barriers no more than a few hundred Angstroms wide, thermal excitation of carriers is important in determining the incident electron flux for the tunnelling process. At low temperatures, processes (2) or (3) probably dominate and tunnelling may be the rate-limiting process because of the low density of available interband states. At higher temperatures, process (1) begins to compete, resulting in a strong temperature dependence. At about 1 volt forward bias a sharp decrease in the slope of the characteristics was observed even after correction for series resistance. This bias voltage is almost equal to the barrier potential and corresponds to tunnelling through the conduction band spike dominating the forward current. For cell #1 the low temperature characteristics have the highest current in this bias region. Above 1.2 volts the slope of the 288°K characteristic increases again probably due to thermal emission over the barrier. Figure 4.6 shows the temperature dependence of the forward current at a fixed bias of 0.5 volts. The activation energy of 1.2 eV obtained from the high temperature region is evidence that at these temperatures forward current is due to tunnelling through the conduction band spike with the incident electron flux being thermally activated.

Measurements on an evaporated CdS cell over a limited temperature range also resulted in temperature insensitive V-I characteristics consistent with tunnelling-limited forward current.

The crossover of the V-I characteristics taken in the dark and with illumination on the junction (see figure 4.2) is one of the major unexplained observations in the Cu_2S-CdS cells. The incident

light appears to have two effects; (1) generation of a photocurrent, and (2) increasing the forward current of the cell. The spectral response of the second effect has been shown to be very similar to the spectral response for long wavelength enhancement of photocurrent.[35] Under strong white illumination the forward characteristic approaches that of the non-heat-treated cell where the forward current is independent of illumination (see figure 4.3). These observations are consistent with the proposed model.

Before heat treatment the forward current is independent of illumination and the characteristics in the dark and light are similar to the classical photodiode characteristics in which no crossover is observed. However, the temperature independence of the forward current (figure 4.4) implies a tunnelling process instead of the usual thermally activated current over the barrier. Heat treatment causes diffusion of acceptor states E_2 into the CdS resulting in a widened depletion layer. Even though the barrier height remains unchanged, forward current will be greatly decreased due to the decreased tunnelling probability through a wider barrier. Under illumination with photon energies greater than 1.5 eV the acceptor states E_2 can be populated with holes as explained in connection with photocurrent enhancement. The net acceptor density and the depletion width decrease, tending at high light intensities to the pre-heat-treatment values. The forward current tunnelling process increases toward the limiting pre-heat-treatment value. Since variation of the depletion width by hole occupation of level E_2 is the mechanism responsible for both the enhancement of long wavelength response and the increased forward

current, it is evident that the spectral response of the two effects will be the same.

Shiozawa et al.[23] have suggested that the resistance of the compensated CdS layer is responsible for the degraded long wavelength response in the Cu_2S-CdS cells. Shirland[87] has attributed the cross-over in the V-I characteristics to the presence of a series resistance in the cell. Since photoconductivity of the compensated CdS layer would determine the magnitude of the series resistance, these models predict the same spectral response of enhancement and quenching as the model involving a conduction band spike. The difference between the models is that variation of the depletion width modulates transparency of a barrier in one case, while in the other photoconductivity decreases the internal series resistance of the cell. Recently, van Aerschot et al.[35] have shown that the V-I characteristic in the light cannot be explained by a series resistance that is only light intensity dependent. Using the equation of a photovoltaic cell with a series resistance

$$i_L = i_0[e^{\alpha(V-Ri_L)}-1]-i_s \ , \qquad (6.4)$$

where i_L is the total current under illumination, and i_s is the photocurrent, these authors found that the value of R would have to be a function of the current to fit the observed data. These authors suggest that enhancing radiation has the effect of decreasing the barrier height of the heterojunction. Such a decrease would certainly explain the crossover of the V-I characteristics, but it is not clear

how decreasing the barrier height would increase the collection efficiency for electrons generated in the Cu_2S layer unless a conduction band spike exists.

In the model of Shiozawa et al.[23] a decrease in barrier height is postulated to account for the crossover of the V-I characteristics. However, the lower barrier height in strong light appears to ignore the affinity difference as a barrier to forward current.

The temperature independence of the V-I characteristics suggests that the forward current is not due to thermally activated flow over the barrier. Changes in the depletion width can modulate the tunnelling probability without affecting the barrier height. The observation that the forward characteristics under strong illumination tend to the pre-heat-treated value is consistent with changes in the depletion width and unchanged barrier height.

After strong illumination, the forward characteristics are observed to slowly drift back to the lower current dark value. At increased forward bias the drift is much more rapid. This observation is consistent with recombination of forward bias injected electrons with holes trapped in levels E_2 by the previous illumination. This recombination increases the net acceptor density widening the depletion layer and therefore decreases the forward tunnelling current. With no current flowing, as in the persistence of the enhancement effect in the dark, very long decay times were measured. Electron flow through the depletion region in either the forward or reverse direction increases the recombination rate by which holes are emptied from the traps.

Junction Capacitance

Measurements of the junction capacitance with and without illumination support the idea of a light-modulated depletion width. While it is recognized that capacitance data under strong illumination must be treated cautiously because of free carrier effects, it is still possible to gain some knowledge of depletion width behavior under illumination.

Capacitance-voltage measurements in the dark show that the depletion layer is widened by heat treatment (see figure 4.10). Illumination with short wavelength light results in increased capacitance. In some cells for which optical quenching was very strong, additional long wavelength light was observed to quench the short wavelength induced increase in capacitance (see figure 4.11). Since short wavelength light ($\geq$ 1.5 eV) should decrease the effective acceptor density, and long wavelength light should reactivate the acceptors, these results are in accord with the proposed model.

After short wavelength illumination of the cells, the dark capacitance decreases very slowly to the equilibrium dark value. The equilibrium capacitance could be attained very rapidly by illumination with long wavelength light (< 1.5 eV) or by allowing a short period with forward bias voltage applied. Both these relaxation processes are due to emptying of holes from the diffused-in acceptor levels.

Open-Circuit Photovoltage

On many of the heat-treated cells, the maximum open-circuit photovoltage obtained with strong long wavelength illumination exceeds

the photovoltage obtainable with either short wavelength or white illumination. On cell #4, V_{oc} = 0.4 volts for strong illumination with photon energies less than 1.8 eV. Additional illumination of the cell with a weaker secondary source having photon energies greater than 2 eV resulted in quenching of the open-circuit voltage to 0.36 volts. This result cannot be explained by any model invoking series resistance as no net current was flowing through the cell. The proposed model involving light-modulated depletion widths offers a simple explanation of this effect. With intense long wavelength light the depletion width remains wide. Tunnelling through the conduction band spike is inefficient, but sufficient carriers penetrate the spike to build up the photovoltage. Because of the wide depletion region, forward current due to the photovoltage is very small which allows a large photovoltage to build up. Weak secondary illumination causes additional photocurrent to flow, but it also populates levels E_2 with holes, shrinking the depletion region. The forward current which is presumably a tunnelling process is very sensitive to the depletion width and therefore increases rapidly. Because of the higher forward current when the depletion region is narrow, the photocurrent can no longer support as large a photovoltage. The photocurrent and the forward current are therefore equalized at a lower V_{oc}.

The spectral response of open-circuit photovoltage shown in figures 4.14 and 4.20 show that fairly large (≈100 mvolts) open-circuit photovoltages are generated even though the same light intensity resulted in less than 10^{-11} amps of short-circuit photocurrent. It is clear that these open-circuit photovoltages can only be maintained

by such low photocurrent if the cell forward current is extremely low.

6.6 Light-Modulated Zener Breakdown

In sections 5.4 and 5.5, the observation of a large photocurrent gain under reverse bias was described. The experimental observations made on a large number of cells are listed in section 5.4. A model involving light-induced Zener breakdown at high field points on the junctions is proposed to account for these observations.

Figure 6.3 shows the band profile for the reverse-biased Cu_2S-CdS heterojunction. Three conduction band profiles are indicated schematically on the figure. The line labelled (1) represents the band profile at a planar interface between the Cu_2S and the CdS. Line (2) represents the profile at a sharp protuberance of Cu_2S into the CdS. At such a point, the depletion width will be less than for the planar interface and consequently the electric field at the interface is much higher. Line (3) represents further change in the band profile at sharp points caused by photoinjected holes. Band-to-band tunnelling or Zener breakdown occurs from the top of the Cu_2S valence band to the CdS conduction band.

The mechanism for the light-modulation of the tunnelling process is very similar to the process described in connection with long wavelength enhancement of spectral response in these cells. In this case the electric field in the depletion region is modulated by free holes optically generated by bandgap irradiation of the CdS. The holes drift to the Cu_2S-CdS interface in the potential gradient of the valence band. The positive charge due to the free holes causes

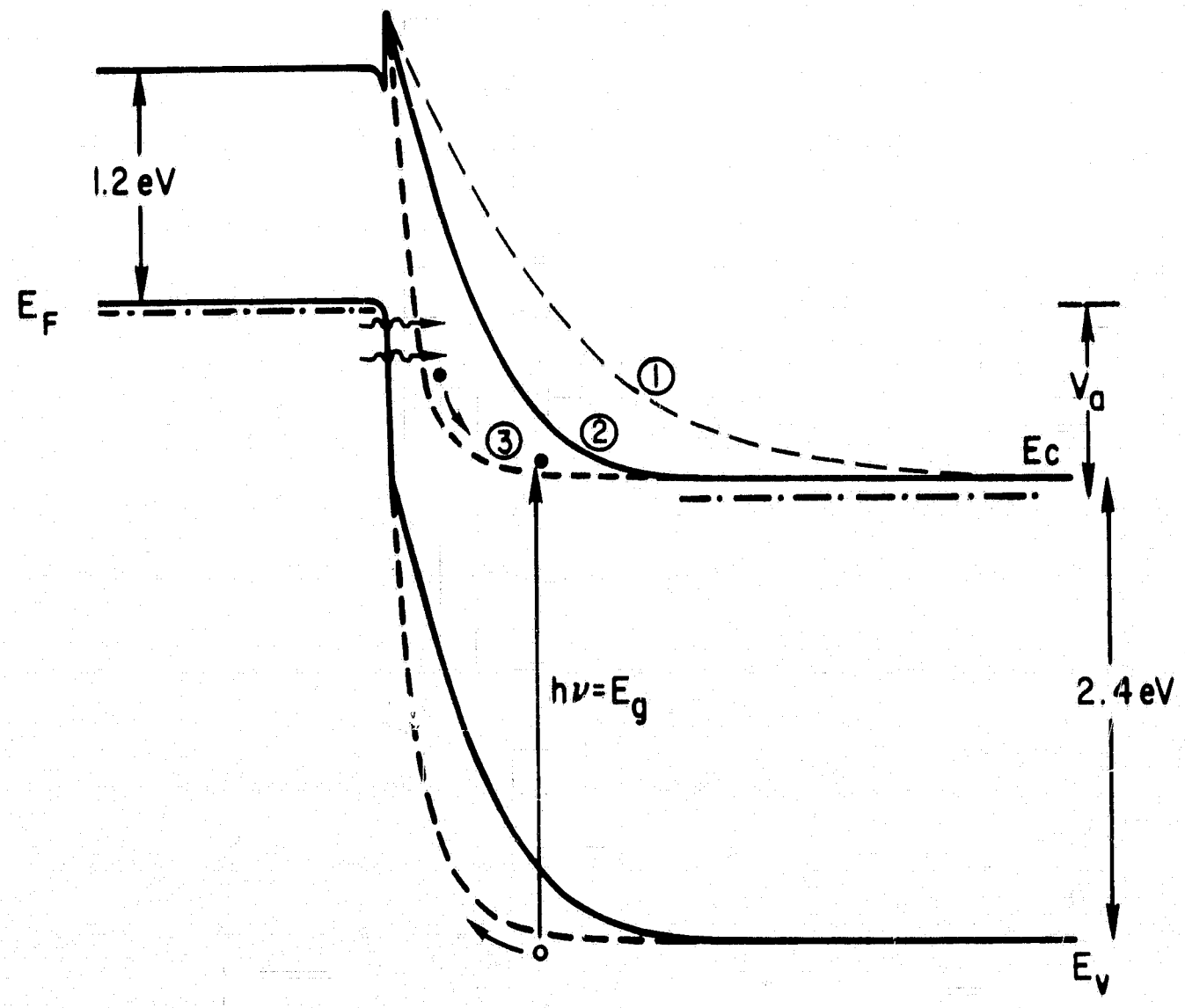

FIGURE 6.3: BAND PROFILE UNDER REVERSE BIAS SHOWING THE LIGHT-MODULATED ZENER BREAKDOWN MECHANISM. CONDUCTION BAND PROFILES ARE SHOWN FOR (1) THE PLANAR INTERFACE, (2) SHARP POINTS ON THE INTERFACE, AND (3) SHARP POINTS WITH NARROWING DUE TO PHOTO-INJECTED HOLES.

the electric field to increase near the interface, narrowing the forbidden region sufficiently for appreciable tunnelling across the bandgap to take place. The magnitude of the observed photocurrent gain and its slow response (2×10^{-4} seconds) requires that the holes be delayed for a short time at or near the Cu_2S-CdS interface.

The mechanism outlined above for depletion width modulation has been invoked to explain the infrared enhancement of electroluminescence in ZnS.[49] Tunnelling through the top of a Schottky barrier was modulated in this instance. Tunnelling from valence to conduction band has also been used to explain electroluminescence experiments in Cu_2S-ZnS heterojunctions[88] but no light modulation was involved.

The light-modulated Zener breakdown described in this thesis is believed to be the first observation of such a process. Because the breakdown only occurs at high field points on the planar junctions, the geometry in the breakdown regions is not known. For this reason no detailed theoretical treatment could be compared with the experiments. In the following subsection a qualitative discussion is presented relating the proposed breakdown mechanism to the experimental observations. The last subsection presents an empirical approach by which the dependence of the breakdown current on reverse bias voltage and light intensity are obtained graphically.

Qualitative Discussion

Two of the experimental observations lead to the conclusion that photo-injected holes are necessary for the light-induced breakdown effect. The first is the sharp threshold at the CdS band edge

for onset of the breakdown effect, and the second observation is that the maximum gain is always obtained with the light probe at the depletion layer edge on the CdS side of the junction.

The photocurrent which is approximately constant on many cells from 1.4 eV to 2.4 eV is an electron current due to photoexcitation in the Cu_2S and is apparently not related to the observed breakdown. The first significant hole injection into the space charge region of the junction occurs with CdS bandgap radiation at 2.4 eV. The increasing gain observed as the light microprobe moves away from the Cu_2S side of the junction is probably due to three effects? (1) increased transit time for holes injected in the space charge region, (2) decreased effect of the electron space charge injected with the holes, and (3) geometry of the field near points where breakdown occurs. In most of the experiments a 20 micron by 1.5 micron line of light parallel to the junction was the source of injected holes. Since points at the Cu_2S-CdS interface are the major breakdown regions the distortions of the electric field near the points will focus injected holes to the high field regions. Simple consideration of the field distortion near such points shows that with increasing distance from the point a longer section of the line image will result in holes which drift to the high field region.

The threshold of 0.2 volts for onset of the light-induced breakdown is expected from the location of the Fermi level in the bulk CdS. In all the crystals investigated the Fermi level lies between 0.1 and 0.2 volts below the conduction band edge. In the Cu_2S layer the Fermi level is at or very near the valence band edge. Since Zener

breakdown requires tunnelling from the Cu_2S valence band to the CdS conduction band, a reverse bias of at least 0.1 to 0.2 volts is needed to bring empty conduction band states opposite the occupied Cu_2S valence band states. Similar breakdown effects observed on an electroplated Cu-CdS barrier cell showed no threshold, with appreciable gain being measurable with less than 10 millivolts reverse bias.

Saturation of the breakdown effect is observed at very low values of reverse bias. At less than 2 volts reverse bias the major increases in the photocurrent have already taken place. Since avalanche breakdown requires that the average kinetic energy of the holes be greater than the bandgap, this mechanism can be ruled out. In the light-induced breakdown model the saturation occurs because the change in the tunnelling barrier width per unit voltage change becomes smaller at higher reverse bias. This point will be seen more clearly in the next subsection.

On several cells the dark current for the entire reverse biased junction was less than the current due to the breakdown induced by the light microprobe (see figure 5.14). Photo-induced breakdown current in excess of the dark current are also seen in the V-I characteristics of uniformly illuminated cells (figure 4.1). Thus dark current modulation by minority carriers[89] could not explain the observed effects.

In a manner very similar to the enhancement of photocurrent, a small number of photoinjected holes control a large current flow. The possibility of the existence of a "p-n hook" giving rise to phototransistor action was investigated.[90] However, the lack of an adequate electron source on the Cu_2S side would not allow such a

structure to supply the observed currents.

The correlation of the breakdown with defects at the junction supports the Zener breakdown model, since the existence of high field points appears to be necessary for significant tunnelling to be possible. The large photocurrent gains observed with the light probe at a defect on the junction and the response time of 2×10^{-4} seconds suggest that the injected holes must be trapped in some fashion at the interface. Transit time and trapping effects in crossing the junction are not responsible as the photocurrent due to photoinjected holes at zero bias shows much faster response than the breakdown current. Hole-trapping in interface states on the CdS side of the junction could result in increased effectiveness of hole space charge leading to the large observed gain. This mechanism was postulated by Tyagi and Garlick in their model of infrared enhanced electroluminescence.[49]

After heat treatment of the cells at 250°C in air the light-induced Zener breakdown is greatly reduced. Widening of the depletion region by diffused-in acceptors reduces the field at the junction. In addition, sharp points on the junction will be regions of high surface energy. During heat treatment there will be a tendency for the radius of curvature of these points to increase in order to minimize the surface energy of the junction. The electric field at larger radius points will be smaller resulting in decreased tunnelling.

The light-modulated Zener tunnelling mechanism appears to be the only model capable of accounting for all the experimental results on reverse biased Cu_2S-CdS heterojunctions. Although a quantitative treatment of the mechanism has not been possible, all the experimental

observations are in satisfactory qualitative agreement with the behavior expected of such a light-induced breakdown.

Semi-Empirical Treatment

The major obstacle to a quantitative treatment of the light-induced Zener breakdown model is the non-uniformity of the effect along the junction (see figure 5.17). Since the breakdown is apparently extremely sensitive to the geometry at the interface with major effects being localized at defects, it is impossible to analyze the problem without at least a good approximation to the shape of the defect. Analysis of the similar problem assuming planar geometry was given by Tyagi and Garlick.[49] In this section, equation (2.10) for the tunnelling probability will be used, in conjunction with a reasonable estimate of the band profile at the highest field point, in order to generate the dependence of the photocurrent on reverse bias voltage and light intensity. An exact solution of the tunnelling problem at a point requires a three dimensional treatment. In the following, a one dimensional treatment is given with modification of the shape of the band profile being introduced to account for the increased field near a point.

The tunnelling probability is given by equation (2.10) as a function of the barrier width, δ. In order to proceed further the functional dependence δ on the applied voltage and on the light intensity F is required. An accurate expression for $\delta(V,F)$ requires a knowledge of the geometry of the junction at the point where tunnelling takes place. Lacking this knowledge, an empirical expression for the barrier

width has been used. In this expression it is assumed that the depletion width at the point is the same as for the planar regions but that the potential is a steeper function at sharp points. The expression for δ is

$$\delta = \frac{d}{V_B^{1/3}} \left[(V_B + V - V_{th})^{1/3} - (V - V_{th})^{1/3} \right] , \qquad (6.5)$$

where d is the zero bias width for a planar step junction, V_B is the diffusion potential, V is the applied reverse bias, and the threshold voltage V_{th} is the potential difference between the Fermi level and the CdS conduction band. The effect of light is introduced by varying the width of the depletion region d as follows

$$d = \left[\frac{\varepsilon V_B}{2q\{N_D - N_A + p(F)\}} \right]^{1/2} , \qquad (6.6)$$

where p(F) is the effective position charge introduced into the depletion region by the light.

In figure 6.4(a), the variation of δ with reverse bias is plotted for dark (F = 0) and three values of light intensity corresponding to p(F) being 1, 10 and 100 times $(N_D - N_A)$ in equation (6.6). The calculations of δ were all made assuming 1Ω-cm CdS bulk resistivity. In figure 6.4(b) the variation of current with δ predicted by equation (2.10) is plotted. The three intersecting lines correspond to the short-circuit photocurrent at the various light intensities. The slope of the line representing the tunnelling current is somewhat less

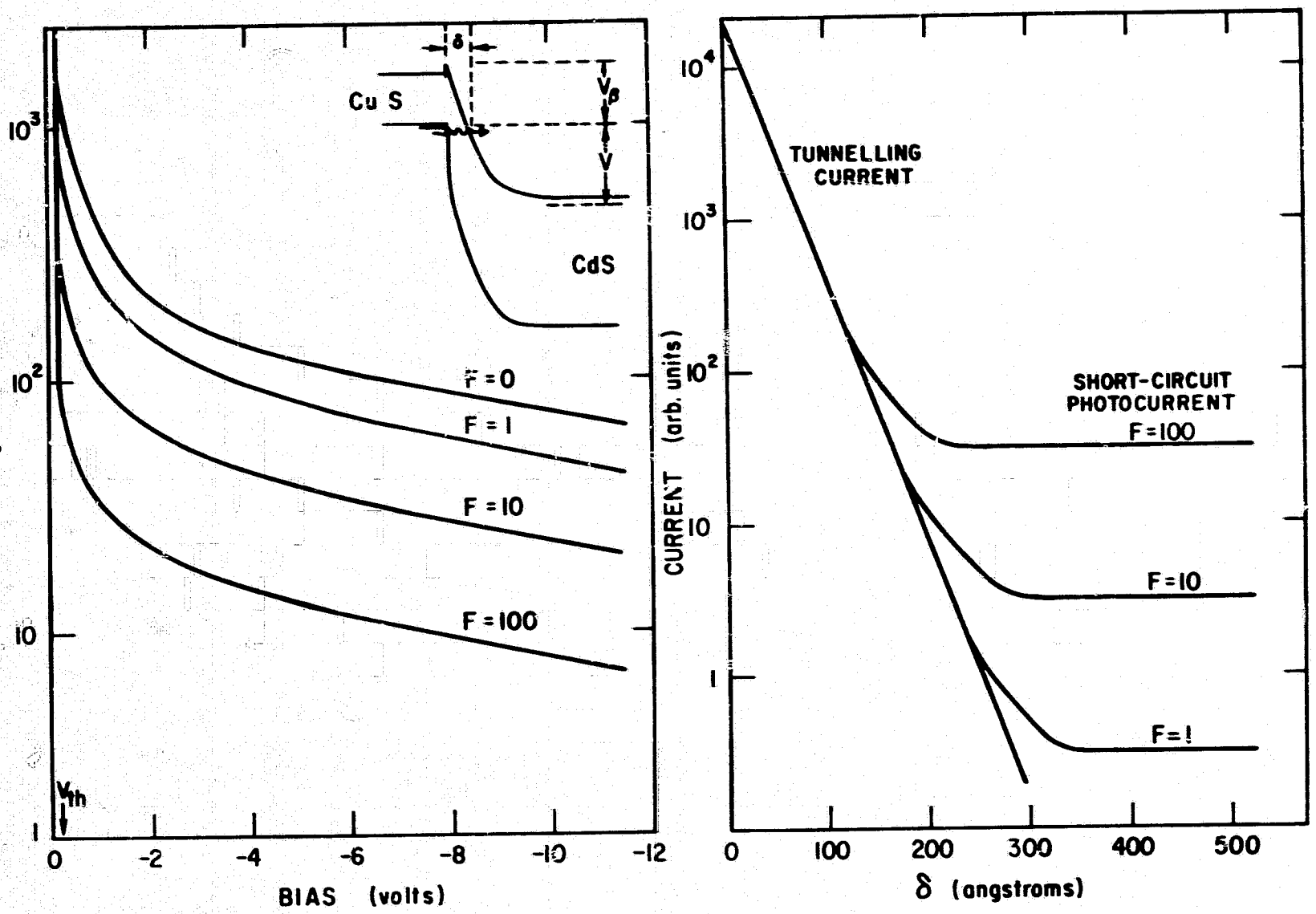

FIGURE 6.4 (a) CALCULATED VARIATION OF THE BARRIER THICKNESS AS A FUNCTION OF BIAS VOLTAGE FOR DIFFERENT LIGHT INTENSITIES ASSUMING LIGHT MODULATED ZENER BREAKDOWN MODEL.

(b) CURRENT VARIATION WITH BARRIER THICKNESS EXPECTED FOR THE TUNNELLING MODEL.

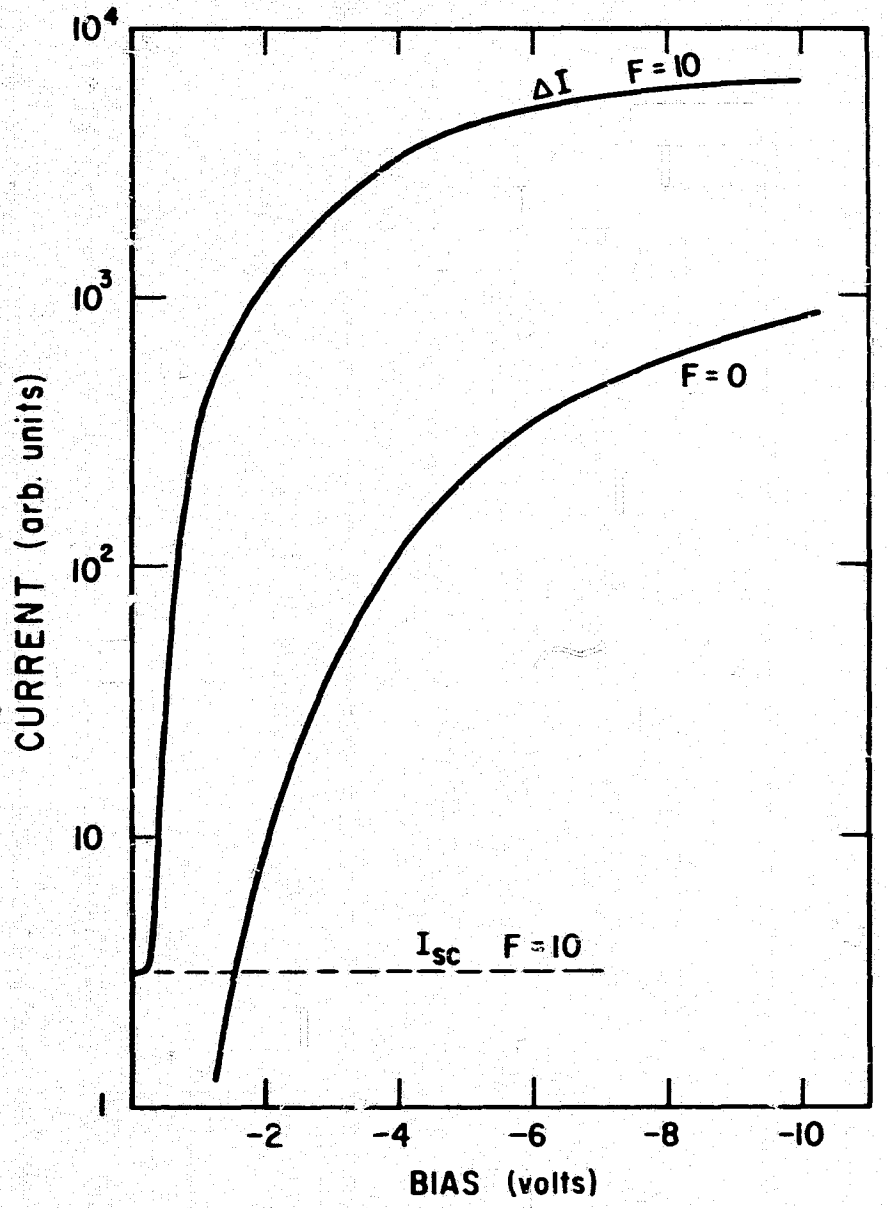

FIGURE 6.5 (a) EXPECTED VARIATION OF DARK CURRENT AND PHOTOCURRENT WITH BIAS FROM CURVES OF FIG. 6.4 (a) AND (b).

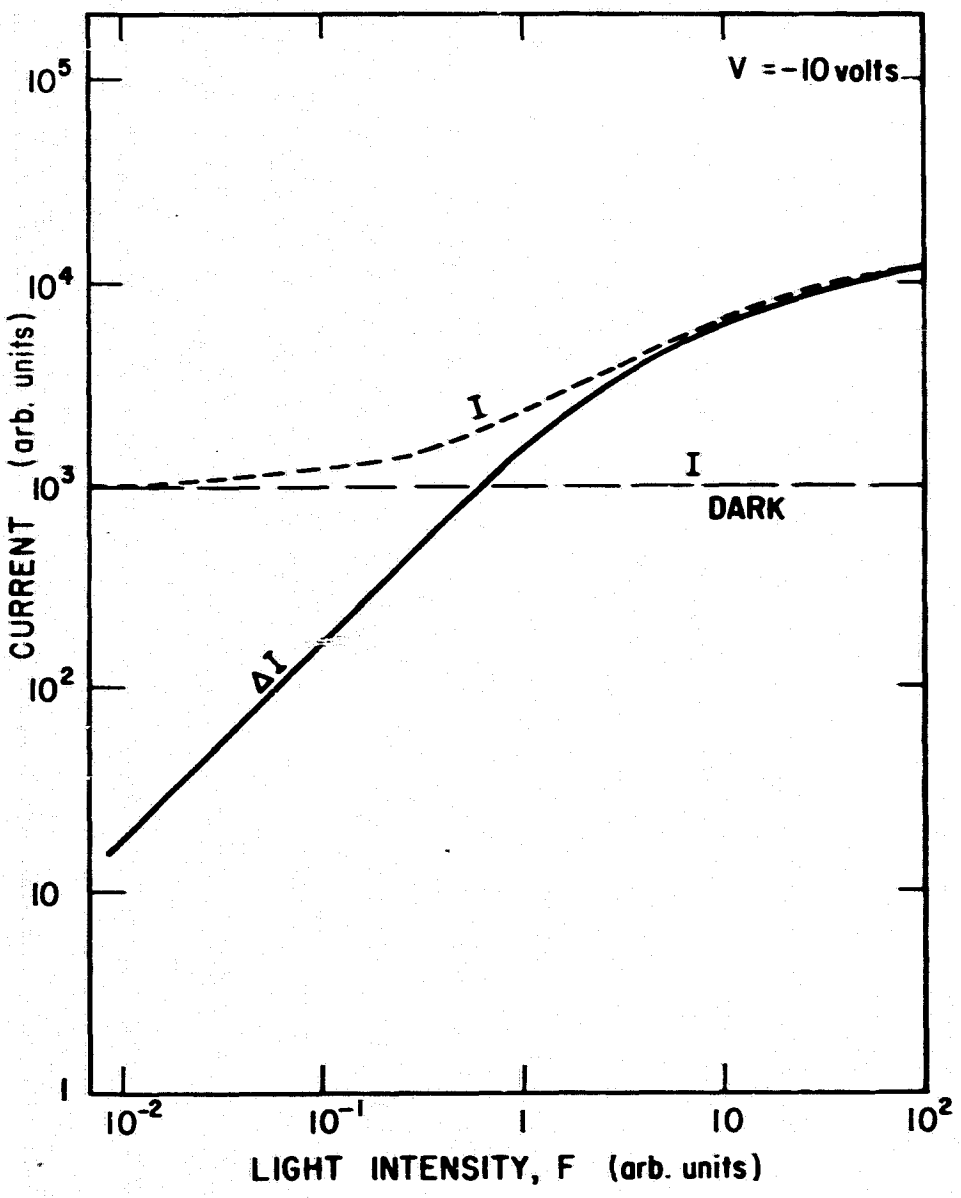

(b) INTENSITY DEPENDENCE OF THE SATURATED PHOTOCURRENT FROM CURVES OF FIG. 6.4 (a) AND (b).

than that calculated from equation (2.10) for the appropriate barrier in CdS since the resulting current versus reverse bias plot is in better qualitative agreement with the experimental curves.

Using figures 6.4(a) and (b) a plot of photocurrent as a function of reverse bias was obtained (figure 6.5(a)). The photocurrent curve, ΔI, was obtained from the total current, with F = 10, minus the dark current, F = 0. Since the experimental data of figures 5.13 and 5.14 were obtained with chopped light and phase sensitive detection of the photocurrent, the experimental data correspond to the graphically determined ΔI. The general features of the calculated photocurrent versus reverse bias curve are seen to be in good agreement with those of the experimental curves. The discrepancy between the calculated coefficient describing the tunnelling current and the coefficient actually used is not serious considering the approximations that have been made in treating the effect of light intensity and the geometry near the points. Since trapping at interface states appears necessary to explain the large gain and slow response of the breakdown effect, it is expected that higher fields may exist at breakdown points than the values predicted from the voltage and light dependence of δ given in equation (6.5) and (6.6).

In figure 6.5(b) the intensity dependence of the saturated breakdown current is plotted. Comparing this curve with figures 5.15 and 5.16, it is observed that the linear dependence at low light intensity followed by the onset of saturation at high intensities is predicted by this treatment of the model.

It is concluded that although an exact analysis of the proposed mechanism has not been possible, the semi-empirical analysis presented here gives qualitative support for the light-modulated Zener breakdown model.

VII. CONCLUSIONS

The photovoltaic effects of efficient Cu_2S-CdS heterojunctions can be consistently explained by a model in which the transparency of a conduction band spike to photoexcited electrons tunnelling from the Cu_2S controls the photoresponse. In the proposed model, the transparency of the barrier can be varied by changing the density of ionized acceptor states in the CdS layer at the junction. Heat treatment of the cells introduces acceptor levels into the CdS. The charge state of these levels can be changed to a less negative value with respect to the lattice either by optical transitions from the levels to the conduction band or by capture of holes excited by intrinsic radiation. In this way, light absorbed in the CdS can decrease the effective acceptor density, resulting in a reduced depletion width at the junction. The conduction band spike narrows with the depletion width, increasing its transparency to photoexcited electrons in the Cu_2S conduction band.

The effects predicted by this model and observed experimentally are:

(1) V-I characteristics having larger forward current under short wavelength illumination than in the dark,

(2) loss of long wavelength response after heat treatment,

(3) existence of fast and slow components in the photoresponse,

(4) enhancement of long wavelength response by relatively low intensity short wavelength secondary illumination,

(5) optical quenching of the photoresponse in two infrared bands,

(6) persistence of the enhancement effect for long dark intervals,

(7) quenching of long-wavelength-generated V_{oc} by additional short wavelength illumination,

(8) increased junction capacitance after short wavelength illumination and rapid return to the equilibrium capacitance on illuminating with infrared.

From optical quenching experiments the positions in the CdS bandgap of the energy levels effective in modulating the photoresponse are 0.3 eV and 1.1 eV above the valence band. The deeper level which is responsible for the persistence of the enhancement has an activation energy for thermal emptying of 0.95 eV and a hole capture cross-section of 2.5×10^{-15} cm^2.

Measurements of the temperature dependence of the forward V-I characteristics of these cells shows that the current fits an equation of the form

$$I = I_o \, (e^{\alpha V} - 1) \, , \qquad (7.1)$$

where α is a temperature independent constant. The temperature independence of I_o for non-heat-treated cells indicates that the forward

characteristics are dominated by a tunnelling process through interface states.

Light microprobe measurements resulted in direct determination of the ambipolar diffusion lengths on both sides of the Cu_2S-CdS heterojunction. On the CdS side diffusion lengths between 3×10^{-4} and 6×10^{-4} cm ±10 percent were measured. On the Cu_2S side the measured diffusion lengths ranged from $\leq 1 \times 10^{-5}$ to 3×10^{-5} cm ±25 percent. The diffusion lengths measured in the CdS are in good agreement with values reported in the literature for undoped CdS crystals. The measurements in the Cu_2S are the first direct determination of diffusion lengths in this material. The values obtained substantiate previous estimates based on the optimum Cu_2S layer thickness for efficient photovoltaic cells.

Reverse breakdown under short wavelength illumination is satisfactorily explained by light-induced Zener breakdown. Light microprobe investigation shows that this breakdown is localized at imperfections such as cracks on the junction. A mechanism in which photoinjected holes modulate the depletion width at high field points on the junction resulting in band-to-band tunnelling is shown to qualitatively explain this phenomenon. The experimental observations explained by this mechanism are:

(1) photocurrent gain in excess of 2000,

(2) a threshold of 0.2 volts reverse bias for the breakdown,

(3) intrinsic excitation of the CdS necessary for light-induced breakdown,

(4) saturation of the breakdown current between 2 and 4 volts reverse bias,

(5) maximum photocurrent observed some distance from the junction on the CdS side,

(6) photocurrents in excess of the incident photon flux and the reverse dark current,

(7) large variations in light-induced breakdown along the junctions,

(8) reduction or elimination of the breakdown effect by short heat treatment of the cells.

Measurements have been concentrated on heterojunctions formed on single crystal CdS. However, measurements made on a Clevite evaporated CdS thin film cell indicate that the conclusions reached in this dissertation are applicable to these cells. The only significant difference observed in the thin film cell was the absence of the lower energy quenching band at 0.8 eV. Absence of this quenching band does not change the main features of the proposed model.

REFERENCES

1) D. C. Reynolds, G. Leies, L. L. Antes, and R. E. Marburger, Phys. Rev. 96, 533 (1954).

2) D. C. Reynolds and S. J. Czyzak, Phys. Rev. 96, 1705 (1954).

3) R. Williams and R. H. Bube, J. Appl. Phys. 31, 968 (1960).

4) E. D. Fabricius, J. Appl. Phys. 33 1597 (1962).

5) H. G. Grimmeiss and R. Memming, J Appl. Phys. 33, 2217, 3596 (1962).

6) J. Woods and J. A. Champion, J. Electron. Control 7, 243 (1960).

7) D. A. Cusano, IRE Transactions ED-9, 504 (1962).

8) D. A. Cusano, Solid-State Electron. 6, 217 (1963).

9) B. Selle, W. Ludwig and R. Mach, Phys. Stat. Sold. 24, K149 (1967).

10) R. R. Bockemuehl, J. E. Kaupilla and D. S. Eddy, J. Appl. Phys. 32, 1324 (1961).

11) P. N. Keating, J. Phys. Chem. Solids 24, 1101 (1963).

12) P. N. Keating, J. Appl. Phys. 36, 564 (1965).

13) N. Duc Cuong and J. Blair, J. Appl. Phys. 37, 1660 (1966).

14) G. Nadjakov et al., Izv. Bulg. Akad. Nauk 4, 10 (1954).

15) F. Cabannes, Compt. Rend. 246, 257 (1958).

16) H. Moss, Proc. National Aeronautical Electronics Conf., 47 (1960).

17) R. R. Chamberlin and J. S. Skarman, Solid-State Electron. 9, 819 (1966).

18) F. A. Sterland and J. R. Hietanen, Proc. 19th Ann. Power Sources Conf., 177 (1965).

19) S. Djurle, Acta Chem. Scand. 12, 1415 (1955).

20) R. Marshall and S. S. Mitra, J. Appl. Phys. 36, 3882 (1965).

21) L. Eisenmann, Ann. Phys. 10, 129 (1952).

22) G. P. Sorokin, Y. M. Papshev and P. T. Oush, Sov. Phys. Solid State 7, 1810 (1966).

23) L. R. Shiozawa, G. A. Sullivan, and F. Augustine, Proc. Seventh Photovoltaic Specialists Conference, 39 (1968).

24) B. Selle and J. Maege, Phys. Stat. Sol. 30, K153 (1968).

25) E. Hirahara, J. Phys Soc. Japan 6, 428 (1951).

26) G. B. Abdullaev, Z. A. Aliyorova, E. H. Zamanova, and G. A. Asadov, Phys. Stat. Sol. 26, 65 (1968).

27) J. Singer and P. A. Faeth, Appl. Phys. Letters 11, 130 (1967).

28) S. Y. Pavelets and G. A. Fedorus, Ukrainian Phys. Jour. 11, 687 (1966).

29) R. J. Mytton, Brit. J. Appl. Phys. 1, 721 (1968).

30) W. Palz and W. Ruppel, Phys. Stat. Sol. 15, 649 (1966).

31) M. Balkanski and B. Chone, Rev. dePhys. Appl. 1, 179 (1966).

32) A. E. Potter, Jr., W. B. Berry, H. W. Brandhorst, Jr. and R. L. Schalla, NASA Technical Note, NASA TN D-4333 (1968).

33) A. E. Potter, Jr., R. L. Schalla, H. W. Brandhorst, Jr., and L. Rosenblum, NASA Technical Memorandum, NASA TM X-52500 (1968).

34) F. Shirland, Adv. Energy Conv. 6, 201 (1966).

35) A. E. van Aerschot, J. J. Capart, K. H. David, M. Fabricotti, K. H. Heffels, J. J, Loferski, and K. K. Reinhertz, Proc. Seventh Photovoltaic Specialists Conf., 22 (1968).

36) H. W. Brandhorst, Jr., NASA Technican Memorandum NASA TM X-52489 (1968).

37) L. J. van Ruyven, Thesis submitted to the Technical High School at Eindhoven, (1964).

38) R. L. Anderson, IBM J. Res. and Dev. 4, 283 (1960).

39) W. G. Oldham and A. E. Milnes, Sol. State Electron. 7, 153 (1964).

40) H. K. Henisch, Rectifying Semiconducting Contacts, Oxford University Press, Fair Lawn, N. J. (1957).

41) W. Shockley, Bell System Tech. J. 28, 435 (1949).

42) T. L. Tansley, Phys. Stat. Sol. 18, 105 (1966).

43) G. Zeidenbergs and R. L. Anderson, Solid-State Electr. 10, 113 (1967).

44) C. Zener, Proc. Roy. Soc. London, Ser. A 145, 523 (1934).

45) W. Franz, Ann. Phys., Lpz. 15, 17 (1952).

46) K. B. Mc Afee, E. J. Ryder, W. Shockley and M. Sparks, Phys. Rev. 83, 650 (1951).

47) A. G. Chynoweth, W. L. Feldmann, A. A. Lee, R. A. Logan, and G. L. Pearson, Phys. Rev. 118, 425 (1960).

48) F. A. Padovani and R. Stratton, Solid-State Electr. 9, 695 (1966).

49) R. C. Tyagi and G. F. J. Garlick, Brit. J. Appl. Phys. 17, 747 (1966).

50) W. van Roosbroeck, Phys. Rev. 91, 282 (1953).

51) L. B. Valdes, Proc. IRE 40, 1420 (1952).

52) W. van Roosbroeck, J. Appl. Phys. 40, 1420 (1952).

53) L. B. Valdes, The Physical Theory of Transistors, p 164-165, Mc Graw-Hill, New York (1961).

54) E. Jahnke and F. Emde, Tables of Functions, 4th ed., pp 236-243, Dover Publications, New York (1945).

55) M. H. Norwood and W. G. Hutchinson. Solid-State Electr. 8, 807 (1965).

56) K. L. Ashley and J. R. Biard, IEEE Trans. Electr. Dev. ED-14, 429 (1967).

57) J. J. Loferski and J. J. Wysocki, RCA Rev. 22, 38 (1961).

58) Crystal grown by R. Fiegelson, Center for Materials Research, Stanford University.

59) Crystal orientations were determined by P. F. Lindquist.

60) J. E. Rowe and R. A. Forman, J. Appl. Phys. 39, 1917 (1968).

61) R. L. Davies and R. E. Gentry, IEEE Trans. Electr. Dev. Ed-11, 313 (1964).

62) The calibrated Si photodiode was obtained from Dr. R. H. Dyck of Fairchild Camera and Instrument Corp.

63) C. van Opdorp and J. Vrakking, Solid-State Electr. 10, 955 (1967).

64) D. Dutton, Phy. Rev. 112, 785 (1958).

65) At the lowest temperatures the V-I characteristic for long wavelength illumination developed a discontinuity near zero volts which disappeared at about 190°K on warming (see figure 4.5). At this temperature the discontinuity could be regenerated by passing large forward current in the dark and then illuminating with long wavelength light. Forward current with the light still on resulted in a slow removal of the discontinuity.

66) H. K. Henisch, Rectifying Semiconductor Contacts, pp 215, Oxford University Press, Fair Lawn, N. J. (1957).

67) L. R. Shiozawa, G. A. Sullivan, and F. Augustine, "Research on the Mechanism of the Photovoltaic Effect in High Efficiency CdS Thin-Film Solar Cells." Third Quarterly Progress Report, Contract AF 33 (615)-5224, Aerospace Research Labs., (March 1967).

68) L. R. Shiozawa, E. A. Sullivan, and F. Augustine, Eleventh Quarterly Progress Report, Contract AF 33(615)-5224, (March 1969).

69) R. H. Bube, Photoconductivity of Solids, pp 60, John Wiley and Sons, Inc., New York (1960).

70) R. H. Bube, Phys. Rev. 99, 1105 (1955).

71) S. O. Hemila and R. H. Bube, J. Appl. Phys. 38, 5258 (1967).

72) D. B. Medved, J. Chem. Phys. 28, 870 (1958).

73) P. Mark, J. Phys. Chem. Solids, 25, 911 (1964).

74) R. H. Bube, Photoconductivity of Solids, pp 53, John Wiley and Sons, Inc., New York (1960).

75) W. E. Spear and J. Mort, Proc. Phys. Soc. 81, 130 (1963).

76) J. Auth and R. Ridder, Ann. Physik (Leipzig) 2, 351 (1959).

77) C. E. Bleil, D. D. Snyder and Y. T. Sihvonen, Phys. Rev. 111, 1522 (1958).

78) H. S. Sommers, R. E. Berry and I. Sochard, Phys. Rev. 101, 987 (1956).

79) K. Maeda and A. Kasami, Proc. Int. Conf. on II-VI Semiconducting Compounds, Providence, Rhode Island, 1323, (1967).

80) M. Aven and J. S. Prener, ed., Physics and Chemistry of II-VI Compounds, John Wiley and Sons, New York (1967), Chapter 10.

81) W. Palz and W. Ruppel, Phys. Stat. Sol. 15, 665 (1966).

82) I. Broser and R. Broser-Warminsky, J. Phys. Chem. Solids 6, 386 (1958), and J. Phys. Chem. Solids 8, 177 (1959).

83) Measurements were made by F. English of Sandia Corp. using the Litton Corp. electron mirror microscope.

84) F. J. Bryant and A. F. J. Cox, Brit. J. Appl. Phys. 16, 463 (1965), and Proc. Phys. Soc. (London) 87, 551 (1966).

85) R. H. Bube, J. Appl. Phys. 35, 586 (1964).

86) F. F. Morehead, J. Phys. Chem. Solids 24, 37 (1963).

87) F. A. Shirland, Adv. Energy Conv. 6, 201 (1966).

88) A. N. Georgobiani and V. I. Steblin, Phys. Stat. Sol, 21, K45 (1967).

89) V. I. Stafeev, Sov. Phys.: J. Tech. Phys. 2, 2037 (1957).

90) W. Shockley, Electrons and Holes in Semiconductors, pp 112, D. Van Nostrand Company, Inc., Princeton, N. J. (1950).